INFRARED PHOTODISSOCIATION SPECTROSCOPY OF SMALL ORGANIC CATIONS

By

JONATHAN DAVID MOSLEY

(Under the Direction of Michael A. Duncan)

ABSTRACT

Small organic cations of the form $[C_n,H_m]^+$ (carbocations) and $[C_x,H_y,O]^+$ (carboxonium ions) are produced in a molecular beam via electrical discharge in a pulsed nozzle source. Size-selected ions are investigated using infrared laser photodissociation spectroscopy in the fingerprint region (600-2150 cm^{-1}) and the C−H and O−H stretching region (2400-3800 cm^{-1}). Quantum chemistry is used to predict structures and frequencies to aid assignment of the infrared spectra. We attempted to produce and characterize the infamous 2-norbornyl carbocation $[C_7,H_{11}]^+$ in the gas phase. Spectral analysis reveals that a previously unanticipated rearrangement occurs. $[C_7,H_9]^+$ is produced from norbornene, and an unusual structural isomer of the well-known protonated toluene is found. The mass 31 cation $[C,H_3,O]^+$ exists in two structural configurations, protonated formaldehyde and the triplet methoxy cation. Cation analogs to formaldehyde $[C,H_2,O]^+$ and methanol $[C,H_4,O]^+$ both have radically different structural isomers. $[C_2,H_3,O]^+$ can exist as the remarkably stable acetyl cation, or as its more energetic protonated ketene isomer, depending on the complex reaction pathways involved in the ion source.

INDEX WORDS: Ion Infrared Spectroscopy, Carbocations, Carboxonium Ions

INFRARED PHOTODISSOCIATION SPECTROSCOPY OF SMALL ORGANIC CATIONS

By

JONATHAN DAVID MOSLEY

B.S., University of Florida, 2007

A Dissertation Submitted to the Graduate Faculty of the University of Georgia

in Partial Fulfillment of the Requirements for the Degree

DOCTOR OF PHILOSOPHY

ATHENS, GEORGIA

2014

INFRARED PHOTODISSOCIATION SPECTROSCOPY OF SMALL ORGANIC CATIONS

By

JONATHAN DAVID MOSLEY

Major Professor: Michael A. Duncan

Committee: Gary E. Douberly
Paul v. R. Schleyer

Electronic Version Approved:

Julie Coffield
Dean of the Graduate School
The University of Georgia
August 2014

DEDICATION

I dedicate this dissertation to my wife Nicole Pacheco. Thank you for your loving acceptance of me and for the giving of everything you have for the greater good.

"Sometimes you've *got* to think about more than your own safety. Sometimes you've *got* to think about the greater good." – J. K. Rowling

ACKNOWLEDGEMENTS

Firstly, I would like to thank my Higher Power, whom I choose to call God, for reaching me through all the wonderful people who have supported me on my journey down the Road of Happy Destiny.

I would like to thank my parents Michael and Juliana Mosley for instilling in me a strong work ethic and a desire to be of service to others. Without these fundamental principles, I would be helpless in discovering my true potential as a human being. I would also like to thank my wife Nicole Pacheco, without whom the completion of graduate school while raising four children would have just been a nightmare. To my loving children (if you ever actually read this), I thank you for showing me the meaning of unconditional love.

Lastly, I would like to thank Professor Michael Duncan for the opportunity to work in his laboratory. Neither one of us knew what we were getting ourselves into when I joined up five years ago. I am indebted to him for allowing me the space to twist, turn, and finally spring forth into the light of spectroscopy. I will never forget the lessons that I learned while under his tutelage. Above all, he has taught me the importance of being able to simply relate to others the fundamental principles of science that so completely captivate our minds.

"If you do what you've always done, you'll get what you've always gotten." – Anthony Robbins

TABLE OF CONTENTS

Page

CHAPTER 1

INTRODUCTION

The structures of ions have been of particular interest in mass spectrometry[1-4] and astrochemistry.[5-9] Ion reactivity studies and collisional dissociation dynamics can indicate the presence of more than one isomer, though spectroscopy can give more direct structural information.[1-4] Additionally, the observation of ions in space requires spectroscopy in the laboratory to confirm their presence and abundance in interstellar environments. However, ion spectroscopy is difficult due to the high internal temperatures and low densities per quantum state resulting from standard ion production methods.[4] On the other hand, quantum chemistry can provide structural information of ions as well as the relative energies of isomers. Indeed, theory and spectroscopy are both needed to corroborate which isomers exist.[1, 3, 4] Recent developments in ion production methods and infrared laser technology make it possible to obtain the spectra of mass-selected ions via laser photodissociation.[10-15] This work utilizes infrared photodissociation spectroscopy and mass spectrometry to investigate the structure and bonding of small organic cations of the form $[C_m,H_n]^+$ and $[C_x,H_y,O]^+$.

Ions of the form $[C_m,H_n]^+$, known as carbocations, are well known in mass spectrometry.[1-3] Carbocations are known in organic chemistry as reaction intermediates, such as in electrophilic aromatic substitutions.[16-18] They also exist in interstellar clouds and planetary atmospheres, and are key elements in reactions producing complex organic molecules in space.[4-9] Carbocations are interesting in their own right in terms of their structure and bonding. Their "nonclassical" configurations contain bridging hydrogen and methyl moieties, which participate

in three-center two-electron (3c-2e) bonding. Carbocations can also have carbon atoms which connect to more than four other atoms, giving rise to the term "hypervalent". "Classical" structures consist of carbon atoms engaging in single, double, and triple bonds with ordinary binding configurations, but neighboring orbitals can interact in these structures to introduce subtle effects, such as hyperconjugation. Carbocations often pose problems within quantum chemistry because of these structural issues. Carbocations of a particular mass to charge ratio can have more than one structural isomer, often with competing "classical" and "nonclassical" forms.[1, 3] The actual structures that form depend on the ion production methods, what precursor is used to produce the ion, the inherent stability of the binding configurations and the local environment. Carbocations are thus compelling targets for infrared spectroscopy.

Extending beyond pure carbocations, $[C_x,H_y,O]^+$, known as carboxonium ions, are prevalent among mass spectra of oxygen-containing organic molecules.[1-4] The name itself reflects their hybrid nature, possessing characteristics of carbocations and oxonium ions (those containing positively charged trivalent oxygen atoms). Indeed, multiple isomers are expected for a wide variety of carboxonium ions that differ in the location of the positive charge on neighboring C and O atoms.[1, 3, 4, 19] These ions have been implicated as reaction intermediates in organic chemistry, such as in Friedel-Crafts acylation reactions.[19, 20] Like carbocations, they are present in the interstellar medium, and are critical intermediates in reactions producing complex polyatomic molecules in space.[4-9] Therefore, carboxonium ions are also fascinating subjects for studies utilizing modern spectroscopy techniques.

The observation of carbocations and carboxonium ions in space requires known spectral signatures to confirm their presence and abundance in interstellar environments. Indeed, CH^+, one of first known diatomic molecules in space, was detected by its well-known electronic

spectrum.[21] While only a handful of these organic cations have been detected in space, many more are believed to be present.[7-9] A diagram of astrochemical pathways for several carbocations and carboxonium ions (see Figure 1.1) reveals just a small portion of the richly complex astrochemical pathways that involve these fascinating species. The detection of new species requires spectroscopy in the laboratory. Generally, to perform electronic spectroscopy, an ion must contain low lying electronic states which give rise to transitions that are accessible by modern lasers. Laser light up to the vacuum-UV region is available, but adds substantial experimental difficulty due to atmospheric absorptions. To date, a limited number of organic ions have been studied with electronic spectroscopy.[21-23] Rotational spectra have been measured for some of these ions.[24-26] However, rotational spectroscopy of ions is difficult due to inherently low signal levels, and thus has only been successful for a few cases. A very recent development allows for mass-selected rotational spectra to be obtained.[26] Still, the application is limited only to ions with a permanent dipole moment. On the other hand, vibrational spectroscopy is generally applicable to carbocations and carboxonium ions, regardless of the presence of low lying electronic states or permanent dipole moments.

Because of the extreme difficulties in performing ion spectroscopy, there have been very few previous investigations into the exact structures of carbocations and carboxonium ions. Infrared and NMR spectroscopy have been performed for several ions in so-called "superacid" matrices, which stabilize the ions with counteranions in a solvation environment.[17-19] X-ray crystallography measurements have also been reported for some of these systems, but determining the effects of solvent and counterions is difficult.[27, 28] Thus, gas-phase experiments are ideal for ion characterization, because they remove these undesirable complications.

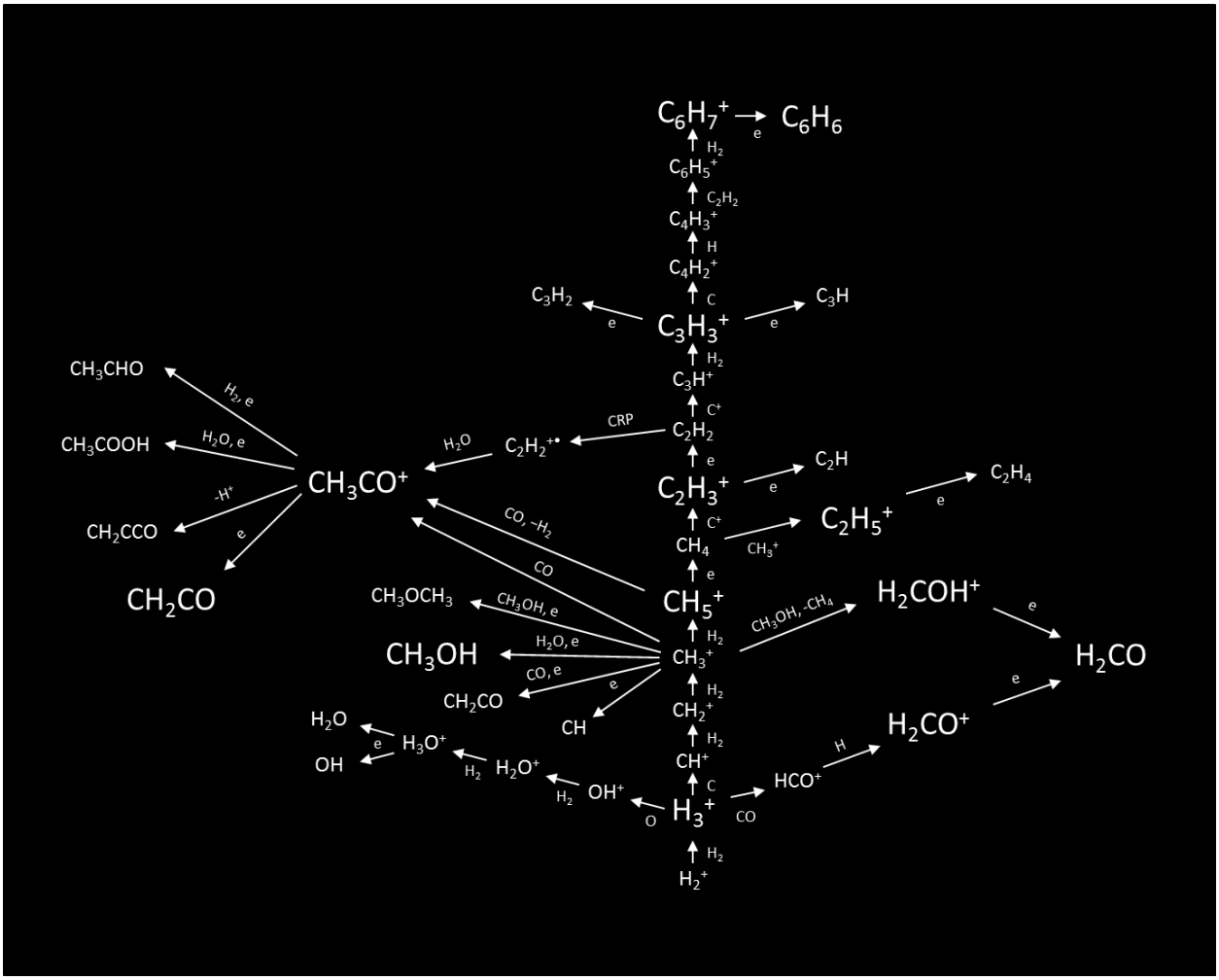

Figure 1.1. A diagram showing a few astrochemical pathways involving carbocations and carboxonium ions as reaction intermediates.

Unfortunately, standard gas-phase ion production methods, such as plasmas and electron impact ionization, are highly energetic processes, and result in complex mixtures of ions and neutral molecules. Spectral detection of any particular ionic species is therefore complicated by overlapping signals from neutral molecules which absorb in the same wavelength regions and are present in much higher concentrations. Additionally, hot ions have complex spectra due to the large amounts of excess energy spread over the molecular ion's internal degrees of freedom. The present work addresses these issues with improvements in ion production and detection methods. A pulsed discharge in a supersonic expansion produces abundant cold ions which are isolated and studied with mass-selected infrared laser photodissociation spectroscopy. These methods provide new spectral signatures for pure carbocations and carboxonium ions and elucidate the role of structural isomers.

Previous vibrational spectroscopic studies have employed a wide variety of techniques, including measurements in superacid matrices,[17-19] photoelectron spectroscopy of radicals,[29-38] infrared laser absorption in plasmas,[39-41] infrared laser absorption in molecular beams with pulsed discharges,[42] infrared absorption in rare gas matrices,[43, 44] and discharges or electron impact ionization followed by mass-selected infrared laser photodissociation.[12, 13] Each technique suffers from disadvantages, including solvent and counterion effects, inefficient ion cooling, low densities of ions, and limited laser tuning ranges. Nevertheless, significant insights into the structural configurations of carbocations and carboxonium ions have been made using these techniques. Some early developments in ion spectroscopy made by T. Oka utilized discharges or plasmas to measure high resolution absorption spectra for ions such as CH_5^+ and $C_2H_3^+$.[40, 41] These studies suffer from overlapping signal of the more abundant neutral CH_4 and C_2H_2. Interestingly, the CH_5^+ spectrum has yet to be assigned. The Nesbitt group measured this

ion at higher resolution more recently, prompting several theoretical studies of the highly complex vibrational dynamics of this hypervalent carbocation.[42, 45-50] The advent of velocity modulation enabled the selective detection of ions within discharge tubes, and these methods have been applied to a limited number of ions, including the rotationally resolved spectrum of HCO^+ in the C−H stretching region measured by Saykally.[51-53] Sears et al measured the ν_3 fundamental band of HCO^+ in the 2200 cm^{-1} region using similar methods.[54] T. Amano measured the high resolution spectrum of the O−H stretch of H_2COH^+.[55] Maier and coworkers have developed a method for studying electronic spectra of carbocations using discharges in molecular beams, mass selection, and deposition in rare gas matrices.[22] The same authors have reported the infrared spectrum of $C_3H_3^+$ in a similar matrix isolation study.[43] Newer matrix isolation studies have also been performed for ions such as $C_6H_7^+$ using solid *para*-hydrogen matrices.[44]

Perhaps the most definitive measurements have been performed using infrared laser photodissociation with mass-selected ions. The first such measurements were performed by Y. T. Lee on ions such as CH_5^+ and $C_2H_7^+$.[12, 13] The same group first discussed the method of spectator atom "tagging" to enhance infrared dissociation yield, where photon energies are much lower than covalent bond energies.[10, 11, 13] Using this technique, Dopfer and Maier measured the infrared spectra of several carbocations, including CH_3^+, $C_3H_3^+$ and $C_6H_7^+$, and the carboxonium ions HCO^+ and $HOCO^+$.[56-60] However, these studies were limited to the higher frequency C−H and O−H stretching regions by the available infrared lasers. The use of free electron lasers by these and other authors enabled the measurement of spectra in the fingerprint region, but the spectra were broad and shifted unpredictably due to multiphoton dissociation effects.[61-64] The experiments described here utilize the gas-phase ion production methods and mass-selected

photodissociation measurements similar to those described previously by Y. T. Lee[10, 11, 13] and those of Dopfer and Maier,[56-60] but use improved ion cooling in supersonic expansions. Recent developments in infrared optical parametric oscillators (OPO) have significantly improved the spectral analysis of organic cations throughout the infrared region. The Duncan group has recently used these methods to measure the extended infrared spectra of several carbocations, including $C_2H_3^+$, $C_3H_3^+$, $C_3H_5^+$, $C_4H_9^+$, $C_6H_7^+$ and $C_{10}H_9^+$.[65] The same group has also measured the spectra of $HOCO^+$ and $C_3H_7O^+$.[66, 67] Johnson and coworkers have recently reported spectra for $CH_3OH_2^+$ and $CH_3CH_2OH_2^+$ recorded using similar OPO's.[68]

This present work applies infrared photodissociation spectroscopy, mass spectrometry and computational chemistry to the investigation of a structural isomer of the infamous 2-norbornyl cation, $C_7H_{11}^+$. Additionally, the spectrum of $C_7H_9^+$ is obtained and analyzed to reveal another isomer of protonated toluene. This method is also used to probe the structure and bonding of the mass 31 cation, $[C,H_3,O]^+$, which is ubiquitous among mass spectra of oxygen-containing molecules. The cation analogs of the well-known organic molecules formaldehyde and methanol are studied as well. Finally, the acetyl cation, CH_3O^+, and its higher energy isomers are investigated. This ion is an important reaction intermediate and is believed to be present in space, but has yet to be discovered there, due to a lack of known gas-phase spectroscopic data.

References

(1) Baer, T.; Ng, C.; Powis, I., *The Structure, Energetics, and Dynamics of Organic Ions*. Wiley: New York, 1996.

(2) Beynon, J. H., *Mass Spectrometry*. Elsevier: Amsterdam, 1960.

(3) Holmes, J. L.; Aubrey, C.; Mayer, P. M., *Assigning Structures to Ions in Mass Spectrometry*. CRC Press: Boca Raton, FL, 2007.

(4) Bowers, M. T., *Gas Phase Ion Chemistry*. Academic Press: New York, 1984; Vol. I-III.

(5) Hartquist, T. W.; Williams, D. A., eds., *The Molecular Astrophysics of Stars and Galaxies*. Clarendon Press: Oxford, 1998.

(6) Tielens, A. G. G. M., *The Physics and Chemistry of the Interstellar Medium*. Cambridge University Press: Cambridge, U.K., 2005.

(7) Petrie, S.; Bohme, D. K., Ions in space. *Mass Spectrom. Rev.* **2007**, *26* (2), 258-280.

(8) Snow, T. P.; Bierbaum, V. M., Ion chemistry in the interstellar medium. *Annu. Rev. Anal. Chem.* **2008**, *1* (1), 229-259.

(9) Klemperer, W., Astronomical chemistry. *Annu. Rev. Phys. Chem.* **2011**, *62*, 173-184.

(10) Okumura, M.; Yeh, L. I.; Lee, Y. T., The vibrational predissociation spectroscopy of hydrogen cluster ions. *J. Chem. Phys.* **1985**, *83* (7), 3705-3706.

(11) Okumura, M.; Yeh, L. I.; Myers, J. D.; Lee, Y. T., Infrared spectra of the cluster ions $H_7O_3^+ \cdot H_2$ and $H_9O_4^+ \cdot H_2$. *J. Chem. Phys.* **1986**, *85* (4), 2328-2329.

(12) Yeh, L. I.; Price, J. M.; Lee, Y. T., Infrared-spectroscopy of the penta-coordinated carbonium-ion $C_2H_7^+$. *J. Am. Chem. Soc.* **1989**, *111* (15), 5597-5604.

(13) Boo, D. W.; Lee, Y. T., Infrared-spectra of CH_5^+ core in CH_5^+ (H_2). *Chem. Phys. Lett.* **1993**, *211* (4-5), 358-363.

(14) Bieske, E. J.; Dopfer, O., High-resolution spectroscopy of cluster ions. *Chem. Rev.* **2000**, *100*, 3963-3998.

(15) Duncan, M. A., Frontiers in the spectroscopy of mass-selected molecular ions. *Int. J. Mass Spectrom.* **2000**, *200*, 545-569.

(16) Aue, D. H., Carbocations. *Wiley Int. Rev.: Comp. Mol. Sci.* **2011**, *1* (4), 487-508.

(17) Olah, G. A.; Prakash, G. K., *Carbocation Chemistry*. John Wiley and Sons: New York, 2004.

(18) Schleyer, P. V. R.; Prakash, G. K., *Stable Carbocation Chemistry*. John Wiley and Sons: New York, 1997.

(19) Olah, G. A.; Laali, K. K.; Wang, Q.; Prakash, G. K. S., *Onium Ions*. John Wiley & Sons: New York, 1998.

(20) Olah, G. A., *Friedel-Crafts Chemistry*. Wiley: New York, 1973.

(21) Douglas, A. E.; Herzberg, G., Band spectrum and structure of the CH^+ molecule; identification of three interstellar lines. *Can. J. Res.* **1942**, *20a* (6), 71-82.

(22) Jochnowitz, E. B.; Maier, J. P., Electronic spectroscopy of carbon chains. *Annu. Rev. Phys. Chem.* **2008**, *59*, 519-544.

(23) Bieske, E. J.; Maier, J. P., Spectroscopic studies of ionic complexes and clusters. *Chem. Rev.* **1993**, *93* (8), 2603-2621.

(24) Dixon, T. A.; Woods, R. C., Microwave absorption spectrum of the CO^+ ion. *Phys. Rev. Lett.* **1975**, *34* (2), 61-63.

(25) Woods, R. C.; Dixon, T. A.; Saykally, R. J.; Szanto, P. G., Laboratory microwave spectrum of HCO^+. *Phys. Rev. Lett.* **1975**, *35* (19), 1269-1272.

(26) Sandra, B.; Lars, K.; Alexander, S.; Oskar, A.; Stephan, S., Laboratory rotational spectrum of *l*-C_3H^+ and confirmation of its astronomical detection. *Astrophys. J. Lett.* **2014**, *783* (1), L4/1-4.

(27) Laube, T., X-ray crystal structures of carbocations stabilized by bridging or hyperconjugation. *Acc. Chem. Res.* **1995**, *28* (10), 399-405.

(28) Davlieva, M. G.; Lindeman, S. V.; Neretin, I. S.; Kochi, J. K., Isolation, x-ray structures, and electronic spectra of reactive intermediates in friedel−crafts acylations. *J. Org. Chem.* **2005**, *70* (10), 4013-4021.

(29) Houle, F. A.; Beauchamp, J. L., Detection and investigation of allyl and benzyl radicals by photoelectron-spectroscopy. *J. Am. Chem. Soc.* **1978**, *100* (11), 3290-3294.

(30) Houle, F. A.; Beauchamp, J. L., Photoelectron-spectroscopy of methyl, ethyl, isopropyl, and tert-butyl radicals - implications for the thermochemistry and structures of the radicals and their corresponding carbonium-ions. *J. Am. Chem. Soc.* **1979**, *101* (15), 4067-4074.

(31) Schultz, J. C.; Houle, F. A.; Beauchamp, J. L., Photoelectron-spectroscopy of 1-propyl, 1-butyl, isobutyl, neopentyl, and 2-butyl radicals - free-radical precursors to high-energy carbonium-ion isomers. *J. Am. Chem. Soc.* **1984**, *106* (14), 3917-3927.

(32) Jarvis, G. K.; Weitzel, K. M.; Malow, M.; Baer, T.; Song, Y.; Ng, C. Y., High-resolution pulsed field ionization photoelectron-photoion coincidence study of C_2H_2: Accurate 0 K dissociation threshold for C_2H^+. *Phys. Chem. Chem. Phys.* **1999**, *1* (22), 5259-5262.

(33) Weitzel, K. M.; Malow, M.; Jarvis, G. K.; Baer, T.; Song, Y.; Ng, C. Y., High-resolution pulsed field ionization photoelectron-photoion coincidence study of CH_4: Accurate 0 K dissociation threshold for CH_3^+. *J. Chem. Phys.* **1999**, *111* (18), 8267-8270.

(34) Xing, X.; Wang, P.; Woo, H. K.; Bahng, M. K.; Baek, S. J.; Ng, C. Y., Rotationally resolved infrared-vacuum ultraviolet-pulsed field ionization-photoelectron depletion method for infrared spectroscopic studies of neutral molecules. *Chem. Phys. Lett.* **2008**, *455* (4-6), 321-324.

(35) Willitsch, S.; Wuest, A.; Merkt, F., High-resolution photoelectron spectroscopy and ab initio quantum chemistry. *Chimia* **2004**, *58* (5), 281-286.

(36) Willitsch, S.; Merkt, F., Rovibronic photoionization dynamics of asymmetric-top molecules. *Int. J. Mass Spectrom.* **2005**, *245* (1-3), 14-25.

(37) Worner, H. J.; Merkt, F., Diradicals, antiaromaticity, and the pseudo-Jahn-Teller effect: Electronic and rovibronic structures of the cyclopentadienyl cation. *J. Chem. Phys.* **2007**, *127* (3), 034303/1-16.

(38) Schulenburg, A. M.; Meisinger, M.; Radi, P. P.; Merkt, F., The formaldehyde cation: Rovibrational energy level structure and coriolis interaction near the adiabatic ionization threshold. *J. Mol. Spectrosc.* **2008**, *250* (1), 44-50.

(39) Oka, T., Observation of the infrared spectrum of H_3^+. *Phys. Rev. Lett.* **1980**, *45* (7), 531-534.

(40) Crofton, M. W.; Jagod, M. F.; Rehfuss, B. D.; Oka, T., Infrared spectroscopy of carbo-ions. V. Classical vs nonclassical structure of protonated acetylene $C_2H_3^+$. *J. Chem. Phys.* **1989**, *91* (9), 5139-5153.

(41) White, E. T.; Tang, J.; Oka, T., CH_5^+: The infrared spectrum observed. *Science* **1999**, *284* (5411), 135-137.

(42) Huang, X.; McCoy, A. B.; Bowman, J. M.; Johnson, L. M.; Savage, C.; Dong, F.; Nesbitt, D. J., Quantum deconstruction of the infrared spectrum of CH_5^+. *Science* **2006**, *311* (5757), 60-63.

(43) Wyss, M.; Riaplov, E.; Maier, J. P., Electronic and infrared spectra of $H_2C_3H^+$ and cyclic $C_3H_3^+$ in neon matrices. *J. Chem. Phys.* **2001**, *114* (23), 10355-10361.

(44) Bahou, M.; Wu, Y.-J.; Lee, Y.-P., A new method for investigating infrared spectra of protonated benzene ($C_6H_7^+$) and cyclohexadienyl radical (c-C_6H_7) using *para*-hydrogen. *J. Chem. Phys.* **2012**, *136* (15), 154304/1-8.

(45) Schreiner, P. R.; Kim, S. J.; Schaefer, H. F.; Schleyer, P. V., CH_5^+ - the never-ending story or the final word. *J. Chem. Phys.* **1993**, *99* (5), 3716-3720.

(46) Marx, D.; Parrinello, M., Molecular spectroscopy - CH_5^+: The cheshire cat smiles. *Science* **1999**, *284* (5411), 59-61.

(47) Bunker, P. R.; Ostojic, B.; Yurchenko, S., A theoretical study of the millimeterwave spectrum of CH_5^+. *J. Mol. Struct.* **2004**, *695*, 253-261.

(48) Fleming, F. P.; Barbosa, A. G. H.; Esteves, P. M., Nature of the chemical bond in protonated methane. *J. Phys. Chem. A* **2006**, *110* (43), 11903-11905.

(49) Kumar, P.; Marx, D., Understanding hydrogen scrambling and infrared spectrum of bare CH_5^+ based on ab initio simulations. *Phys. Chem. Chem. Phys.* **2006**, *8* (5), 573-586.

(50) Lin, Z.; McCoy, A. B., Signatures of large-amplitude vibrations in the spectra of H_5^+ and D_5^+. *J. Phys. Chem. Lett.* **2012**, *3* (24), 3690-3696.

(51) Gudeman, C. S.; Saykally, R. J., Velocity modulation infrared-laser spectroscopy of molecular-ions. *Annu. Rev. Phys. Chem.* **1984**, *35*, 387-418.

(52) Gudeman, C. S.; Begemann, M. H.; Pfaff, J.; Saykally, R. J., Velocity-modulated infrared laser spectroscopy of molecular ions: The ν_1 band of HCO^+. *Phys. Rev. Lett.* **1983**, *50* (10), 727-731.

(53) Stephenson, S. K.; Saykally, R. J., Velocity modulation spectroscopy of ions. *Chem. Rev.* **2005**, *105* (9), 3220-3234.

(54) Foster, S. C.; McKellar, A. R. W.; Sears, T. J., Observation of the ν_3 fundamental band of HCO^+. *J. Chem. Phys.* **1984**, *81* (1), 578-579.

(55) Amano, T.; Warner, H. E., Laboratory detection of protonated formaldehyde (H_2COH^+). *Astrophys. J.* **1989**, *342* (2), L99-L101.

(56) Olkhov, R. V.; Nizkorodov, S. A.; Dopfer, O., Infrared photodissociation spectra of CH_3^+–Ar_n complexes (n=1–8). *J. Chem. Phys.* **1998**, *108* (24), 10046-10060.

(57) Dopfer, O.; Roth, D.; Maier, J. P., Infrared spectra of $C_3H_3^+$-N_2 dimers: Identification of proton-bound c-$C_3H_3^+$-N_2 and H_2CCCH^+-N_2 isomers. *J. Am. Chem. Soc.* **2002**, *124* (3), 494-502.

(58) Solcà, N.; Dopfer, O., Protonated benzene: IR spectrum and structure of $C_6H_7^+$ *Angew. Chem. Int. Ed.* **2002**, *41* (19), 3628-3631.

(59) Nizkorodov, S. A.; Dopfer, O.; Ruchti, T.; Meuwly, M.; Maier, J. P.; Bieske, E. J., Size effects in cluster infrared spectra: The ν_1 band of Ar_n-HCO^+ (n = 1-13). *J. Phys. Chem.* **1995**, *99* (47), 17118-17129.

(60) Dopfer, O.; Olkhov, R. V.; Roth, D.; Maier, J. P., Intermolecular interaction in proton-bound dimers.: Infrared photodissociation spectra of RG–$HOCO^+$ (RG=He, Ne, Ar) complexes. *Chem. Phys. Lett.* **1998**, *296* (5–6), 585-591.

(61) Jones, W.; Boissel, P.; Chiavarino, B.; Crestoni, M. E.; Fornarini, S.; Lemaire, J.; Maitre, P., Infrared fingerprint of protonated benzene in the gas phase. *Angew. Chem. Int. Ed.* **2003**, *42* (18), 2057-2059.

(62) Polfer, N.; Sartakov, B. G.; Oomens, J., The infrared spectrum of the adamantyl cation. *Chem. Phys. Lett.* **2004**, *400* (1–3), 201-205.

(63) Lorenz, U. J.; Solcà, N.; Lemaire, J.; Maître, P.; Dopfer, O., Infrared spectra of isolated protonated polycyclic aromatic hydrocarbons: Protonated naphthalene. *Angew. Chem. Int. Ed.* **2007**, *46* (35), 6714-6716.

(64) Chiavarino, B.; Crestoni, M. E.; Fornarini, S.; Lemaire, J.; Mac Aleese, L.; Maître, P., Infrared absorption features of gaseous isopropyl carbocations. *ChemPhysChem* **2004**, *5* (11), 1679-1685.

(65) Duncan, M. A., Infrared laser spectroscopy of mass-selected carbocations. *J. Phys. Chem. A* **2012**, *116* (47), 11477-11491.

(66) Douberly, G. E.; Ricks, A. M.; Ticknor, B. W.; Duncan, M. A., Structure of protonated carbon dioxide clusters: Infrared photodissociation spectroscopy and ab initio calculations. *J. Phys. Chem. A* **2008**, *112* (5), 950-959.

(67) Douberly, G. E.; Ricks, A. M.; Ticknor, B. W.; Duncan, M. A., The structure of protonated acetone and its dimer: Infrared photodissociation spectroscopy from 800 to 4000 cm^{-1}. *Phys. Chem. Chem. Phys.* **2008**, *10* (1), 77-79.

(68) Roscioli, J. R.; McCunn, L. R.; Johnson, M. A., Quantum structure of the intermolecular proton bond. *Science* **2007**, *316* (5822), 249-254.

CHAPTER 2

EXPERIMENTAL SETUP

Organic cations are produced in a supersonic expansion via pulsed electrical discharge using needle or ring electrodes. Ions are produced using expansion gas(es) consisting of He, H_2, Ne, and/or Ar seeded with the vapor pressure of a solid or liquid organic precursor molecule. A General Valve Series 9 nozzle, operated at a frequency of 10 Hz and pulse duration ranging from 200-400 microseconds, is employed in these experiments. The backing pressure used varies with the gas mixture, diameter of the expansion hole, nozzle pulse duration, and electrical discharge setup and conditions. Typical backing pressures range from 50-200 psig. The original design of the molecular beam machine used to conduct these experiments can be traced to the Smalley group.[1, 2] The reflectron time-of-flight (TOF) apparatus is original to the Duncan group and has been described previously for the photodissociation of mass-selected ions.[3-5] This work utilizes TOF mass spectrometry with powerful infrared lasers to obtain the infrared photodissociation spectra of organic cations.

Figure 2.1 illustrates the molecular beam apparatus used to conduct these experiments. Ion production occurs in the first vacuum chamber, known as the "source". This chamber has an operating pressure of approximately 10^{-6} Torr, and is maintained by a Varian VHS-10 diffusion pump (6600 l/s of He). A diagram of the needle electrode discharge setup is shown in Figure 2.2. Two needles are mounted using a specially designed Teflon plate with Cu mounting blocks so that a 0.25 mm gap occurs between the tips of the needles, and the gap is centered to the expansion hole. The needles are positioned 8.7 mm downstream from the last expansion

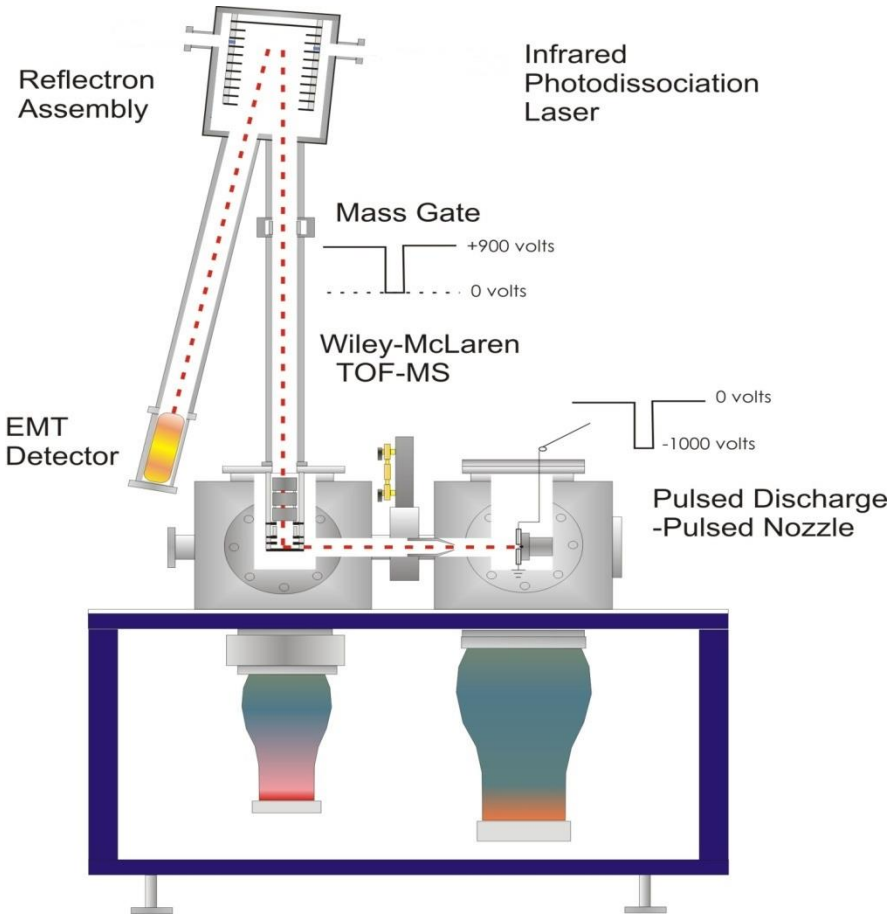

Figure 2.1. Schematic of the molecular beam apparatus.

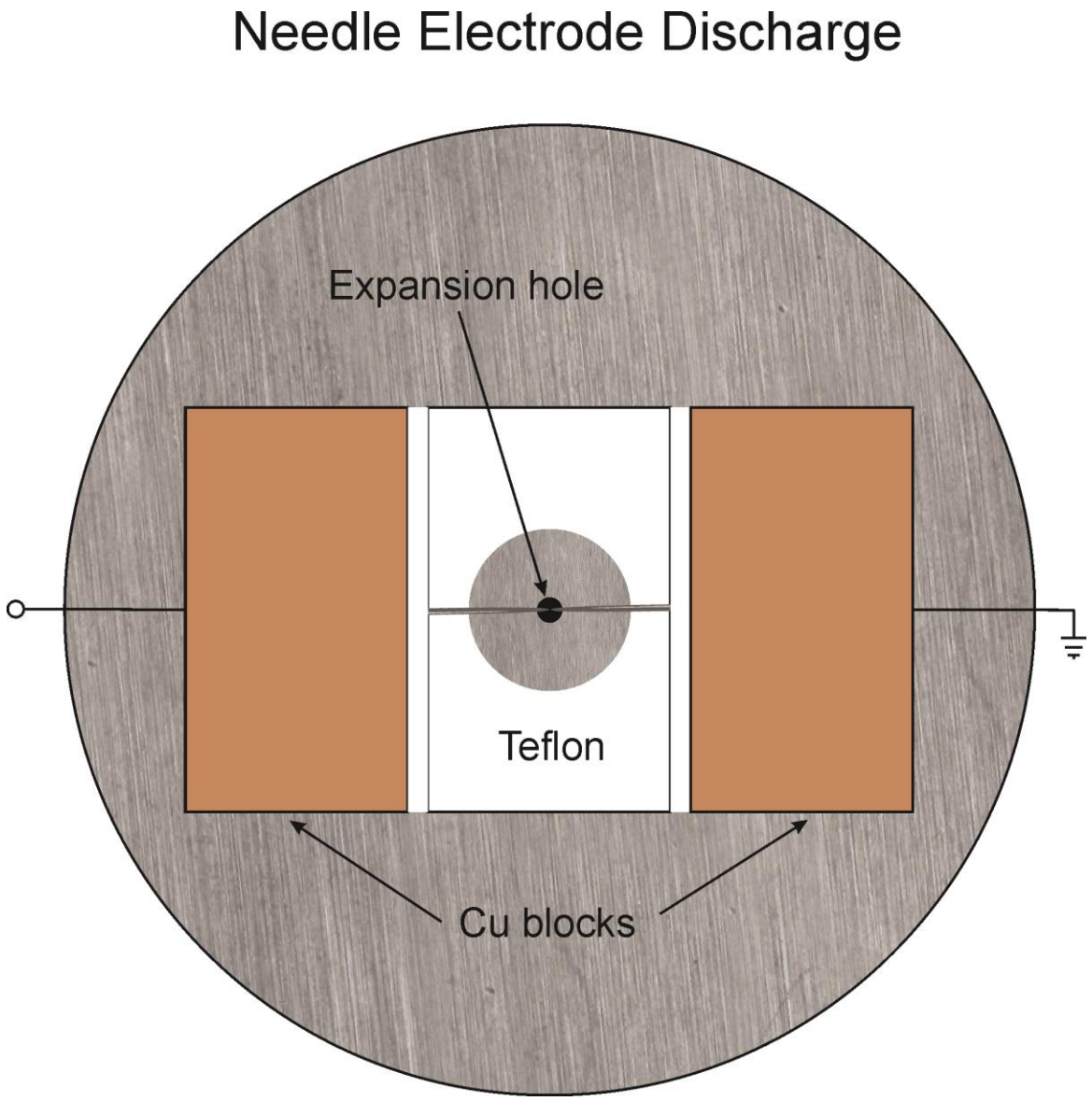

Figure 2.2. A diagram of the needle electrode discharge source.

aperture. One needle is maintained at a ground potential, while the other is connected to the output of a Directed Energies (DEI) PVX-4140 high voltage pulsing circuit. The voltage is controlled by an external power supply (Bertan) that operates from 0-3000 V. The pulse width is controlled by an externally generated 5V pulse (Stanford Research Systems) and is variable over the nanosecond to millisecond range. Typical pulse widths for optimal ion production are from 4-15 microseconds. Highly efficient cooling in the supersonic expansion is achieved by pulsing the discharge in the middle of the nozzle gas pulse. The resulting plasma contains a variety of neutrals, cations and anions.

Ions are entrained in the molecular beam and skimmed (Beam Dynamics 3mm nozzle) into a second, differentially pumped, mass spectrometer chamber. Cations are pulse extracted into the first flight tube of a homemade Wiley-McClaren TOF mass spectrometer in the reflectron configuration.[3, 4, 6] The mass spectrometer chamber is maintained at an operating pressure of approximately 10^{-6} – 10^{-7} Torr using a Varian VHS-6 diffusion pump (3000 l/s of He) to reduce collisions of the ion beam with background gases. Because pulse extraction occurs perpendicularly to the molecular beam axis, a pair of deflection plates (~40V) is used to correct for lateral motion of the ion beam. The ions are extracted in between the "draw-out grid" and repeller plate of the Wiley-McClaren stack which, combined with a third ground plate downstream, creates a two-field acceleration region. This setup minimizes the energy spread due to the finite width of the molecular beam along the electric field lines and greatly improves the resolution of the TOF mass spectrometer. Voltages are supplied to the acceleration plates by fast high voltage switches (Behlke HTS-50) and the timings are controlled by digital delay generators (Stanford Research Systems). After extraction, the ion beam passes through an einzel lens (~400V) which counteracts space-charge effects and creates a tightly focused ion packet. The

ions then enter a field free region, an ion mirror, and another field free region and ultimately terminate their flight at an ion detector (EMT Hamamatsu R-590). The output of the detector is pre-amplified and sent to a digital oscilloscope, which measures the time taken for the ions to traverse the mass spectrometer.

Ions accelerated in a TOF instrument have essentially the same kinetic energy. Their flight time is determined by both their kinetic energy and their mass, as shown by equation (1):

$$Kinetic\ Energy = {}^{1}/_{2}\, mv^2 \tag{1}$$

Where m is the mass of the ion and v is its velocity, which is equal to distance, d over time, t. Time zero is defined here to coincide with the pulsing of the acceleration plates. Thus, by substitution and rearrangement, mass is shown to be proportional to the square of the flight time:

$$m = {}^{2KE}/_{({}^{d}/_{t})^2} \tag{2}$$

So, ions with lighter mass will travel more quickly than heavier ions, and if the kinetic energy and distance traveled is precisely known, the mass of the ion can be obtained by measuring the flight time with an oscilloscope. However, exactly measuring these parameters is difficult in practice, so a reference mass is used to calibrate the mass spectrum. Since all ions have the same kinetic energy, equation (1) can be expressed as:

$$m_1 v_1^2 = m_2 v_2^2 \tag{3}$$

Which when rearranged, can give a simple way in which to express the mass of an unknown ion in terms of its flight time and that of an ion with known mass:

$$m_1 = m_2\left(t_1/t_2\right)^2 \tag{4}$$

The reference ion usually varies with the precursor used. Initial calibration is often done using the known flight time of the hydronium ion in our mass spectrometer (m/z = 19, 33.4 microseconds). Homemade software utilizes a two-point calibration system to allow for calibration over a large range of masses:

$$\text{offset} = \frac{(m_2^2 * t_1) - (m_1^2 * t_2)}{m_2^2 - m_1^2} \tag{5}$$

Which corrects for the error introduced by the difference in time zero between very small and very large masses.

The tunable infrared light used in these experiments is generated by a LaserVision infrared optical parametric oscillator (OPO)/ optical parametric amplifier (OPA) laser system. An illustration of this system is shown in Figure 2.3. The OPO is pumped by the fundamental (1064 nm) of a Spectra Physics Pro 230 Nd:YAG laser operated at 10 Hz and approximately 430 mJ/pulse. The pump beam enters the OPO/OPA box and is first split by a 30/70 beam splitter. The 30% beam is frequency doubled in a potassium dihydrogen phosphate (KDP) crystal to

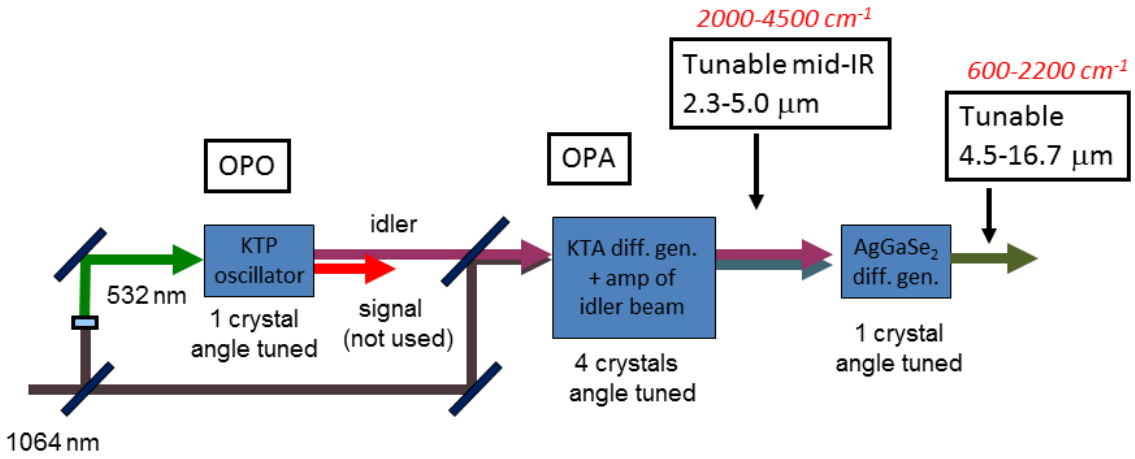

Figure 2.3. A schematic of the Laservision OPO/OPA setup.

generate light at 532 nm (~ 18800 cm^{-1}), while the higher energy fraction is sent to the OPA via the delay line. A dichroic mirror dumps the residual 1064 beam and directs the 532 nm light through a potassium titanyl phosphate (KTP) crystal in the OPO. This crystal splits the incident beam into two beams (signal and idler) that are governed by the following equations:

$$\omega_{\text{signal}} \neq \omega_{\text{idler}} \tag{6}$$

$$\omega_{\text{signal}} > \omega_{\text{idler}} \tag{7}$$

$$\omega_{\text{pump}} = \omega_{\text{signal}} + \omega_{\text{idler}} \tag{8}$$

where ω is frequency in cm^{-1}. Equation 8 holds true due to the law of conservation of energy. The signal beam, which is tunable from 710 – 880 nm (14084 – 11364 cm^{-1}) is blocked and the idler beam, which is tunable from 1340 – 2120 nm (4715 – 7436 cm^{-1}), is sent to the amplification stage, where it recombines with the delayed 1064 nm beam (9398 cm^{-1}). The OPA consists of four potassium titanyl arsenate (KTA) crystals. Without the transmitted idler beam from the OPO stage, the delay beam would be frequency doubled, generating green light. With the idler beam overlapping the delay beam in time and space, difference frequency mixing occurs within the KTA media, generating tunable mid-IR light approximately between 2000 and 4700 cm^{-1} with a linewidth of 1.2 cm^{-1}. The phase matching conditions cause the new idler (mid-IR) and signal (near-IR) beams to be orthogonally polarized. This allows them to be efficiently separated with a polarizer, allowing for continuously tunable mid-IR or near-IR lasing. Optionally, the use of a silver gallium selenide ($AgGaSe_2$) crystal allows for a second stage of difference frequency generation, mixing the mid-IR and near-IR beams to generate tunable light from 600-2000 cm^{-1}. The OPO/OPA laser system covers most of the infrared

region from 600-7400 cm^{-1}, with only a small gap from 4700 – 4715 cm^{-1}. Most fundamental vibrations occur in the fingerprint region (300-2000 cm^{-1}) and the higher frequency stretching region (2500-4500 cm^{-1}). Thus, this system is widely applicable for vibrational spectroscopy of carbocations and carboxonium ions.

The TOF mass spectrometer described here is used for photodissociation experiments. This type of experiment is only possible with a tandem mass spectrometer (MS/MS) experimental design, which allows for the mass-selection of the parent ion and the separation of parent and fragment ions. Using a special type of TOF instrument known as a reflectron, MS/MS is accomplished within the same mass spectrometer (see Figure 2.1). Mass selection occurs in the first flight tube using pulsed deflection plates. Connecting two flight tubes is a turning region, or "ion mirror", which consists of several grids separated by resistors and having increasingly positive voltages. Thus, ions entering the turning region from the first flight tube act as a ball rolling up a hill. The photodissociation laser intersects the mass-selected ion packet within the turning region of the reflectron (i.e. the top of the hill). This minimizes the timing difficulty associated with overlapping a nanoseconds−wide laser pulse with a fast ion packet in a TOF instrument. The ions have zero longitudinal velocity for 1-2 microseconds, whereas the laser pulse is present for only about 5 nanoseconds. Upon reacceleration (rolling down the hill), parent and fragment ions receive the same kinetic energy and can be separated again by mass within the second flight tube. A secondary result of using a reflectron is an improved resolution for ions of the same mass. Due to the finite spread of ions within the molecular beam, some ions will exit the TOF acceleration region with a slightly greater kinetic energy than other ions of the same mass, creating an uncertainty in the arrival time of any given mass-to-charge ratio. The reflectron decreases this uncertainty, by increasing the temporal resolution of the arrival time.

Basically, ions with greater energy penetrate farther into the reflectron electric field, and thus have a greater transit time through the reflectron. This allows the slower ions to "catch up" with the faster same-mass ions, and all ions of the same mass-to-charge ratio reach the detector within a narrower time interval.

A typical mass spectrum using the TOF mass spectrometer described here is presented in Figure 2.4 (top trace, black). This spectrum was recorded using the vapor pressure of ethanol at room temperature seeded in an expansion of pure Ar. Several peaks are seen with unit resolution (using the full-width half-maximum definition). As shown in Figure 2.4, the full spectrum can be recorded, or a single peak can be detected with mass selection (middle trace, navy). This allows for an increase in ion signal by increasing the (negative) voltage applied to the detector. Additional ion intensity can be obtained by applying a large positive voltage (~2500 V) to a post-accelerator tube positioned within the second flight tube. Because the ion density produced in the TOF mass spectrometer is too low for direct absorption measurements (10^6–10^7 molecules/cm^3), absorption must be detected by its effect on the ion. This action spectroscopy is accomplished with photodissociation in the TOF mass spectrometer. However, the energy of an infrared photon (~ 0.5 eV) is much less than the energy required to break a covalent bond (4-5 eV), thus the method of rare gas tagging is used to greatly enhance the photodissociation yield. Using a rare gas atom, such as Ar, a weak (~0.1 eV) intermolecular bond is formed in the Ar-tagged complex. Ar is highly polarizable, and charge-induced dipole interactions stabilize the weakly bound complex in the absence of external stimuli. Infrared absorption by the molecular ion induces fast intramolecular vibrational relaxation (IVR) processes on the order of picoseconds, and enough energy transfers into the normal mode corresponding to the Ar stretching motion to break the intermolecular bond. This process is highly efficient, with nearly

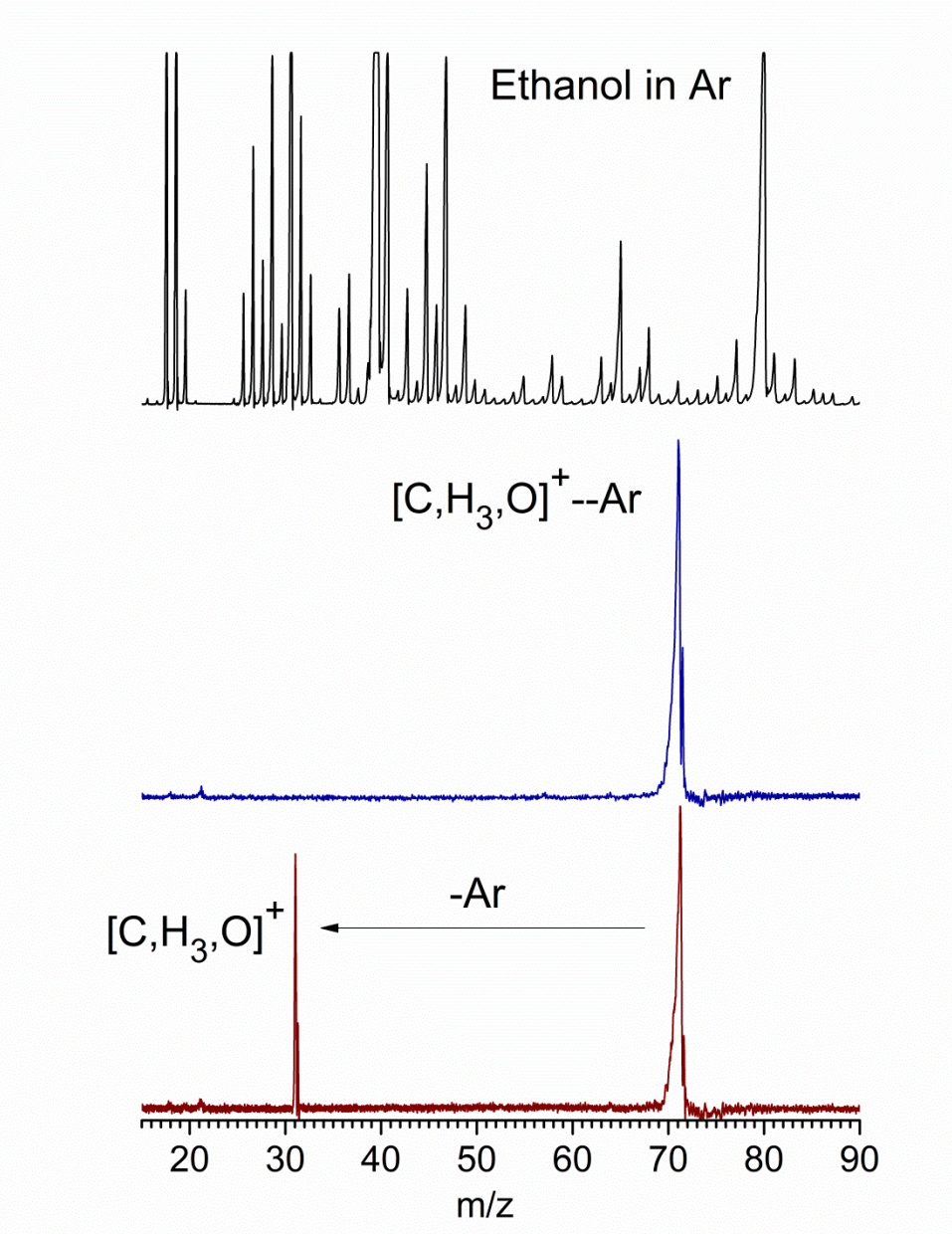

Figure 2.4. A breakdown mass spectrum of $[C,H_3,O]^+$−Ar produced using ethanol vapor seeded in an expansion of Ar.

100% photodissociation yield upon absorption. Due to the high ionization potential (IP) of Ar (15.8 eV), the charge remains on the organic cation (9-10 eV typical IP for neutral organic molecules) and a loss of neutral Ar is observed, as shown in Figure 2.4 (bottom trace, wine). Thus, by integrating the fragment ion intensity while tuning the infrared laser, an infrared photodissociation spectrum analogous to the molecular ion's absorption spectrum can be obtained. This is accomplished by recording a photodissociation mass spectrum averaged over a pre-defined number of laser shots per wavelength and transferring at high speeds to a PC which contains homemade integration software. The same software controls the laser scanning parameters to ensure precise wavelength correlation. A typical infrared photodissociation spectrum is obtained over 300-1000 laser shots.

References

(1) Powers, D. E.; Hansen, S. G.; Geusic, M. E.; Puiu, A. C.; Hopkins, J. B.; Dietz, T. G.; Duncan, M. A.; Langridge-Smith, P. R. R.; Smalley, R. E., Supersonic metal cluster beams: Laser photoionization studies of copper cluster (Cu_2). *J. Phys. Chem.* **1982**, *86* (14), 2556-2560.

(2) Dietz, T. G.; Duncan, M. A.; Powers, D. E.; Smalley, R. E., Laser production of supersonic metal cluster beams. *J. Chem. Phys.* **1981**, *74* (11), 6511-6512.

(3) Cornett, D. S.; Peschke, M.; LaiHing, K.; Cheng, P. Y.; Willey, K. F.; Duncan, M. A., Reflectron time-of-flight mass spectrometer for laser photodissociation. *Rev. Sci. Instrum.* **1992**, *63* (4), 2177-2186.

(4) LaiHing, K.; Cheng, P. Y.; Taylor, T. G.; Willey, K. F.; Peschke, M.; Duncan, M. A., Photodissociation in a reflectron time-of-flight mass spectrometer: A novel mass spectrometry/mass spectrometry configuration for high-mass systems. *Anal. Chem.* **1989**, *61* (13), 1458-1460.

(5) Duncan, M. A., Invited review article: Laser vaporization cluster sources. *Rev. Sci. Instrum.* **2012**, *83* (4), 041101/1-19.

(6) Wiley, W. C.; McLaren, I. H., Time-of-flight mass spectrometer with improved resolution. *Rev. Sci. Instrum.* **1955**, *26* (12), 1150-1157.

CHAPTER 3

STRUCTURAL ISOMERIZATION OF 2-NORBORNYL CATION IN THE GAS PHASE REVEALED BY INFRARED SPECTROSCOPY AND COMPUTATIONAL CHEMISTRY

The 2-norbornyl cation ($C_7H_{11}^+$; $2NB^+$) is the most famous and controversial nonclassical carbocation.[1, 2] On the basis of unusual solvolysis reaction rates and products of 2-exo- and 2-endo-norbornyl derivatives,[3-8] Winstein proposed a symmetrically bridged nonclassical structure for the ionic intermediate.[5] In sharp disagreement, H. C. Brown favored rapidly equilibrating classical structures and advocated steric hindrance to account for the difference in solvolysis rates.[9] This dispute continued vehemently for three decades. Experimental investigations of the nature of $2NB^+$, e.g., under "stable ion" conditions in "superacid" media supported the non-classical structure (as did theoretical computations at ever-more sophisticated levels).[10-22] Notably, Saunders demonstrated that the deuterium isotope effects on the ^{13}C-NMR spectra showed no rapidly equilibrating carbon signatures[14] and Yannoni, et al.'s cryogenic (5K) ^{13}C-NMR spectra showed a static symmetrically bridged structure.[15] However, proponents of the classical structure argued that these results were not definitive because of the relatively long NMR time scale. Recently, the long-sought X-ray crystal structure of the 2-norbornyl cation finally was obtained (by overcoming double-disorder problems), confirming the nonclassical structure of $2NB^+$ in the condensed phase.[23] Nevertheless, questions remain about the nature of this ion in the gas phase. Although aspects of its chemistry have been studied by mass spectrometry,[24-28] no gas-phase vibrational spectroscopy of $2NB^+$ has been recorded. Hence, our initial objective was to explore the structure of the mass-selected $C_7H_{11}^+$ ion with infrared laser

spectroscopy. Much to our surprise, the structure of $C_7H_{11}^+$ obtained by protonating norbornene under our conditions, was *not* that of $2NB^+$, but instead corresponded to a much more stable rearranged ion. The identification of the structure of this unexpected $C_7H_{11}^+$ isomer is the subject of the present paper.

Previous gas phase mass spectrometry investigations of $2NB^+$ explored its ion-molecule reactions and collision induced dissociation behavior.[24-28] Fragmentation patterns of $C_7H_{11}^+$ produced by different methods are similar, and energetic thresholds were consistent with the expected thermochemistry for $2NB^+$.[28] However, rearrangements are common in ion fragmentation and these experiments did not establish the actual ion structures. Since $2NB^+$ is so well-known as an ion pair in the condensed phase, it is not generally appreciated that this ion is far from being the $C_7H_{11}^+$ global energy minimum. Limited computational studies have explored some other $C_7H_{11}^+$ isomers, but there has been no comprehensive study of the potential energy surface.[20, 29, 30] Our investigation of the $C_7H_{11}^+$ isomer produced by highly energetic norbornene protonation was based on comparison of its experimental infrared spectrum with those predicted computationally for various $C_7H_{11}^+$ isomers. Theory finds that several of these are more stable than $2NB^+$, but that only the $C_7H_{11}^+$ global energy minimum gives a good match with the IR experiment.

$C_7H_{11}^+$ ions are produced using a previously-described pulsed electrical discharge source.[31] The expansion gas composed of 5% H_2/95% argon (total pressure ~20 atm) is seeded with norbornene vapor (Sigma-Aldrich, 99%) heated to ~40 °C. Ions are formed and cooled collisionally in the supersonic expansion. The molecular beam is skimmed into a second differentially-pumped vacuum chamber, where the ions are pulse-extracted by a reflectron time-of-flight (TOF) mass spectrometer. $C_7H_{11}^+$ tagged with argon (m/z 135) is mass-selected in the

first section of the TOF, and the selected ion packet is irradiated in the turning region of the reflectron by the beam from a tunable infrared photodissociation laser (LaserVision OPO/OPA).[31] Parent and fragment ions are reaccelerated into a second flight tube and detected at different times with an ion detector. IR spectra are recorded by integrating the $C_7H_{11}^+$ ion signal resulting from argon elimination while tuning the infrared laser. MP2 computations were carried out with the GAMESS-US package (version 1 May 2012 (R1)).[32] CCSD(T) computations employed the CFOUR program (Version 1.0).[33]

The infrared spectrum of our $C_7H_{11}^+$ isomer, obtained by photodissociation of argon tagged species[31] is shown in Figure 3.1 (top). The $C_7H_{11}^+$Ar ion was produced in a mixture of norbornene and H_2 in argon; H_3^+ forms abundantly and serves as the protonating agent. After mass selection, the spectrum was recorded as the wavelength dependent yield of the $C_7H_{11}^+$ photofragment. The spectrum consists of a strong broad band at 2910 cm^{-1} in the C−H stretching region, whose appearance is insensitive to laser power or to the tagging employed (one or two 2 Ar's or N_2). Much weaker absorptions appear at higher frequencies, but sharper structures characterize the fingerprint region, with bands at 995, 1230, 1333, 1389, 1421, 1482, and the most prominent peak at 1525 cm^{-1}. Notably, this spectrum DOES NOT correspond to that predicted for the 2-norbornyl cation (Figure 3.1, blue trace, bottom) by the MP2/cc-pVTZ level of theory. Likewise, our band patterns DO NOT match those measured for 2NB+ in superacid films.[13, 23] In particular, $2NB^+$ has no 1525 cm^{-1} feature nor are its stronger bands in the 1300–1400 cm^{-1} region and the strong feature near 850 cm^{-1} detected. We confirmed the surprising conclusion that our spectrum is *not* that of the $2NB^+$ cation by showing that its vibrational spectrum computed at DFT/B3LYP and CCSD(T) levels of theory was in essential agreement with that shown in Figure 3.1.

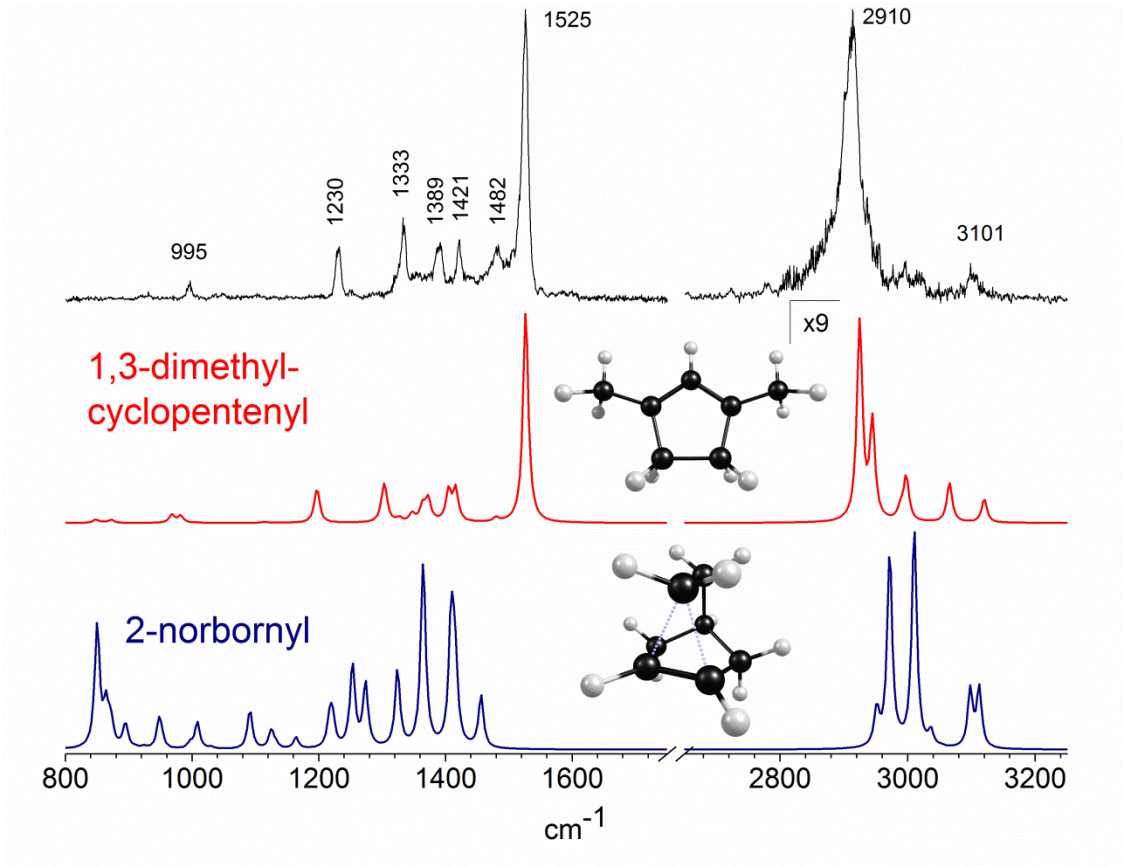

Figure 3.1. Comparison of the gas phase infrared spectrum of $C_7H_{11}^+$ with spectra predicted for two candidate structures of $C_7H_{11}^+$. The experimental trace (black) is shown on top. Theoretical results for 1,3-dimethylcyclopentenyl cation (**A,** red) are shown in the middle. Theoretical results for the 2-norbornyl cation (**F**, royal) are shown at the bottom. Harmonic frequencies were computed at the MP2/cc-pVTZ level of theory and scaled by a factor of 0.956.

The ion we produced was identified by a more extensive computational investigation into possible $C_7H_{11}^+$ isomers than performed previously.[20, 29, 30] The six lowest energy isomers of the 13 $C_7H_{11}^+$ structures examined are shown in Figure 3.2. The energies of isomers **A**, **B** and **D** were computed further at the CCSD(T)/ANO0 level, but their relative energies (Table 3.1) agree. As is apparent in Figure 3.2 and Table 3.1, $2NB^+$ is far from being the most stable $C_7H_{11}^+$ isomer. In line with *post facto* chemical intuition, the 1,3-dimethylcyclopentenyl cation ($DMCP^+$) is the $C_7H_{11}^+$ global energy minimum, being 23.4 and 16.9 kcal/mol more stable than $2NB^+$ at the CCSD(T) and the MP2 levels, respectively. Computed vibrational spectra for each of the 13 $C_7H_{11}^+$ isomers were compared with the measured spectrum. Only the $DMCP^+$ isomer has a computed spectrum (Figure 3.1, middle trace) matching experiment remarkably well. All of the main experimental features are accounted for, and there are no obvious bands predicted that are not observed. Evidently, our experiment produced the $DMCP^+$ global minimum $C_7H_{11}^+$ isomer *exclusively*.

Previous gas phase studies employed gentler norbornene protonation conditions to give the $2NB^+$ ion.[24-28] In contrast, the protonation method employed here was highly exothermic (by nearly 100 kcal/mol) and the ion produced in our experiment had ample excess energy to isomerize into the monocyclic DMCP structure. The rearrangement observed is quite understandable when the experimental energetics are considered: the protonating agent H_3^+ has a much lower proton affinity (PA=100.9 kcal/mol)[34] than that of norbornene (198.8 kcal/mol).[27] Hence, the exothermic protonation step results in rearrangement since the energy suffices to dissociate the $2NB^+$ framework. Merino and coworkers have carried out a complimentary molecular dynamics investigation of the global $2NB^+$ potential energy surface in a study of its rearrangement pathways.[35] According to their findings, ring-opening steps for $2NB^+$ require

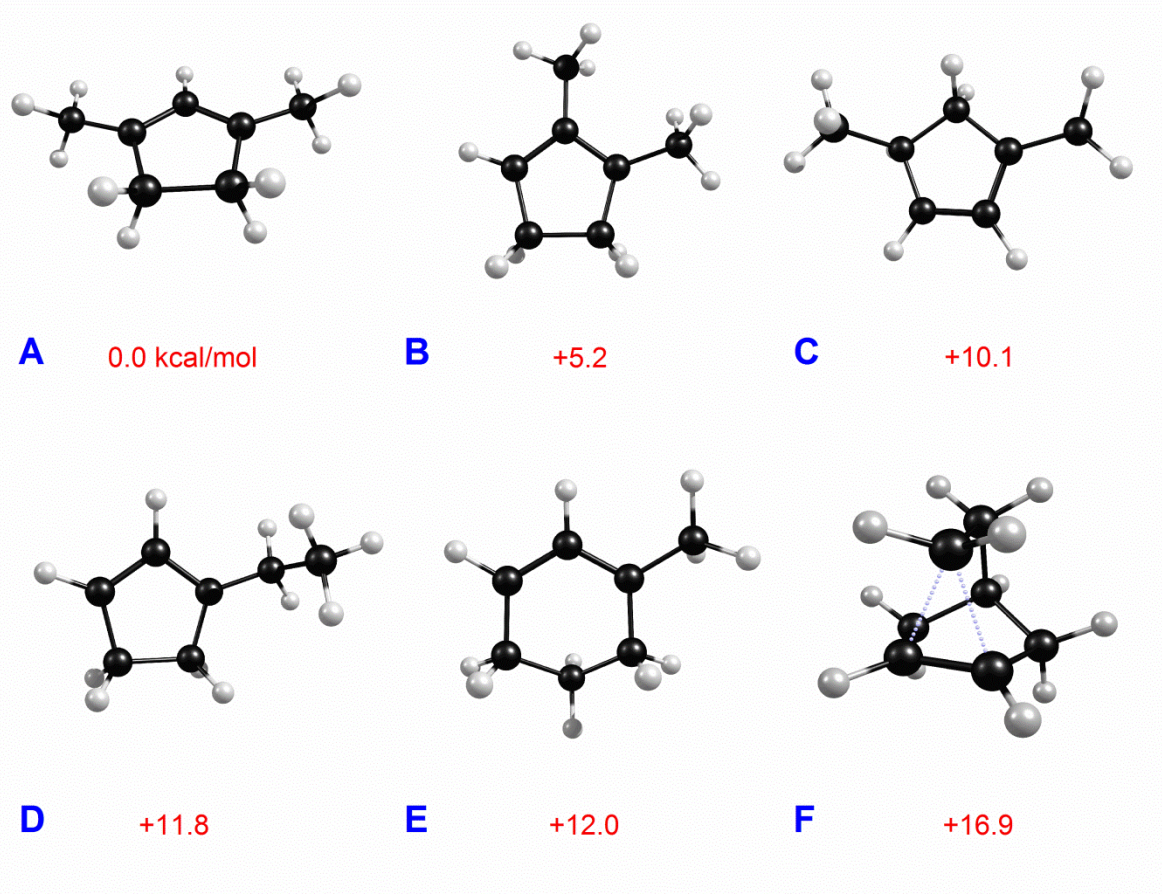

Figure 3.2. Six low energy $C_7H_{11}^+$ isomers. **F** is believed to be a stable minimum in the gas phase. Our computations show **A** to be the most stable isomer in the gas phase.

Table 3.1. Structural isomers of the $C_7H_{11}^+$ cation predicted on the 0 K potential energy surface (PES). All structures were fully optimized at the MP2/cc-pVTZ level of theory and confirmed to be minima by harmonic vibrational frequency analysis. Selected low energy isomers were evaluated further at the CCSD(T)/ANO0 level of theory. Theoretical results confirm that isomer **A** is the global minimum.

Isomer	MP2/cc-pVTZ [hartree]	ΔE [kcal mol^{-1}]	CCSD(T)/ANO0 [hartree]	ΔE [kcal mol^{-1}]
1,3-dimethylcyclopentenyl **(A)**	-272.469199	0.0	-272.401776	0.0
1,2-dimethylcyclopentenyl **(B)**	-272.460872	+5.2	−−−	−−−
1,4-dimethylcyclopentenyl **(C)**	-272.453815	+10.1	−−−	−−−
1-ethylcyclopentenyl **(D)**	-272.452139	+11.8	−−−	−−−
1-methylcyclohexenyl **(E)**	-272. 452273	+12.0	-272.386235	+11.0
2-norbornyl **(F)**	-272.446965	+16.9	-272.368925	+23.4

activation energies well below the exoergicity of norbornene protonation by H_3^+. Previous gas phase studies of $2NB^+$ employed much less exothermic norbornene protonation reactions, or generated ions from norbornyl halide precursors.[24-28] Unfortunately, our initial attempts to observe authentic gas phase $2NB^+$ spectra were unsuccessful due, e.g., to limitations of our present apparatus. But we plan to persevere and report our results subsequently.

The $DMCP^+$ cation we observed (evidently for the first time in the gas phase) is a fascinating species in its own right. It has been characterized before in the condensed phase in zeolite matrices.[36-38] Methanol-to-gasoline conversion studies showed that small hydrocarbon precursors such as ethylene can lead to this ion, whose presence was confirmed by ^{13}C-NMR studies as an ion pair component in the acid catalyst.[36, 37] Haw, et al. obtained a low resolution condensed phase Raman spectrum of $DMCP^+$.[38] Its structure combines carbocation-stabilizing features: five-membered ring allyl resonance and optimally-placed methyl substituents. The C-C-C asymmetric allyl stretch corresponds to the strong 1525 cm^{-1} vibration. This frequency is lower than the corresponding vibrations of the allyl cation (1581 cm^{-1})[39] or of protonated benzene (1607 cm^{-1}).[40] The prominent 2910 cm^{-1} absorption corresponds to the overlapping C–H stretches of the CH_3 and CH_2 groups. Lower frequency bands arise from C–H bending and carbon stretching modes. (See the vibrational assignments in Table 3.2; also as shown, three bands observed in the condensed-phase Raman experiment are shifted only slightly from our gas phase values.) Therefore, the assignment of the $C_7H_{11}^+$ ion in our experiment to $DMCP^+$, the $C_7H_{11}^+$ global minimum, is unambiguous.

Merino's related study[35] reveals an even richer variety of structures on the $C_7H_{11}^+$ cation potential surface connecting to the $2NB^+$ cation. Besides $DMCP^+$, other cations lower in energy than $2NB^+$ are highly relevant in the mechanistic dynamics of this PES. Thus far, we only have

Table 3.2. Vibrational bands for the 1,3-dimethylcyclopentenyl (C_{2v} symmetry) cation compared to the predictions of theory and previous Raman experiments. Frequencies are in cm^{-1}; intensities in parentheses are in km/mol.

Exp.[a]	MP2[b]	CCSD(T)[c]	Raman[d]	symmetry	Assignment[e]
995	977 (22.6)	987 (81.9)	1000	b_1	ip CH_3 δ_{asym}/CH_2 twist/CH out-of-plane wag
1230	1197 (67.6)	1219 (707.9)		b_2	ip CH_2/CH wag
1333	1300 (18.1)	1322 (48.7)		a_1	ip C_2 (ring) stretch, ip CH_3 umbrella
	1304 (68.2)	1324 (156.2)		b_2	oop C_2 (ring) stretch, ip CH_2 wag
1389	1363 (35.7)	1381 (5.6)	1375	b_2	oop CH_2 scissors, asym ring distortion
	1372 (51.8)	1392 (68.8)		a_1	ip CH_2 scissors
1421	1404 (60.7)	1435 (25.2)	1440	b_1	ip CH_3 asym bend
	1418 (45.5)	1425 (20.8)		b_2	oop CH_3 asym bend/CH in-plane wag
1482	1479 (9.5)	1456 (1.2)		a_1	C_3 (allyl) sym stretch
1525	1528 (446.8)	1514 (223.8)		b_2	C_3 (allyl) asym stretch
2910	2923 (41.9)	2890 (25.0)		b_2	oop CH_3 sym stretch
	2945 (19.5)	2929 (12.5)		a_1	ip CH_2 sym stretch
2995					
3017	3065 (8.8)	3034 (10.3)		b_2	oop CH_3 in-plane C–H stretch
3101	3119 (4.7)	3121 (783.9)		a_1	allyl C–H stretch

[a]This work. [b]Frequencies of $C_7H_{11}^+Ar$ scaled by a factor of 0.956; basis sets were cc-pVTZ for C and H atoms, aug-cc-pVDZ for Ar atoms. [c]Anharmonic frequencies for $C_7H_{11}^+$ from harmonic frequencies computed at the CCSD(T) level using a truncated atomic natural orbital basis set (ANO0) and anharmonic corrections obtained at the MP2/ANO0 level coupled with second-order vibrational perturbation theory (VPT2). [d]From ref. 36. [e]ip=in phase; oop=out of phase.

detected $DMCP^+$ spectroscopically. Future studies with carefully chosen reactants and conditions may allow other $C_7H_{11}^+$ isomers to be characterized, hopefully including the authentic $2NB^+$ cation.

References

(1) Aue, D. H., Carbocations. *Wiley Int. Rev.: Comp. Mol. Sci.* **2011**, *1* (4), 487-508.

(2) Olah, G. A.; Prakash, G. K., *Carbocation Chemistry*. John Wiley and Sons: New York, 2004.

(3) Schmerling, L., The exchange of hydrogen and chlorine between bicyclo (2,2,1) heptane and t-butyl chloride. *J. Am. Chem. Soc.* **1946**, *68* (2), 195-196.

(4) Roberts, J. D.; Urbanek, L.; Armstrong, R., The chlorination of bicyclo [2,2,1] heptane (norbornylane). *J. Am. Chem. Soc.* **1949**, *71* (9), 3049-3051.

(5) Winstein, S.; Trifan, D. S., The structure of the bicyclo[2,2,1]2-heptyl (norbornyl) carbonium ion. *J. Am. Chem. Soc.* **1949**, *71* (8), 2953-2953.

(6) Winstein, S.; Morse, B. K.; Grunwald, E.; Jones, H. W.; Corse, J.; Trifan, D.; Marshall, H., Neighboring carbon and hydrogen. VII. Reactivity of some alicyclic and bicyclic derivatives1,2,3. *J. Am. Chem. Soc.* **1952**, *74* (5), 1127-1132.

(7) Winstein, S.; Trifan, D., Neighboring carbon and hydrogen. XI. Solvolysis of exo-norbornyl p-bromobenzenesulfonate1,2,3. *J. Am. Chem. Soc.* **1952**, *74* (5), 1154-1160.

(8) Winstein, S.; Trifan, D., Neighboring carbon and hydrogen. X. Solvolysis of endo-norbornyl arylsulfonates1,2,3. *J. Am. Chem. Soc.* **1952**, *74* (5), 1147-1154.

(9) Brown, H. C.; Schleyer), w. c. b. P. v. R., *The Nonclassical Ion Problem*. Plenum Press: New York, 1977.

(10) Schleyer, P. V.; Comisaro.Mb; Olah, G. A.; Fort, R. C.; Watts, W. E., Stable carbonium ions .10. Direct nuclear magnetic resonance observation of 2-norbornyl cation. *J. Am. Chem. Soc.* **1964**, *86* (24), 5679-5680.

(11) Saunders, M.; Schleyer, P. V.; Olah, G. A., Stable carbonium ions .11. Rate of hydride shifts in 2-norbornyl cation. *J. Am. Chem. Soc.* **1964**, *86* (24), 5680-5681.

(12) Olah, G. A.; Commeyras, A.; Lui, C. Y., Stable carbonium ions. LXXII. Raman and N.M.R. spectroscopic study of the nortricyclonium ion [protonated tricyclo[2.2.1.02,6]heptane] and its relation to the 2-norbornyl [bicyclo[2.2.1]heptyl]cation. The nature of the stable long-lived norbornyl cation in strong acid solutions. *J. Am. Chem. Soc.* **1968**, *90* (14), 3882-3884.

(13) Olah, G. A.; White, A. M.; Demember, J. R.; Commeyra.A; Lui, C. Y., Stable carbonium ions .100. Structure of norbornyl cation. *J. Am. Chem. Soc.* **1970**, *92* (15), 4627-4640.

(14) Saunders, M.; Kates, M. R., Deuterium isotope effect on the carbon-13 NMR spectrum of the bicyclo[2.2.1]heptyl cation. Nonclassical norbornyl cation. *J. Am. Chem. Soc.* **1980**, *102* (22), 6867-6868.

(15) Yannoni, C. S.; Macho, V.; Myhre, P. C., Resolved ^{13}C NMR spectra of carbonium ions at cryogenic temperatures. The norbornyl cation at 5 K. *J. Am. Chem. Soc.* **1982**, *104* (25), 7380-7381.

(16) Raghavachari, K.; Haddon, R. C.; Schleyer, P. V.; Schaefer, H. F., Effects of electron correlation on the energies of 2-norbornyl cation structures - evaluation of the non-classical stabilization energy. *J. Am. Chem. Soc.* **1983**, *105* (18), 5915-5917.

(17) Brown, H. C., The energy of the transition states and the intermediate cation in the ionization of 2-norbornyl derivatives. Where is the nonclassical stabilization energy? *Acc. Chem. Res.* **1983**, *16* (12), 432-440.

(18) Olah, G. A.; Prakash, G. K. S.; Saunders, M., Stable carbocation .249. Conclusion of the classical non-classical ion controversy based on the structural study of the 2-norbornyl cation. *Acc. Chem. Res.* **1983**, *16* (12), 440-448.

(19) Olah, G. A.; Prakash, G. K. S.; Saunders, M., Structure of the 2-norbornyl cation - reply. *Acc. Chem. Res.* **1985**, *18* (10), 292-293.

(20) Schleyer, P. v. R.; Sieber, S., The classical 2-norbornyl cation rigorously defined ab initio. *Angew. Chem. Int. Ed.* **1993**, *32* (11), 1606-1608.

(21) Schreiner, P. R.; Schleyer, P. V.; Schaefer, H. F., Why the classical and nonclassical norbornyl cations do not resemble the 2-endo- and 2-exo-norbornyl solvolysis transition states. *J. Org. Chem.* **1997**, *62* (13), 4216-4228.

(22) Kong, J.; Roy, D.; Lenoir, D.; Zhang, X. W.; Zou, J. J.; Schleyer, P. V., 2-norbornyl ion-pair leakage in electrophilic addition of HCl to nortricyclene and norbornene. *Org. Lett.* **2009**, *11* (20), 4684-4687.

(23) Scholz, F.; Himmel, D.; Heinemann, F. W.; Schleyer, P. v. R.; Meyer, K.; Krossing, I., At last, the crystal structure determination of the non-classical 2-norbornyl cation. *Science* **2013**, *341* (6141), 62-64.

(24) Kaplan, F.; Cross, P.; Prinstein, R., Gas-phase stabilities of bicyclic cations. *J. Am. Chem. Soc.* **1970**, *92* (5), 1445-1446.

(25) Saluja, P. P. S.; Kebarle, P., Heat of formation of the 2-norbornyl cation in the gas phase. *J. Am. Chem. Soc.* **1979**, *101* (5), 1084-1087.

(26) Solomon, J. J.; Field, F. H., Reversible reactions of gaseous ions. X. The intrinsic stability of the norbornyl cation. *J. Am. Chem. Soc.* **1976**, *98* (6), 1567-1569.

(27) Staley, R. H.; Wieting, R. D.; Beauchamp, J. L., Carbenium ion stabilities in the gas phase and solution. An ion cyclotron resonance study of bromide transfer reactions involving alkali ions, alkyl carbenium ions, acyl cations, and cyclic halonium ions. *J. Am. Chem. Soc.* **1977**, *99* (18), 5964-5972.

(28) Blanchette, M. C.; Holmes, J. L.; Lossing, F. P., Characterizing the 2-norbornyl cation in the gas phase. *J. Am. Chem. Soc.* **1987**, *109* (5), 1392-1395.

(29) Kirmse, W., Metastable norbornyl cations. *Acc. Chem. Res.* **1986**, *19* (2), 36-41.

(30) Fuchs, J.-F.; Mareda, J., Ab initio and DFT gas phase investigations of the $C_7H_{11}^+$ potential energy surfaces of bicyclobutonium species and related carbocations. *J. Mol. Struct.: THEOCHEM* **2005**, *718* (1–3), 93-104.

(31) Duncan, M. A., Infrared laser spectroscopy of mass-selected carbocations. *J. Phys. Chem. A* **2012**, *116* (47), 11477-11491.

(32) Schmidt, M. W.; Baldridge, K. K.; Boatz, J. A.; Elbert, S. T.; Gordon, M. S.; Jensen, J. H.; Koseki, S.; Matsunaga, N.; Nguyen, K. A.; Su, S.; Windus, T. L.; Dupuis, M.; Montgomery, J. A., General atomic and molecular electronic structure system. *J. Comput. Chem.* **1993**, *14* (11), 1347-1363.

(33) CFOUR, a quantum chemical program package written by J. F. Stanton, J. Gauss, M. E. Harding, P. G. Szalay with contributions from A. A. Auer, R. J. Bartlett, U. Benedikt, C. Berger, D.E. Bernholdt, Y.J. Bomble, L. Cheng, O. Christiansen, M. Heckert, O. Heun, C. Huber, T.-C. Jagau, D. Jonsson, J. Jusélius, K. Klein, W.J. Lauderdale, D.A. Matthews, T. Metzroth, L.A. Mück, D.P. O'Neill, D.R. Price, E. Prochnow, C. Puzzarini, K. Ruud, F. Schiffmann, W. Schwalbach, C. Simmons, S. Stopkowicz, A. Tajti, J. Vázquez, F. Wang, J.D. Watts and the integral packages MOLECULE (J. Almlöf and

P.R. Taylor), PROPS (P.R. Taylor), ABACUS (T. Helgaker, H.J. Aa. Jensen, P. Jørgensen, and J. Olsen), and ECP routines by A. V. Mitin and C. van Wüllen. For the current version, see http://www.cfour.de.

(34) Hunter, E. P.; Lias, S. G., Proton Affinity Evaluation. In *NIST Chemistry Webbook, NIST Standard Reference Database Number 69*, Linstrom, P. J.; Mallard, W. G., Eds. National Institute of Standards and Technology: Gaithersburg, MD, 20899, http://webbook.nist.gov.

(35) Merino, G., private communication.

(36) Xu, T.; Haw, J. F., Cyclopentenyl carbenium ion formation in acidic zeolites: An in situ NMR study of cyclic precursors. *J. Am. Chem. Soc.* **1994**, *116* (17), 7753-7759.

(37) Haw, J. F.; Nicholas, J. B.; Song, W. G.; Deng, F.; Wang, Z. K.; Xu, T.; Heneghan, C. S., Roles for cyclopentenyl cations in the synthesis of hydrocarbons from methanol on zeolite catalyst HZSM-5. *J. Am. Chem. Soc.* **2000**, *122* (19), 4763-4775.

(38) Chua, Y. T.; Stair, P. C.; Nicholas, J. B.; Song, W. G.; Haw, J. F., UV raman spectrum of 1,3-dimethylcyclopentenyl cation adsorbed in zeolite H-MFI. *J. Am. Chem. Soc.* **2003**, *125* (4), 866-867.

(39) Douberly, G. E.; Ricks, A. M.; Schleyer, P. v. R.; Duncan, M. A., Infrared spectroscopy of gas phase $C_3H_5^+$: The allyl and 2-propenyl cations. *J. Chem. Phys.* **2008**, *128*, 021102.

(40) Douberly, G. E.; Ricks, A. M.; Schleyer, P. v. R.; Duncan, M. A., Infrared spectroscopy of gas phase benzenium ions: Protonated benzene and protonated toluene, from 750 to 3400 cm^{-1}. *J. Phys. Chem. A* **2008**, *112* (22), 4869-4874.

CHAPTER 4

INFRARED SPECTROSCOPY AND COMPUTATIONAL CHEMISTRY REVEAL ANOTHER STRUCTURAL ISOMER OF PROTONATED TOLUENE

Introduction

The structures of ions have been of particular interest in mass spectrometry.[1-3] Ion reactivity studies and collisional dissociation dynamics can indicate the presence of more than one isomer, though spectroscopy can give more direct structural information.[1-3] However, ion spectroscopy is difficult due to the high internal temperatures and low densities per quantum state resulting from standard ion production methods.[1] On the other hand, computational chemistry can provide structural information of ions as well as the relative energies of isomers. Indeed, theory and spectroscopy are both needed to corroborate which isomers exist. Recent developments in ion production methods and infrared laser technology make it possible to obtain the spectra of mass-selected ions via laser photodissociation.[4-7] This work investigates the $C_7H_9^+$ carbocation with infrared photodissociation spectroscopy.

Carbocations have attracted much attention in organic chemistry.[8-10] For example, σ-complexes, also known as arenium ions, are reaction intermediates in aromatic electrophilic substitutions.[8, 9] The structure of protonated benzene ($C_6H_7^+$) was confirmed to be the C_{2v} global minimum structure via NMR and IR spectroscopy.[11-14] However, the protonation of toluene, one of the simplest derivatives of benzene, may be associated with rearrangements to isomeric structures.[15] Recently, the $C_3H_3^+$ and $C_3H_5^+$ carbocations were shown via infrared spectroscopy to exist in two forms, cyclopropenyl vs propargyl ($C_3H_3^+$),[16, 17] and allyl vs 2-propenyl ($C_3H_5^+$).[18]

The $C_7H_7^+$ system consists of two isomers, as evidenced by different reactivity for different structural forms.[19-21] These structures are believed to be those of the benzylium and tropylium ions, though limited spectroscopic studies have been performed for this system.[22, 23] Here, we investigate the infrared spectrum of a previously unanticipated isomer of the $C_7H_9^+$ system.

Several studies have been performed previously on $C_7H_9^+$ ions, using mass spectrometric studies,[14, 15, 24-30] NMR spectroscopy,[31-34] infrared spectroscopy,[35-37] and computational chemistry.[14, 36, 38-41] Much of the early interest in this ion was due to its being an alkyl-substituted form of protonated benzene ($C_6H_7^+$).[14, 15, 24-26, 31] In fact, four structural isomers of $C_7H_9^+$ correspond to methyl substitution at different ring positions around the benzenium ring (i.e. CH_3-$C_6H_7^+$, protonated toluene). It is widely recognized that the structure corresponding to para-protonated toluene is the global minimum structure.[14, 24, 26, 31, 35-37, 39] Higher energy isomers with very interesting structures have been studied with experimental[27, 28, 32-34] and theoretical[36, 38, 40, 41] methods. Recently, we attempted to measure the infrared spectra of norbornyl cations in the gas phase made from norbornene protonation.[42] Fortuitously, our attempts led to the discovery of a $C_7H_9^+$ carbocation with a previously unobserved structure. The present work reports the infrared spectrum of a different isomer than those reported previously.

Experimental Methods

$C_7H_9^+$ ions are produced using a previously-described pulsed electrical discharge source.[43] The expansion gas composed of 5% H_2/95% argon (total pressure ~20 atm) is seeded with norbornene vapor (Sigma-Aldrich, 99%) heated to ~40 °C. Ions are formed and cooled collisionally in the supersonic expansion. The molecular beam is skimmed into a second differentially-pumped vacuum chamber, where the ions are pulse-extracted by a reflectron time-of-flight (RTOF) mass spectrometer. $C_7H_9^+$ tagged with argon (m/z 133) is mass-selected in the

first section of the RTOF, and the selected ion packet is irradiated in the turning region of the reflectron by the beam from a tunable infrared photodissociation laser (LaserVision OPO/OPA).[43] Parent and fragment ions are reaccelerated into a second flight tube and detected at different times with an ion detector. IR spectra are recorded by integrating the $C_7H_9^+$ ion signal resulting from argon elimination while tuning the infrared laser. MP2 and B3LYP computations were carried out with the GAMESS-US package (version 1 May 2012 (R1)).[44]

Results and Discussion

The full mass spectrum produced from a mixture of norbornene and H_2 in argon is presented in Figure 4.1. The most abundant ion signal is detected for $C_5H_7^+$, $C_7H_9^+$, and $C_7H_{11}^+$. Several smaller peaks are observed, including those corresponding to $C_2H_5^+$, $C_3H_7^+$, $C_4H_9^+$, $C_5H_6^+$, $C_6H_3^+$, $C_6H_7^+$, $C_6H_9^+$, $C_6H_{11}^+$, and $C_7H_7^+$. A few of the less abundant carbocations have been observed before with infrared spectroscopy ($C_2H_5^+$, $C_4H_9^+$, $C_6H_7^+$), while others, such as $C_5H_6^+$ (cyclopentadiene cation) and $C_7H_7^+$ (benzylium vs tropylium) are intriguing targets for such studies. Reaction products occur at higher mass to charge ratios, along with the Ar-tagged complexes of the more abundant carbocations.

The infrared spectrum of $C_7H_9^+$Ar, obtained by photodissociation of the argon tagged species[43] is shown in Figure 4.2 (black trace, third from top). It contains two prominent features in the fingerprint region at 1475 and 1512 cm^{-1}. An intense higher frequency band is seen at 1616 cm^{-1}. At lower frequency, a partially resolved doublet is observed with at 1263 cm^{-1} (HWHM). Other bands appear at 1100, 1195, 1309, and 1392 cm^{-1}. The C−H stretching region consists of two strong peaks at 2836 and 2908 cm^{-1}, as well as two weaker bands at 3085 and 3124 cm^{-1} (partially resolved doublet). The previously reported spectrum of para-protonated

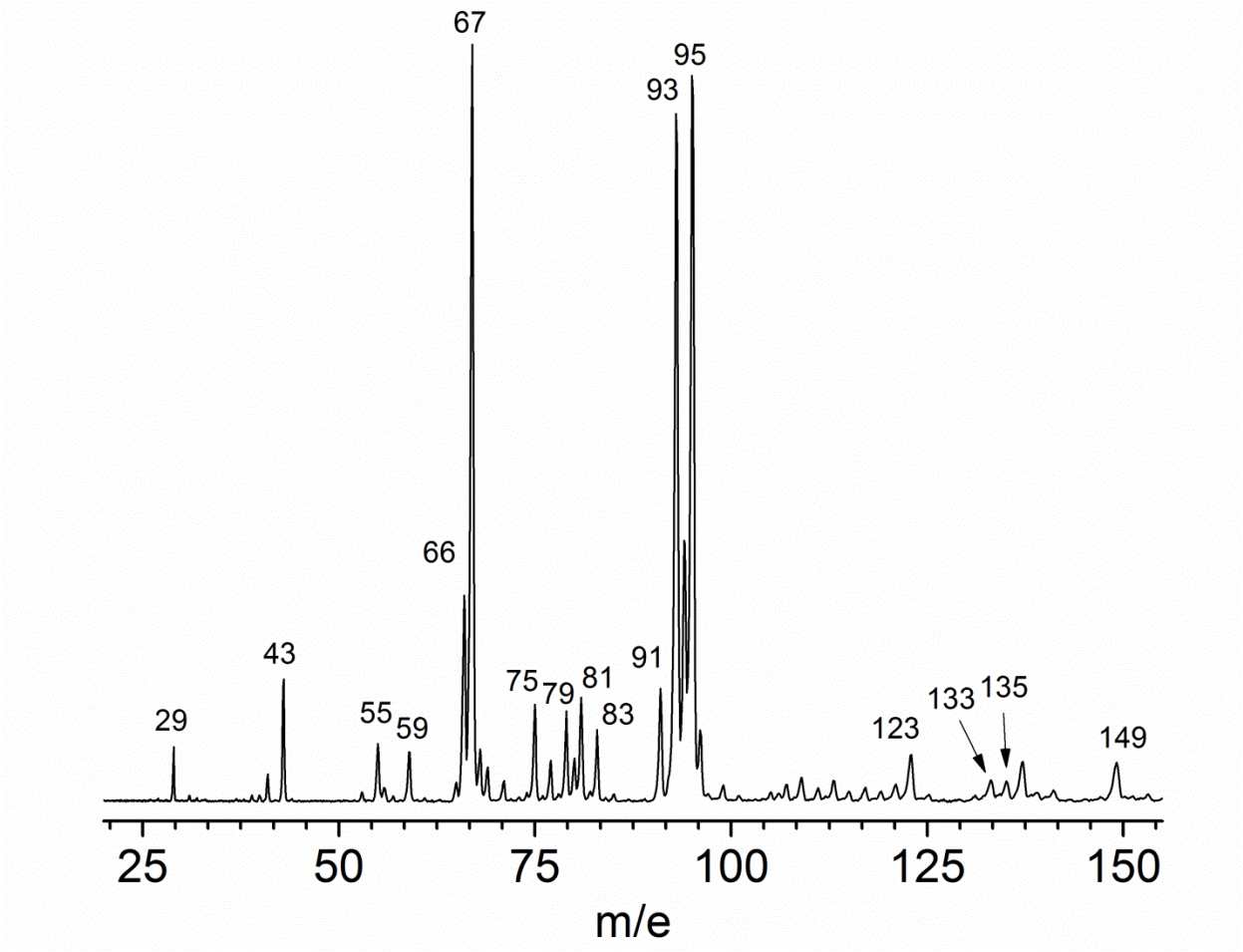

Figure 4.1. The mass spectrum produced from norbornene vapor in an expansion of H_2 and Ar.

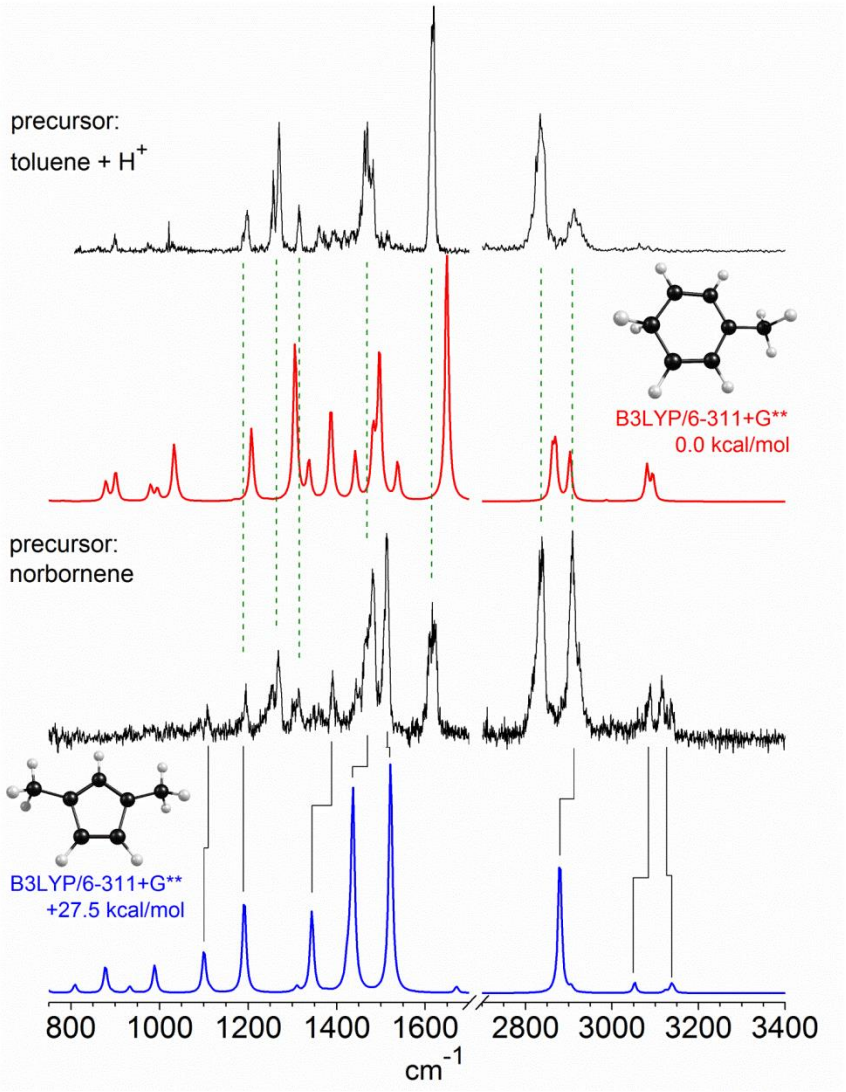

Figure 4.2. Comparison of two gas phase infrared spectra of $C_7H_9^+$ with spectra predicted for two structures of $C_7H_9^+$. Harmonic frequencies were computed at the B3LYP/6-311+G** level of theory and scaled by a factor of 0.969 in the C−H stretching region only.

toluene ($C_7H_9^+$), obtained in this laboratory from toluene protonation, is reproduced for comparison in Figure 4.2 (black trace, top).[37] The common features of the two spectra are highlighted using dashed green lines. The 1195, 1263, and 1309 cm^{-1} bands correspond to peaks reported previously at 1204, 1264/1277, and 1323 cm^{-1}. The band at 1475 cm^{-1} corresponds to overlapping bands at 1473 and 1487 cm^{-1}, but differs in appearance with respect to peak shape. Additionally, the 1263 cm^{-1} band is approximately half as intense as the 1475 cm^{-1} band, whereas the 1277 and 1473 cm^{-1} bands have roughly the same intensities in the previous spectrum. Though we do not normalize to laser power, it is approximately equal at these two frequencies. The 1616 cm^{-1} band corresponds to the most prominent band in the spectrum of para-protonated toluene at 1623 cm^{-1}. Notably, there is a systematic redshift in the values reported here, relative to the previous spectrum in the fingerprint region. This can be attributed to different calibration values between the two experiments. In both cases, calibration is achieved with photoacoustic spectroscopy. Previously, calibration of the higher frequency mid-IR beam of the OPO was used to derive the calibration value in the lower frequency far-IR beam. The current calibration was achieved in the fingerprint region with photoacoustic spectroscopy of ammonia and methane. In the C−H stretching region, two prominent bands exist at 2836 and 2908 cm^{-1}. The 2836 cm^{-1} band matches protonated toluene's most intense C−H stretch, reported previously at 2835 cm^{-1}. In the present spectrum, the band at 2908 cm^{-1} has comparable intensity to that of the 2836 cm^{-1} peak, whereas the previous spectrum contains a peak at 2914 cm^{-1} with less than half the intensity of the 2835 cm^{-1} band. Because seven bands coincide with para-protonated toluene's spectral signature, we conclude that this structure is present in the current experiment. The bands observed previously below 1000 cm^{-1} do not appear in the spectrum from norbornene protonation, presumably due to lower signal levels in the current experiment.

New features are apparent in the fingerprint region at 1100, 1392, and 1512 cm^{-1}, and at 3085 and 3124 cm^{-1} in the C−H stretching region, as shown in Figure 4.2. Additionally, the band at 1473 cm^{-1} is twice as intense as the 1263 cm^{-1} band in the present spectrum, whereas the analogous bands in para-protonated toluene's spectrum have approximately equal intensities. Likewise, the strongest C−H stretching bands observed at 2836 cm^{-1} and 2908 cm^{-1} in the current spectrum are roughly similar in intensity. Previously, the 2835 cm^{-1} band was by far the most intense peak in this region. These observations suggest that an additional structural isomer is present alongside para-protonated toluene when $C_7H_9^+$ is produced using norbornene as a precursor. Norbornene protonation has recently been shown to produce an unexpected structural isomer of the 2-norbornyl cation ($C_7H_{11}^+$) in the gas phase, that of the 1,3-dimethylcyclopentenyl cation (DMCP).[42] This unexpected rearrangement is the result of complex reaction pathways which are present in our ion source. Similarly complex chemistry is expected to occur for the $C_7H_9^+$ ion using identical source conditions. Indeed, the $C_7H_{11}^+$ and $C_7H_9^+$ ions were generated in the same plasma (Figure 4.1) and their spectra were recorded on the apparatus simultaneously.

To investigate other possible isomers, we performed an extensive investigation of the $C_7H_9^+$ potential energy surface (PES). Nine structures were found in addition to the global minimum structure, para-protonated toluene (**1**). Their relative energies computed at the MP2/aug-cc-pVDZ level of theory are presented in Table 4.1, and their structures are shown in Figure 4.3. These values are corrected for zero point vibrational energy effects. The well-known ortho- (**2**), meta- (**3**) and ipso- (**4**) isomers of protonated toluene are +1.2, +4.1 and +8.5 kcal/mol higher in energy than **1**. The 1,3- (**5**), 1,2- (**6**) and 1,4- (**8**) isomers of protonated cycloheptatriene lie higher in energy on the PES at +19.2, +22.2, and +27.6 kcal/mol, respectively. **1**, **2**, and **6** have been investigated with infrared spectroscopy before.[35-37] We find the bicyclic 3-notricyclyl ion (**7**) to be 24.7 kcal/mol above the global minimum structure. Olah measured the NMR

Table 4.1. Structural isomers of the $C_7H_9^+$ cation predicted on the 0 K potential energy surface (PES). All structures were fully optimized at the MP2/aug-cc-pVDZ level of theory and confirmed to be minima by harmonic vibrational frequency analysis.

Isomer	MP2/aug-cc-pVDZ [hartree]	ΔE [kcal/mol]
para-protonated toluene (**1**)	-271.029811	0.0
ortho-protonated toluene (**2**)	-271.027964	+1.2
meta-protonated toluene (**3**)	-271.023164	+4.1
ipso-protonated toluene (**4**)	-271.017963	+8.5
1,3-protonated cycloheptatriene (**5**)	-271.001151	+19.2
1,2-protonated cycloheptatriene (**6**)	-270.996509	+22.2
3-notricyclyl (**7**)	-270.993259	+24.7
1,4-protonated cycloheptatriene (**8**)	-270.986666	+27.6
1,3-dimethylcyclopentadienyl (**9**)	-270.981002	+28.9
1,2-dimethylcyclopentadienyl (**10**)	-270.969032	+36.1

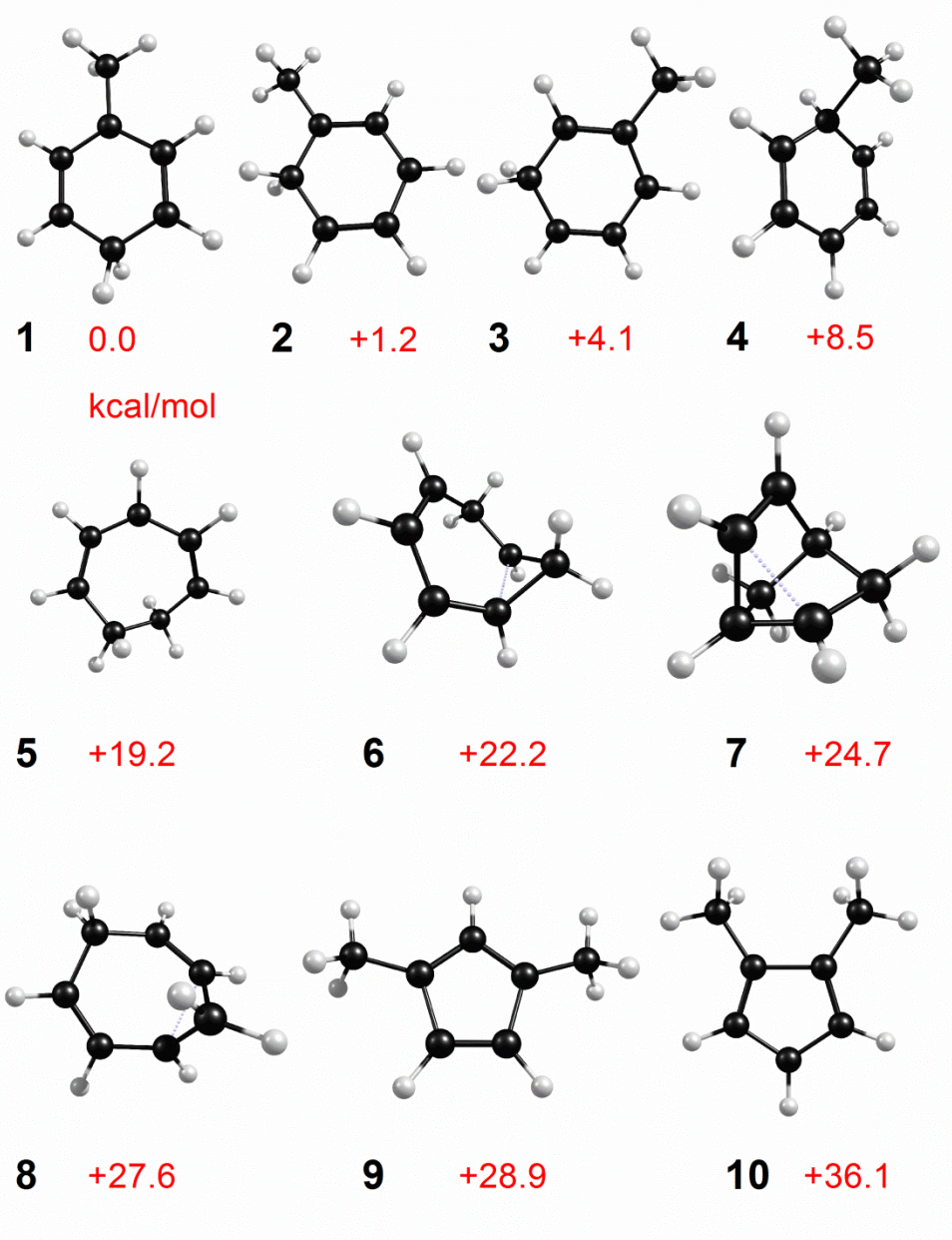

Figure 4.3. Ten $C_7H_9^+$ structures optimized at the MP2/aug-cc-pVDZ level of theory. Relative energies are corrected for zero-point energy effects.

spectrum for **7** in a superacid matrix.[32] This structural isomer is analogous to the infamous 2-norbornyl cation. The remaining two structures are the 1,3- (**9**) and 1,2- (**10**) isomers of dimethylcyclopentadienyl cation. These structures are much more energetic than para-protonated toluene, lying +28.9 and +36.1 kcal/mol higher in energy. Of particular interest is **9**, which is analogous to the $C_7H_{11}^+$ global minimum structure, DMCP. Previous results show that DMCP is present in our ion source under the conditions used here. [42] When we compare the predicted spectra for the nine higher energy isomers computed at the B3LYP/6-311+G** level of theory to our spectrum, only those peaks predicted for **9** satisfactorily match any of the new bands.

The predicted spectrum for **9**−Ar, obtained at the B3LYP/6-311+G** level of theory, is presented in Figure 4.2 (blue trace, bottom). The higher frequency vibrations corresponding to C−H stretching modes are scaled by a factor of 0.969 to correct for vibrational anharmonicity,[45] whereas the lower frequency vibrations are presented unscaled. The predicted frequencies and their infrared intensities are given in Table 4.2 in comparison to the observed infrared bands. Several bands are predicted in the fingerprint region at 1097, 1186, 1343, 1421, 1431 and 1519 cm^{-1}. These bands arise from C−H bending and carbon stretching modes (see vibrational assignments in Table 4.2). In the C−H stretching region, a single strong band is predicted for **9**-Ar, corresponding to overlapping methyl stretches. Two bands with moderate intensity are predicted at 3051 cm^{-1} and 3137 cm^{-1}, corresponding to the methyl and allyl C−H stretches. All of the new experimental features are accounted for, and there are no obvious bands predicted for **9**−Ar above 1000 cm^{-1} that are not observed. Evidently, our experiment produces **9** in addition to **1**.

Figure 4.2 shows the predicted spectrum of **1**−Ar (red trace, second from top) in comparison to the experimental spectra. The fingerprint region of the predicted spectrum is presented unscaled. All of the predicted bands appear to the blue of the experimental bands for

Table 4.2. Vibrational bands for **1** and **9** compared to the predictions of theory. Frequencies are in cm^{-1}; intensities in parentheses are in km/mol.

Exp.[a]	DFT [**1**][b]	Toluene−H^{+}[c]	DFT[**9**][b]	Assignment[d]
1100			1097 (70.8)	iph methyl ip CH wag/allyl CH wag
1195	1207 (47.2)	1204	1186 (154.3)	allyl ip CH wag
1263		1264/1277		
1309	1339 (43.0)	1323		
1392			1343 (177.6)	ooph methyl CH_2 scissors
1475		1473/1487	1421 (86.0)	iph δ-methyl deform
			1431.7 (325.4)	ooph δ-methyl deform/allyl CH wag
1512			1519 (368.5)	asym allyl CCC str
1616	1649 (185.6)	1623		
2836	2862 (32.9)	2835		
	2870 (38.7)			
2908	2903 (35.6)	2914	2880 (175.5)	ooph sym methyl str
	2903 (35.6)		2907 (12.7)	iph asym methyl str
3085			3051 (14.4)	ooph methyl ip CH str
			3051 (14.3)	iph methyl ip CH str
3124	3094 (16.0)		3137 (13.2)	allyl CH str

[a]This work. [b]C−H stretching frequencies scaled by 0.969; low frequencies are left unscaled; basis sets were 6-311+G** for all atoms. [c]From ref. 3. [d]Notation: in phase (iph), out of phase (ooph), in plane (ip), out of plane (oop).

1−Ar. However, when standard scaling is applied, the agreement between experiment and theory is not as good. Hence, we choose to report the values in this region as unscaled harmonic vibrations. In contrast, the predicted bands for **9**−Ar appear very close to, or at slightly lower frequencies than the experimental bands. The C−H stretching region is scaled by a factor of 0.969.[45] Again, predictions for **1**−Ar are not a perfect match, but the agreement is reasonable. Any differences between theory and experiment in this region can be attributed to imperfect scaling, both for the predicted spectrum of **1** and that of **9**.

The cation we observed (apparently for the first time) is fascinating in its own right. Although this structure has been investigated via X-ray crystallography as a ligand in neutral π-hydrocarbon complexes,[46, 47] it has never been characterized in its cationic state to our knowledge. The strong 1512 cm^{-1} band corresponds to the C−C−C asymmetric allyl stretch. This frequency is very close to the corresponding vibration of DMCP at 1525 cm^{-1}. Additionally, the corresponding vibrations of the allyl cation (1581 cm^{-1}),[18] protonated benzene (1607 cm^{-1}),[37] protonated toluene (1623 cm^{-1}),[37] and protonated naphthalene (1620 cm^{-1}),[48] are all higher in frequency. Apparently, this is the lowest frequency measured yet for this type of vibration. The prominent 2908 cm^{-1} absorption corresponds to overlapping methyl C−H stretches, which are observed at 2910 cm^{-1} for DMCP. **9**'s allyl C−H stretch occurs at 3124 cm^{-1}. The corresponding vibration of DMCP occurs at 3101 cm^{-1}. The spectral similarities between **9** and DMCP are due do the very similar structural motifs. Thus, the assignment of the new bands to **9** is unambiguous.

Like the analogous DMCP cation, **9**'s structure contains carbocation-stabilizing features: a five-membered ring allyl resonance and optimally-placed methyl substituents. Unlike DMCP, however, **9** is much higher in energy than the corresponding global minimum structure. This can be explained in part due to a special carbocation problem: with 4 π electrons, **9** is anti-aromatic.

Despite its apparent instability, we observe this structure, and not any of the other higher energy isomers observed previously (see Figure 4.3).[27, 28, 32] The complex plasma reaction pathways form this ion in our source, possibly via H_2 loss from DMCP, in addition to the global minimum structure. That the higher energy isomer survives long enough for spectral analysis (on the order of milliseconds) means there must be a significant local well on the potential energy surface, and rapid collisional cooling traps the metastable ion behind a barrier. Thus, infrared spectroscopy in a supersonic expansion allows for the capture and study of transient species.

Conclusion

The $C_7H_9^+$ carbocation is produced from norbornene and characterized with infrared spectroscopy. The global minimum structure is observed, as well as another higher energy isomer. An extensive investigation of the potential surface reveals multiple $C_7H_9^+$ isomers. Comparison between theory and experiment confirms that the structure of the dimethyl-cyclopentadienyl cation is produced along with para-protonated toluene. This metastable species is formed via an unknown mechanism in our source and kinetically trapped, allowing to measure its infrared spectrum for the first time.

References

(1) Bowers, M. T., *Gas Phase Ion Chemistry, Vol 3: Ions and Light*. Academic Press: New York, 1984.

(2) Baer, T.; Ng, C.; Powis, I., *The Structure, Energetics, and Dynamics of Organic Ions*. Wiley: New York, 1996.

(3) Holmes, J. L.; Aubrey, C.; Mayer, P. M., *Assigning Structures to Ions in Mass Spectrometry*. CRC Press: Boca Raton, FL, 2007.

(4) Yeh, L. I.; Lee, Y. T., Infrared-spectroscopy of the penta-coordinated carbonium-ion $C_2H_7^+$. *J. Am. Chem. Soc.* **1989**, *111* (15), 5597-5604.

(5) Boo, D. W.; Lee, Y. T., Infrared-spectra of CH_5^+ core in CH_5^+ (H_2). *Chem. Phys. Lett.* **1993**, *211* (4-5), 358-363.

(6) Bieske, E. J.; Dopfer, O., High-resolution spectroscopy of cluster ions. *Chem. Rev.* **2000**, *100*, 3963-3998.

(7) Duncan, M. A., Frontiers in the spectroscopy of mass-selected molecular ions. *Int. J. Mass Spectrom.* **2000**, *200*, 545-569.

(8) Olah, G. A.; Prakash, G. K., *Carbocation Chemistry*. John Wiley and Sons: New York, 2004.

(9) Schleyer, P. V. R.; Prakash, G. K., *Stable Carbocation Chemistry*. John Wiley and Sons: New York, 1997.

(10) Aue, D. H., Carbocations. *Wiley Int. Rev.: Comp. Mol. Sci.* **2011**, *1* (4), 487-508.

(11) Olah, G. A.; Schlosberg, R. H.; Kelly, D. P.; Mateescu, G. D., Stable carbonium ions. IC. Benzenonium ion ($C_6H_7^+$) and its degenerate rearrangement. *J. Am. Chem. Soc.* **1970**, *92* (8), 2546-2548.

(12) Olah, G. A.; Staral, J. S.; Asencio, G.; Liang, G.; Forsyth, D. A.; Mateescu, G. D., Stable carbocations. 215. Carbon-13 nuclear magnetic resonance spectroscopic study of the benzenium, naphthalenium, and anthracenium ions. *J. Am. Chem. Soc.* **1978**, *100*, 6299.

(13) Perkampus, H. H.; Baumgarten, E., Proton-Addition Complexes of Aromatic Hydrocarbons. *Angewandte Chemie International Edition in English* **1964**, *3* (12), 776-783.

(14) Hehre, W. J.; McIver, R. T.; Pople, J. A.; Schleyer, P. V., Alkyl substituent effects on stability of protonated benzene. *J. Am. Chem. Soc.* **1974**, *96* (22), 7162-7163.

(15) Kuck, D.; Schneider, J.; Grutzmacher, H. F., A Study of Gaseous Benzenium and Toluenium Ions Generated from 1,4-Dihydro-Benzoic and 1-Methyl-1,4-Dihydro-Benzoic Acids. *J. Chem. Soc. Perk. T. 2* **1985**, (5), 689-696.

(16) Dopfer, O.; Roth, D.; Maier, J. P., Interaction of C3H3+ isomers with molecular nitrogen: IR spectra of C3H3+-(N-2)(n) clusters (n=1-6). *Int. J. Mass Spectrom.* **2002**, *218* (3), 281-297.

(17) Ricks, A. M.; Douberly, G. E.; Schleyer, P. v. R.; Duncan, M. A., Communications: Infrared spectroscopy of gas phase $C_3H_3^+$ ions: The cyclopropenyl and propargyl cations. *J. Chem. Phys.* **2010**, *132* (5), 051101.

(18) Douberly, G. E.; Ricks, A. M.; Schleyer, P. v. R.; Duncan, M. A., Infrared spectroscopy of gas phase $C_3H_5^+$: The allyl and 2-propenyl cations. *J. Chem. Phys.* **2008**, *128*, 021102.

(19) Dunbar, R. C., Nature of the $C_7H_7^+$ ions from toluene parent ion photodissociation. *J. Am. Chem. Soc.* **1975**, *97* (6), 1382-1384.

(20) Lifshitz, C.; Gotkis, Y.; Ioffe, A.; Laskin, J.; Shaik, S., Is the tropylium ion (Tr^+) formed from toluene at its thermochemical threshold? *Intl. J. Mass Spectrom. Ion Proc.* **1993**, *125* (1), R7-R11.

(21) Lifshitz, C., Tropylium ion formation from toluene: Solution of an old problem in organic mass spectrometry. *Acc. Chem. Res.* **1994**, *27* (5), 138-144.

(22) Nagy, A.; Fulara, J.; Garkusha, I.; Maier, J. P., On the benzylium/tropylium ion dichotomy: Electronic absorption spectra in neon matrices. *Angew. Chem.* **2011**, *123* (13), 3078-3081.

(23) Dryza, V.; Chalyavi, N.; Sanelli, J. A.; Bieske, E. J., Electronic absorptions of the benzylium cation. *J. Chem. Phys.* **2012**, *137* (20), 204304.

(24) Devlin, J. L.; Wolf, J. F.; Taft, R. W.; Hehre, W. J., The proton affinities of toluene. *J. Am. Chem. Soc.* **1976**, *98* (7), 1990-1992.

(25) Arnett, E. M.; Abboud, J. L. M., Baker-nathan effect on solvation energies of benzenonium and other organic ions. *J. Am. Chem. Soc.* **1975**, *97* (13), 3865-3867.

(26) Lau, Y. K.; Kebarle, P., Substituent effects on the intrinsic basicity of benzene: proton affinities of substituted benzenes. *J. Am. Chem. Soc.* **1976**, *98* (23), 7452-7453.

(27) Salpin, J. Y.; Mormann, M.; Tortajada, J.; Nguyen, M. T.; Kuck, D., The gas-phase basicity and proton affinity of 1,3,5-cycloheptatriene - energetics, structure and interconversion of dihydrotropylium ions. *Eur. J. Mass Spectrom.* **2003**, *9* (4), 361-376.

(28) Mormann, M.; Kuck, D., Hydride abstraction from 1,3,5-cycloheptatriene by gaseous carbenium ions, as studied by Fourier transform ion cyclotron resonance kinetics and deuterium labeling. *J. Phys. Org. Chem.* **2003**, *16* (10), 746-752.

(29) Mormann, M.; Salpin, J.-Y.; Kuck, D., Gas-phase titration of $C_7H_9^+$ ion mixtures by FT-ICR mass spectrometry: Semiquantitative determination of ion populations generated by CI-induced protonation of C_7H_8 isomers and by EI-induced fragmentation of some monoterpenes. *Int. J. Mass Spectrom.* **2006**, *249–250* (0), 340-352.

(30) Kuck, D., Half a century of scrambling in organic ions: complete, incomplete, progressive and composite atom interchange. *Int. J. Mass Spectrom.* **2002**, *213* (2–3), 101-144.

(31) Olah, G. A.; Schlosberg, R. H.; Porter, R. D.; Mo, Y. K.; Kelly, D. P.; Mateescu, G. D., Stable carbocations .124. Benzenium ion and monoalkylbenzenium ions. *J. Am. Chem. Soc.* **1972**, *94* (6), 2034.

(32) Olah, G. A.; Liang, G., Stable carbocations. CLXXVI. 3-Nortricyclyl cations. Question of charge delocalization in rigid cyclopropylcarbinyl systems. *J. Am. Chem. Soc.* **1975**, *97* (7), 1920-1927.

(33) Masamune, S.; Sakai, M.; Ona, H.; Jones, A. J., Nature of the $(CH)_5^+$ species. II. Direct observation of the carbonium ion of 3-hydroxyhomotetrahedrane derivatives. *J. Am. Chem. Soc.* **1972**, *94* (25), 8956-8958.

(34) Kemp-Jones, A. V.; Nakamura, N.; Masamune, S., A bishomo square-pyramidal carbonium ion. *J. Chem. Soc. Chem. Commun.* **1974**, (3), 109-110.

(35) Dopfer, O.; Lemaire, J.; Maître, P.; Chiavarino, B.; Crestoni, M. E.; Fornarini, S., IR spectroscopy of protonated toluene: Probing ring hydrogen shifts in gaseous arenium ions. *Int. J. Mass Spectrom.* **2006**, *249–250* (0), 149-154.

(36) Schroder, D.; Schwarz, H.; Milko, P.; Roithova, J., Dissociation routes of protonated toluene probed by infrared spectroscopy in the gas phase. *J. Phys. Chem. A* **2006**, *110* (27), 8346-8353.

(37) Douberly, G. E.; Ricks, A. M.; Schleyer, P. V. R.; Duncan, M. A., Infrared spectroscopy of gas phase benzenium ions: Protonated benzene and protonated toluene, from 750 to 3400 cm^{-1}. *J. Phys. Chem. A* **2008**, *112* (22), 4869-4874.

(38) Gassman, P. G.; Creary, X., C_7H_9 cation manifold. Interconversion of a series of potentially bishomoantiaromatic ions. *J. Am. Chem. Soc.* **1973**, *95* (20), 6852-6853.

(39) Dewar, M. J. S.; Dieter, K. M., Evaluation of AM1 calculated proton affinities and deprotonation enthalpies. *J. Am. Chem. Soc.* **1986**, *108* (25), 8075-8086.

(40) Rasul, G.; Prakash, G. K. S.; Olah, G. A., Comparative study of the hypercoordinate ions $C_7H_9^+$ and $C_8H_9^+$ by the ab initio/GIAO-CCSD(T) method. *J. Phys. Chem. A* **2006**, *110* (39), 11320-11323.

(41) Siehl, H.-U., The interplay between experiment and theory: computational NMR spectroscopy of carbocations. In *Advances in Physical Organic Chemistry*, Richard, J. P., Ed. Academic Press: 2007; Vol. 42, pp 125-165.

(42) Mosley, J. D.; Young, J. W.; Agarwal, J.; Schaefer, H. F.; Schleyer, P. v. R.; Duncan, M. A., Structural isomerization of the gas phase 2-norbornyl cation revealed with infrared spectroscopy and computational chemistry. *Angew. Chem. Int. Ed.* **2014**, in press.

(43) Duncan, M. A., Infrared laser spectroscopy of mass-selected carbocations. *J. Phys. Chem. A* **2012**, *116* (47), 11477-11491.

(44) Schmidt, M. W.; Baldridge, K. K.; Boatz, J. A.; Elbert, S. T.; Gordon, M. S.; Jensen, J. H.; Koseki, S.; Matsunaga, N.; Nguyen, K. A.; Su, S.; Windus, T. L.; Dupuis, M.; Montgomery, J. A., General atomic and molecular electronic structure system. *J. Comput. Chem.* **1993**, *14* (11), 1347-1363.

(45) Merrick, J. P.; Moran, D.; Radom, L., An evaluation of harmonic vibrational frequency scale factors. *J. Phys. Chem. A* **2007**, *111* (45), 11683-11700.

(46) Kirss, R. U., Electrocyclic reactions of open metallocenes: Carbon-carbon bond formation during thermolysis of bis(2,4-dimethyl-1,3-pentadienyl)ruthenium and -osmium. *Organometallics* **1992**, *11* (2), 497-499.

(47) Kirss, R. U.; Quazi, A.; Lake, C. H.; Churchill, M. R., Synthesis of unsymmetrical ruthenocenes by gas phase electrocyclic reactions of pentadienylruthenium complexes. *Organometallics* **1993**, *12* (10), 4145-4150.

(48) Ricks, A. M.; Douberly, G. E.; Duncan, M. A., The infrared spectrum of protonated naphthalene and its relevance for the unidentified infrared bands. *Astrophys. J.* **2009**, *702* (1), 301-306.

CHAPTER 5

INFRARED SPECTROSCOPY OF THE MASS 31 CATION: PROTONATED FORMALDEHYDE VS METHOXY

Introduction

The ion at m/z = 31 is produced as an abundant fragment in the ionization of methanol, ethanol, dimethyl ether, and other small oxygen-containing molecules.[1] This ion has been the subject of much study and discussion in the mass spectrometry community for many years.[2-22] Two important structures are recognized, the CH_2OH^+ protonated formaldehyde ion and the CH_3O^+ methoxy cation. The $HCOH_2^+$ oxonio-methylene ion was also proposed on the basis of computational studies,[8] but there is apparently no experimental evidence for this species. In early studies on low temperature ions, evidence was found for a weakly bound $HCO^+–H_2$ complex.[4-6] As shown in Figure 5.1, protonated formaldehyde has a singlet ground state and is by far the most stable structure. Methoxy cation lies +96.0 kcal/mol above this, with a triplet ground state. Therefore, interconversion of these two ions requires a curve crossing, which has been estimated to lie +14.3 kcal/mol above the methoxy ground state.[20] Oxonio-methylene is also a singlet, lying +82.9 kcal/mol above protonated formaldehyde.[8] The collisional dissociation of a variety of ions having m/z=31 produces fragmentation with an m/z = 15:14 peak ratio of about 0.03, suggesting that the most common structure produced is protonated formaldehyde. Different fragmentation (an intense m/z=15 peak) attributed to methoxy cation can be produced by charge reversal of the corresponding anions.[7, 12] Attempts to detect methoxy by ionization of neutral CH_3O radicals from various sources were unsuccessful.[17] Instead, HCO^+ ions were detected at a higher photoionization threshold, presumably by prompt fragmentation of the nascent CH_3O^+. Collisional dissociation of $[C,H_3,O]^+$ proceeds by elimination of H_2 with significant translational energy release.[15, 19-21] However, the energy release is the

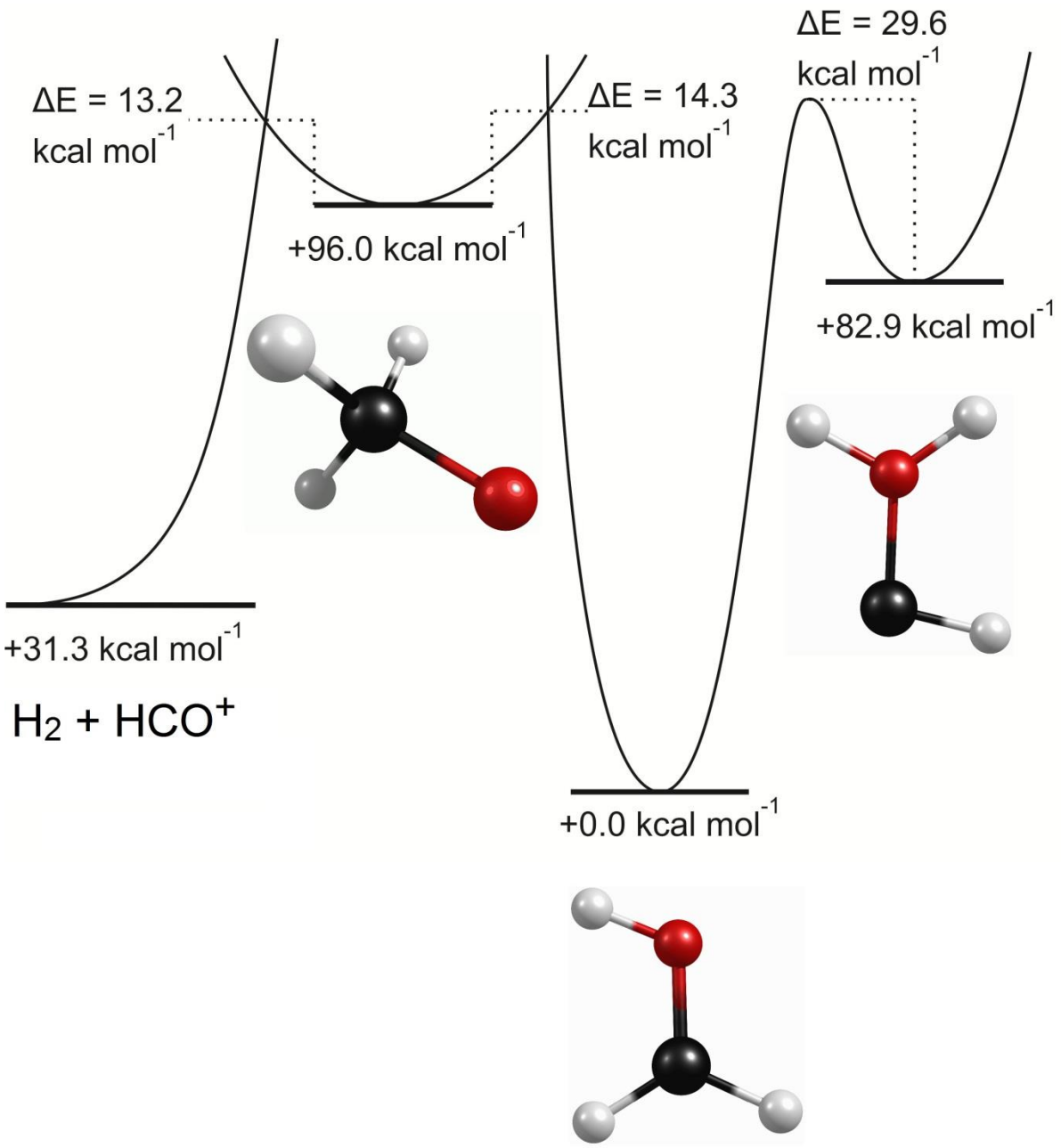

Figure 5.1. Schematic energy level diagram showing the relative energies of methoxy, protonated formaldehyde and oxonio-methylene as well as the energies of the curve crossings connecting these species.

same for ions believed to have either the CH_3O^+ or CH_2OH^+ structures. This has been interpreted to indicate that methoxy crosses over into the protonated formaldehyde structure before dissociating, although it has also been proposed that methoxy dissociates directly to $HCO^+ + H_2$.[20] The protonated formaldehyde ion has been characterized with gas phase infrared spectroscopy via an O–H stretching vibration[23] and with millimeter wave measurements;[24] it has also been detected in interstellar space.[25] The vibrational spectrum of protonated formaldehyde has also been investigated computationally,[26-29] but there is no spectroscopy of the methoxy cation to our knowledge. Here we describe the infrared spectroscopy of the mass-selected m/z=31 ion, produced via discharge in a supersonic expansion, which shows that both protonated formaldehyde and the methoxy cation structures are present.

Experimental details

Ions for these experiments are produced in a pulsed discharge/supersonic expansion source using needle electrodes, as described previously.[30] The expansion gas is argon seeded with the ambient vapor pressure of methanol or ethanol at room temperature. The discharge is activated for a 5–10 microsecond duration in the center of a 250–300 microsecond gas pulse. After this, ions expand supersonically to form a dense, cold plasma. This beam is collimated by a skimmer before sampling by a reflectron time-of-flight mass spectrometer (RTOF) in a differentially pumped chamber.[31] Ions are extracted perpendicular to their flight direction from the molecular beam into the RTOF. To select specific ions for photodissociation, pulsed deflection plates are employed at the end of the first flight tube section. Ions are excited with the tunable infrared laser in the turning region of the reflectron, and mass analysis of any fragmentation peaks occurs in a second flight tube section.[31] The IR laser is a Nd:YAG-pumped optical parametric oscillator/amplifier (OPO/OPA; LaserVision). In its normal operating configuration,[32] a KTP oscillator pumped at 532 nm and a KTA difference frequency generation (idler + 1064 nm) amplifier provides tunable output in the 2000-4500 cm^{-1} region with a line width of about 1 cm^{-1}. In a second configuration, another stage of difference frequency generation in $AgGaSe_2$ provides output in the 800-2200 cm^{-1} range.[33]

Computational studies are carried out at the MP2/cc-pVTZ and DFT/B3LYP levels of theory using the Gaussian03 program package.[34] Energetics are reported from the MP2 calculations, while vibrational spectra are those from DFT/B3LYP, taking advantages of the best performance of each method as noted in previous work from our lab.[30] A vibrational scaling factor of 0.9682 was employed for the DFT/B3LYP spectra, as recommended by Radom and coworkers for this level of theory.[35]

Results and discussion

Electrical discharges in methanol or ethanol produce a complex mass spectrum containing many fragment ions and their clusters with precursor molecules and with argon. A representative mass spectrum is shown in Figure 5.2. The m/z 31 ion is seen in high abundance when ethanol is used as the precursor. Several other fragment ions are observed with varying intensities in our source. Notably, the cluster of argon with the m/z 31 ion, observed at m/z 71, is only a few percent as intense as the untagged species. Employing mass selection (Figure 5.2, navy trace, middle) allows for signal amplification of the ion of interest, and efficient photodissociation is observed upon resonant absorption by the m/z 31 ion.

The infrared photodissociation spectrum measured for $[C,H_3,O]^+Ar$ produced in a discharge of ethanol, obtained by loss of Ar is presented in Figure 5.3. An intense resonance near 3182 cm^{-1} dominates the spectrum, but there are vibrational bands throughout the 1000 to 3500 cm^{-1} region. The 3182 cm^{-1} band is in the region where an O–H stretch is expected for protonated formaldehyde, although this band is shifted significantly to lower energy compared to the O–H stretch seen by Amano and coworkers at 3422.8 cm^{-1}.[23] Bands near 2700 cm^{-1} can be associated with C–H stretches, while those in the 1000-1600 cm^{-1} region should be C−H bending and carbonyl stretching vibrations. We use computational chemistry of the three isomer possibilities for these ions to investigate detailed assignments for these bands. Table 5.1 shows the relative energies for the three isomers at both the MP2 and DFT/B3LYP levels of theory. As expected from previous work, protonated formaldehyde is far more stable than either the methoxy or oxonio-methylene ions, and their relative energies are completely consistent with previous results.[2-5, 8, 10, 13, 16, 20] We have not investigated the energies of the singlet/triplet

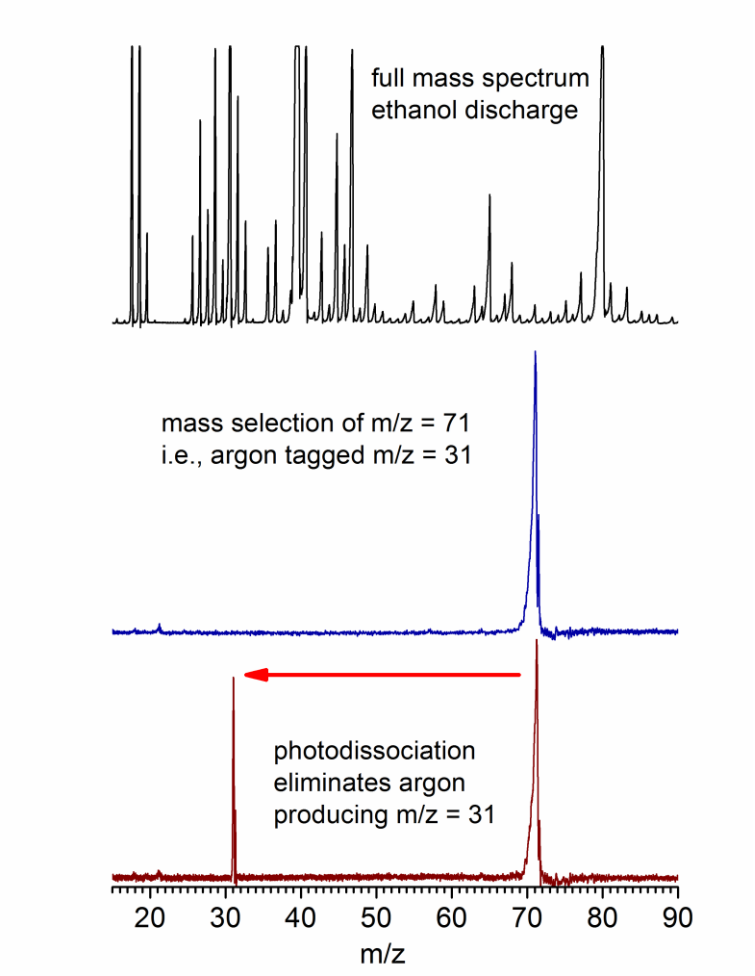

Figure 5.2. The mass spectrum produced from an ethanol discharge (top trace). The middle trace shows the mass-selected m/z = 71 ion corresponding to the m/z = 31 ion tagged with argon. The bottom trace shows the photodissociation of the m/z=71 ion, which proceeds by elimination of argon to produce m/z=31.

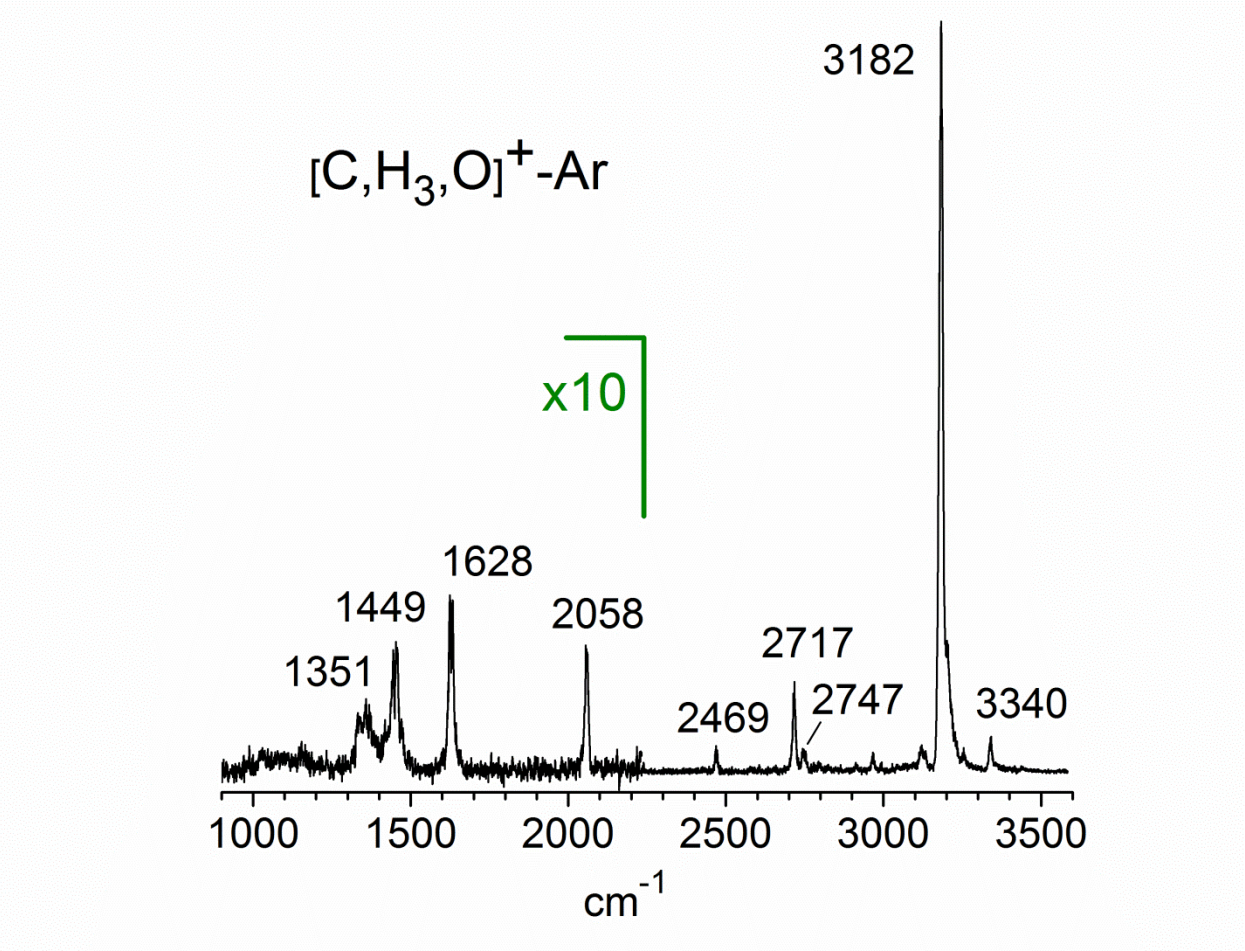

Figure 5.3. The infrared photodissociation spectrum of the mass 31 cation obtained by tagging it with argon and measuring the argon elimination mass channel.

Table 5.1. Relative energies of $[C,H_3,O]^+$ isomers with and without argon at the DFT/B3LYP and MP2 levels of theory with the correlation consistent Dunning triple ζ basis set. All energetics are corrected for zero point energy.

Isomer	ΔE (MP2)	ΔE (B3LYP)
CH_2OH^+	0.0	0.0
$CHOH_2^+$	+81.1	+78.3
CH_3O^+	+91.3	+72.8
CH_2OH^+-Ar	0.0	0.0
$CHOH_2^+$-Ar	+79.8	+76.9
CH_3O^+-Ar (1)	+93.3	+73.8
CH_3O^+-Ar (2)	+93.7	+75.5
CH_3O^+-Ar (3)	+93.9	+75.1

curve crossing for methoxy/protonated formaldehyde; instead, we use here the previous results of Schwarz and coworkers.[20] The oxonio-methylene energetics shown are those from Radom and coworkers.[8]

Figure 5.4 shows an expanded view of the mass 31 ion spectrum compared to the predictions of theory for the protonated formaldehyde, methoxy and oxonio-methylene cations, each with attached argon. The computed band intensities are those for linear absorption, while those in the experiment are determined by the absorption strength, the photodissociation yield and the IR laser power, which falls gradually toward lower energy. We normalize the data to parent ion intensity variations, but not to the laser power because the beam shape and hence the overlap with the ion beam changes across the spectrum. Therefore, band positions are more significant than intensities, especially when comparing different ends of the spectrum.

It is immediately apparent that many of the bands here can be assigned to the protonated formaldehyde cation. The strong 3182 cm^{-1} feature is reproduced reasonably well in position and intensity for the O–H stretch vibration. The different position of this band compared to the vibration in the isolated ion[23] results from the argon atom attaching to the proton, which induces a strong red shift. This can be seen via calculations with and without argon (see Figure 5.5), and large red shifts have been seen for other ions with argon attached at a proton site.[30] Additionally, changing the tag atom to neon largely eliminates the red shift, as shown in Figure 5.6. Just below the 3182 cm^{-1} feature, we see weak bands assigned to the symmetric (2967 cm^{-1}) and asymmetric (3124 cm^{-1}) CH_2 stretches that were not reported previously, but agree well with the predictions of theory. The bands at lower frequency for protonated formaldehyde have also not been reported previously, but all have been predicted before with computational chemistry.[26-29] These include the carbonyl stretch (1628 cm^{-1}), the CH_2 scissors vibration (1449 cm^{-1}) and the COH^+ in-plane hydrogen bend (1351 cm^{-1}). These vibrations are all reproduced well by our theory, including the argon, and are in good agreement with previous theory without argon,[26-29] because the shift from the argon is small. The photodissociation signal drops off below the 1351 cm^{-1}

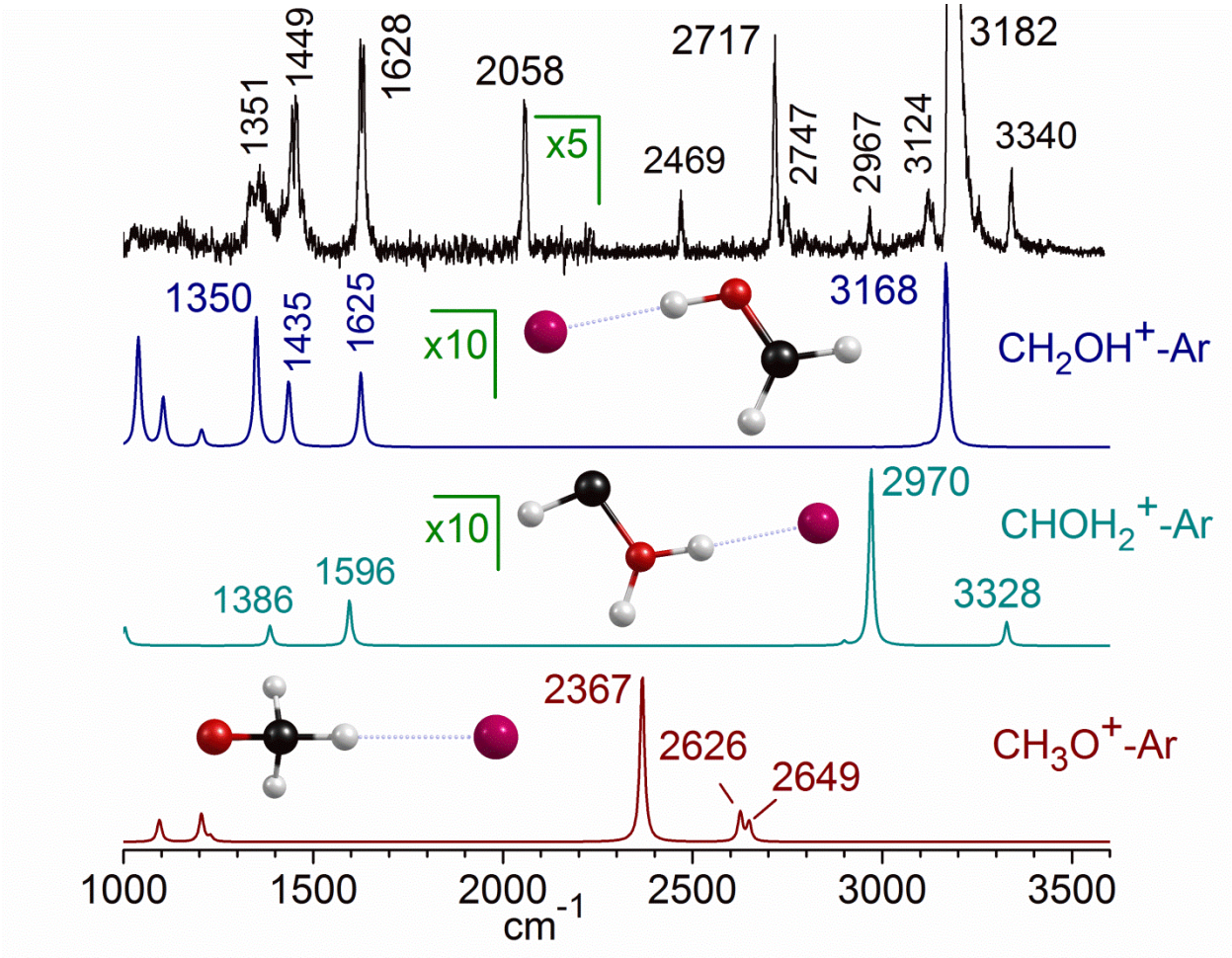

Figure 5.4. An expanded view of the IR spectrum measured for the mass 31 cation compared to the predictions of theory for protonated formaldehyde (second trace/dark blue), oxonio-methylene cation (third trace/turquois) and the methoxy cation (bottom trace/dark red). All computations include the argon atom and frequencies are scaled by a factor of 0.9682.[54]

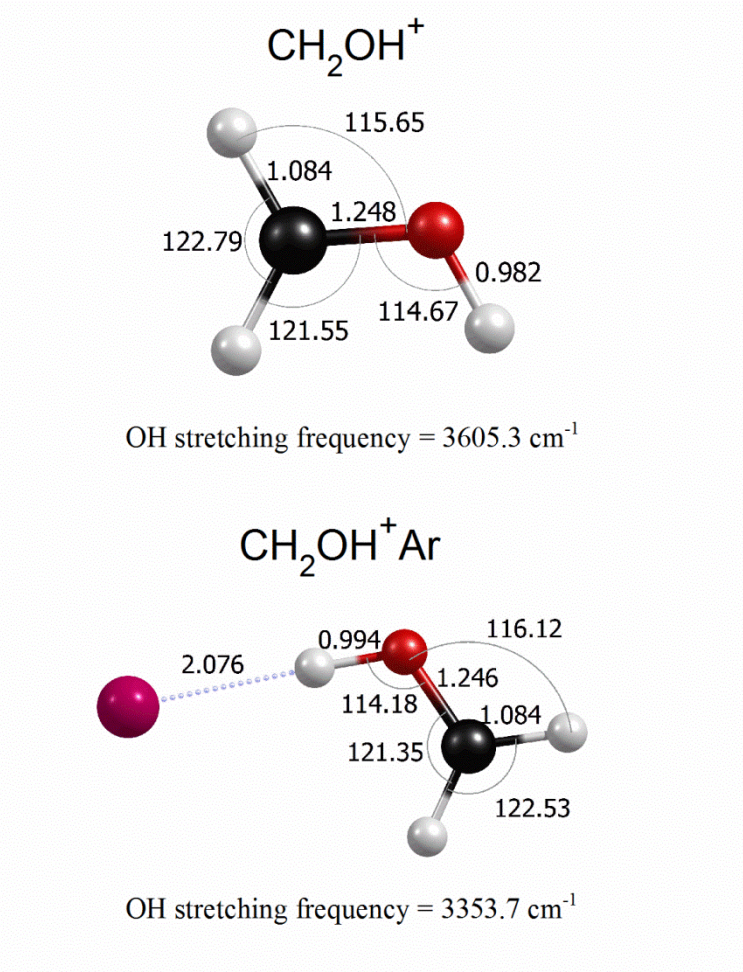

Figure 5.5. The optimized geometries of protonated formaldehyde (CH_2OH^+) with and without argon calculated at the MP2/cc-pVTZ level of theory using Gaussian03. Bond lengths are in Ångstroms. Bond angles are in degrees.

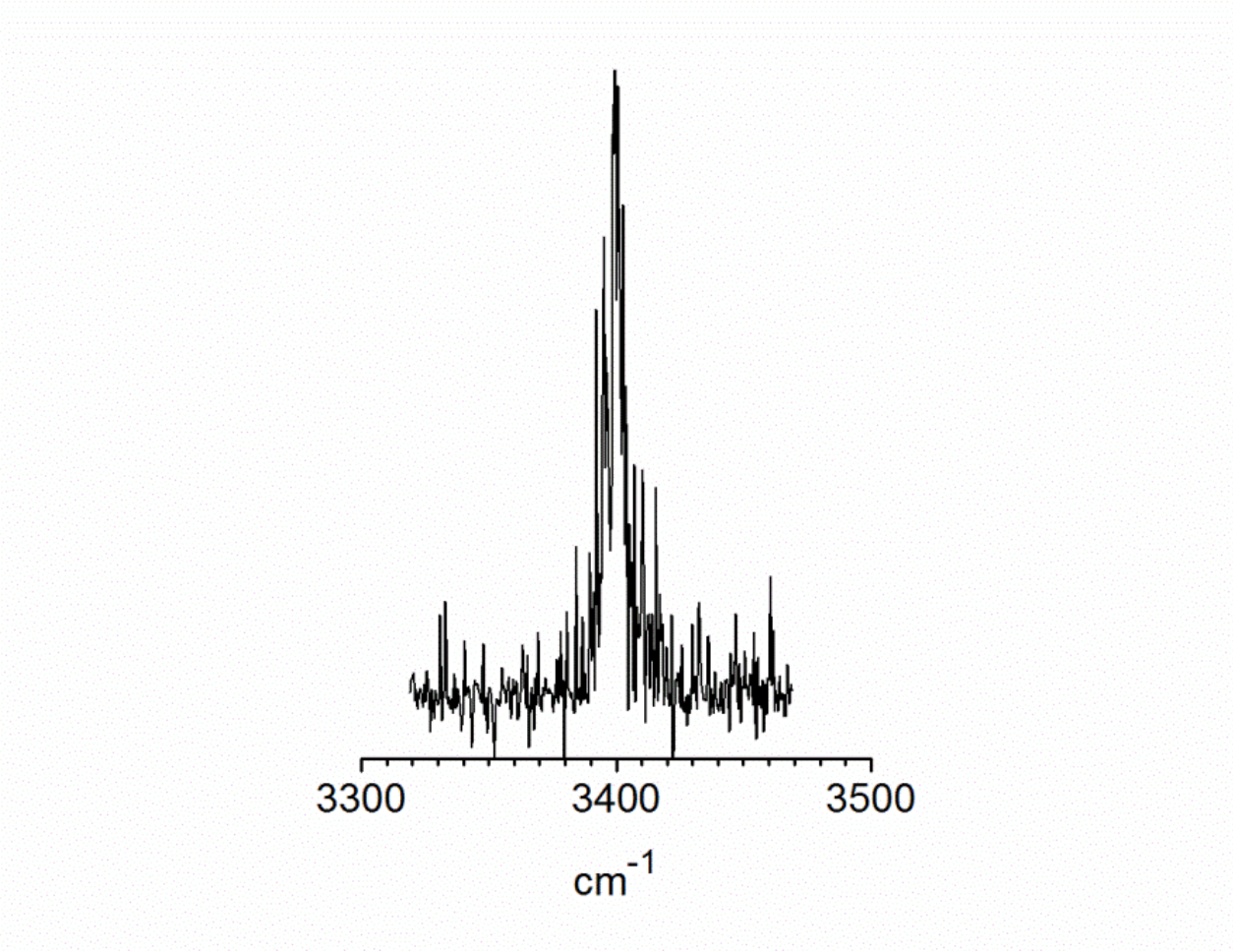

Figure 5.6. The O−H stretching band of $[C,H_3,O]^+Ne$ obtained by loss of neon.

band, most likely due to the bond energy of the argon tag. This is computed to be 4.4 kcal/mol (1540 cm^{-1}) for protonated formaldehyde at the MP2 level and 1.7–2.1 kcal/mol for the different argon isomers of methoxy (see discussion below).

The vibrational frequencies for protonated formaldehyde can be compared to those of formaldehyde itself.[36] The carbonyl stretch of protonated formaldehyde (1628 cm^{-1}) is shifted to much lower frequency than that in formaldehyde (1746.1 cm^{-1}), suggesting that protonation weakens the C=O bond. This presumably is due to the proton's withdrawing electron density from the bond. This is consistent with the computed C=O bond distance in protonated formaldehyde (1.248 Å at the MP2 level; see Figure 5.5) being longer than that in formaldehyde (1.205 Å). Likewise, the CH_2 scissors frequency here (1449 cm^{-1}) is lower than in formaldehyde (1500.1 cm^{-1}), again consistent with a less rigid system. A similar trend is found for the formaldehyde cation,[36] which also has lower C=O (1675 cm^{-1}) and CH_2 scissors (1210 cm^{-1}) vibrations than neutral formaldehyde. The lower frequency bands at 1351, 1449 and 1628 cm^{-1} can also be compared to the vibrations in high Rydberg states of the CH_2OH hydroxymethyl radical that converge to the protonated formaldehyde ground state.[37-39] As shown in Table 5.2, each of these vibrations occurs within a few cm^{-1} of the frequencies seen here.

Bands in the middle of the spectrum are not readily assigned to fundamentals of protonated formaldehyde. These include the feature at 2058 cm^{-1} and the group of bands at 2469, 2717 and 2747 cm^{-1}. Additionally, a less intense but noticeable band at 3340 cm^{-1} cannot be immediately identified. We consider the 2469, 2717 and 2747 cm^{-1} group of bands first. Protonated formaldehyde has no vibrations in this region, but the triplet methoxy cation does have bands predicted here, as shown in the lower trace of Figure 5.4. Although three bands are predicted for CH_3O^+Ar, the pattern of peak positions and intensities from theory does not match the experiment. Because we use the method of argon tagging, and because argon often binds in more than one position on other ions,[40] we conducted a careful study of its binding sites on methoxy and their influence on the vibrational patterns (a similar study on protonated formaldehyde found only the Ar-on-H^+ isomer). Three binding sites for argon attached to methoxy correspond to stable minima. Table 5.1 presents the energies for these complexes, and Figure 5.7 shows

Table 5.2. Vibrational bands of the mass 31 cation tagged with Ar compared with theory and previous experiments. Band positions are in cm^{-1}; IR intensities are in km/mol.

Exp.	Theory (int.)	Previous Exp.	Assignment
1351	1350 (92.5)	1351,[a] 1357,[b] 1370[c]	in phase HCOH bend (CH_2OH^+)
1449	1435 (47.1)	1459,[a] 1465[b]	CH_2 scissors (CH_2OH^+)
1628	1625 (53.4)	1623,[a] 1621,[b] 1650 ± 30[c]	C–O stretch (CH_2OH^+)
2058	2090[d]	-	O–H τ (oop) overtone (CH_2OH^+)
2469	2367 (1028.0)	-	C–H stretch (CH_3O^+)
2717	2626 (181.6)	-	sym. C–H_2 stretch (CH_3O^+)
2747	2649 (120.2)	-	asym. C–H_2 stretch (CH_3O^+)
2967	2977 (0.9)	-	sym. CH_2 stretch (CH_2OH^+)
3124	3111 (8.9)	-	asym. CH_2 stretch (CH_2OH^+)
3182	3168 (1317.7)	3423[e]	O–H stretch (CH_2OH^+)
3254	-	-	-
3340	3356 (36.1)	-	combination band $\nu_1 + \nu_{11}$ (CH_2OH^+)

[a]Ref. 37. [b]Ref. 38. [c]Ref. 39. [d]from anharmonic analysis. [e]Ref. 23.

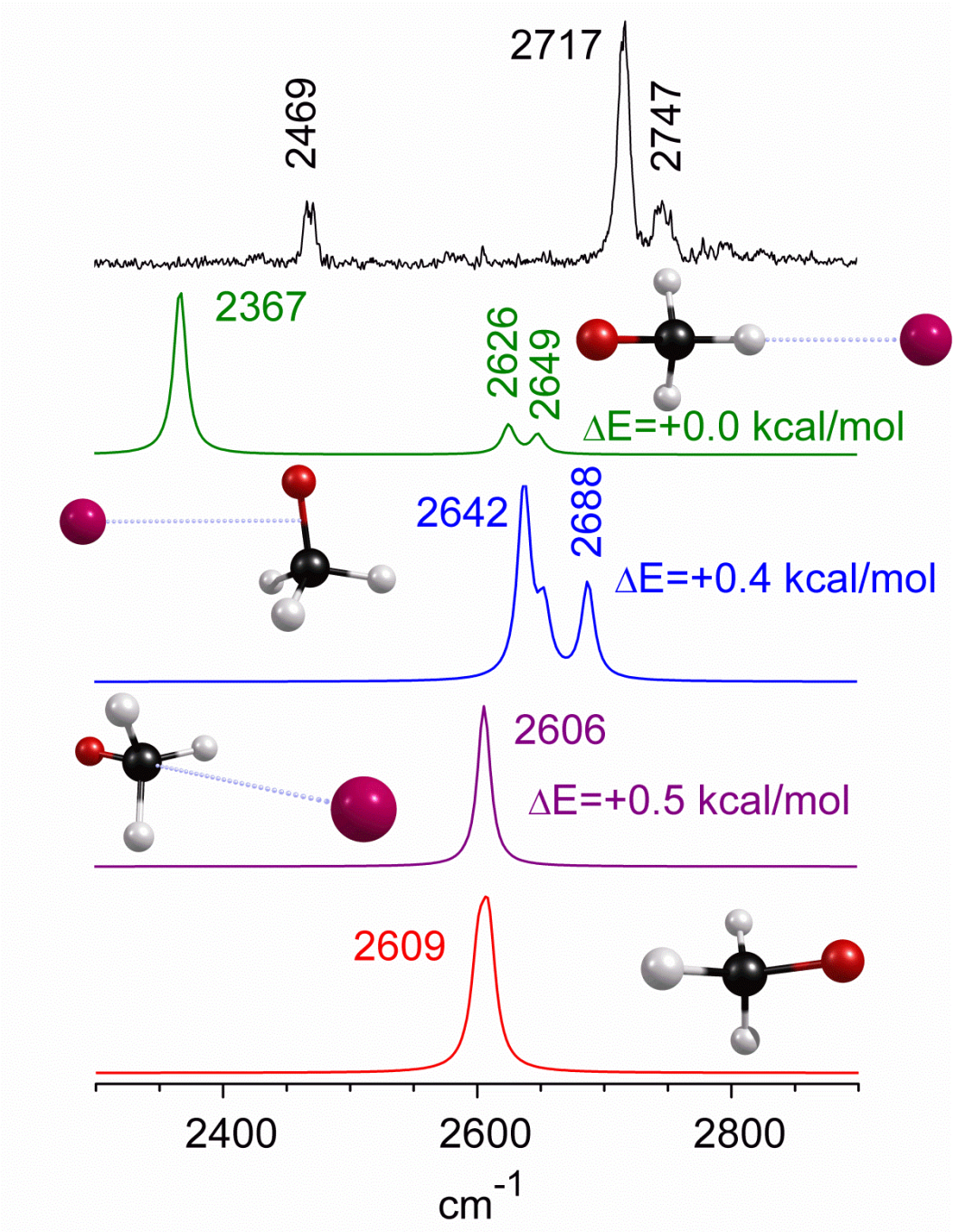

Figure 5.7. The bands attributed to methoxy cation compared to the spectra predicted for isomers with argon at different binding sites.

their spectra compared to the experiment. These include the three-fold pocket between the CH groups (Figure 5.7, purple trace, fourth from top), along the side of the CO bond (blue trace, third from top), and a single CH site (green trace, second from top); the energies of these sites are extremely close. If argon binds in the three-fold pocket on the C_3 axis, the symmetry of the argon-free system is preserved, and two overlapping C–H stretches are predicted (symmetric and degenerate asymmetric stretch) just as seen for the isolated methoxy cation (red trace, bottom). If argon binds alongside the CO bond, the symmetry is broken, and a symmetric/asymmetric pair is split from the remaining . If argon binds on a single CH position, it interacts more strongly with one CH than the others, and this C–H stretch is strongly red shifted with respect to the symmetric/asymmetric CH_2 pair. Unfortunately, none of the vibrational patterns computed for these limiting structures exactly matches the spectrum. The best match is for the Ar-on-CH structure, which is computed to be most stable. It has three bands with about the right spacing, with one more red-shifted than the other two, but the position and relative intensities don't match the spectrum exactly. However, since the energy differences between these sites are so small, it is likely that the potential for argon motion is quite flat and that the argon samples more than one of these configurations. If we acknowledge that the level of theory employed (and perhaps the scaling factors) is not ideal for such weak interactions, and that the zero point motion may exceed the barriers between argon configurations, it is not too surprising that we do not have an exact match to the experimental spectrum. The Ar-on-CH configuration produces a shifted band and a doublet, which is what we see in the experiment, although the exact spacings and relative intensities are not perfect. It is likely that this main configuration, and perhaps some dynamical averaging over nearby configurations, can explain the spectrum. We therefore assign the 2469, 2717 and 2747 cm^{-1} bands to the C–H stretches of the methoxy cation.

Detection of a stable methoxy cation living many hundreds of microseconds is surprising in light of the difficulties in producing this species in the past and its high instability relative to protonated formaldehyde. In additional tests to confirm this assignment, we first varied the precursor used to produce the mass 31 cation. Experiments comparing methanol and ethanol produce the spectra shown in

Figure 5.8. As indicated with the shaded bands, the intensities of the 2469, 2717 and 2747 cm^{-1} bands track together as a group, but the intensity of this group varies significantly with respect to that of the 3182 cm^{-1} band. If these bands were all from the same ion, their relative intensities would remain constant. Therefore, this data strongly supports the assignment of the 2469, 2717 and 2747 cm^{-1} bands to an isomer other than protonated formaldehyde, consistent with our assignment of these bands to methoxy. Using the computed IR intensities of the bands for methoxy versus protonated formaldehyde, and comparing the integrated area of these bands, we can estimate a branching ratio for these two isomers. As shown in the figure, the methoxy:protonated formaldehyde ratio under these discharge conditions is 1:53 for the methanol precursor and 1:12 for the ethanol precursor.

In a second test, we varied the discharge conditions used to produce the ions. We presume that both isomers are produced in some initial branching ratios following the energetic ionization and fragmentation processes, and that the survival of each depends on its cooling rate and efficiency in our source. In particular, survival of methoxy requires that it be cooled and stabilized behind the barrier at the triplet/singlet curve crossing to protonated formaldehyde. The temperature of the plasma should therefore affect the methoxy/protonated formaldehyde branching ratio. To estimate the temperature, we use the computed rotational constants of protonated formaldehyde tagged with argon to simulate a rotational contour for the O–H stretching band, and adjust its linewidth (FWHM) to match that in the experiment (see Figure 5.9). This procedure is not perfect, as the linewidth may also have contributions from predissociation, but it is good enough for a rough estimate. Our normal cold discharge/expansion conditions using ethanol lead to a rotational temperature of about 25K, consistent with ion temperatures measured previously with this source. To change the ion temperature, we increase the discharge voltage level and move its pulse timing relative to the center of the gas pulse. This simultaneously increases the heating of the plasma and reduces the efficiency of the collisional cooling. The comparison of the spectrum obtained with these hotter conditions to that with the normal cold plasma is shown in Figure 5.10. As shown, hotter conditions produce a broader protonated formaldehyde O–H stretching band more

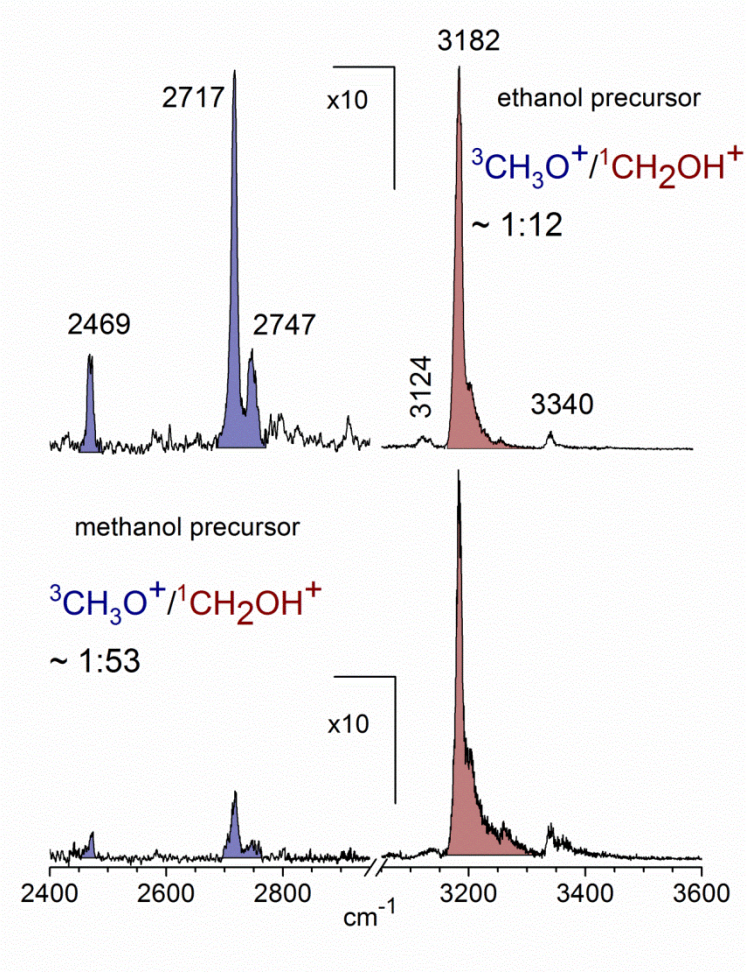

Figure 5.8. The variation in the bands attributed to methoxy (blue) versus protonated formaldehyde (red) when ions are produced from ethanol versus methanol precursors.

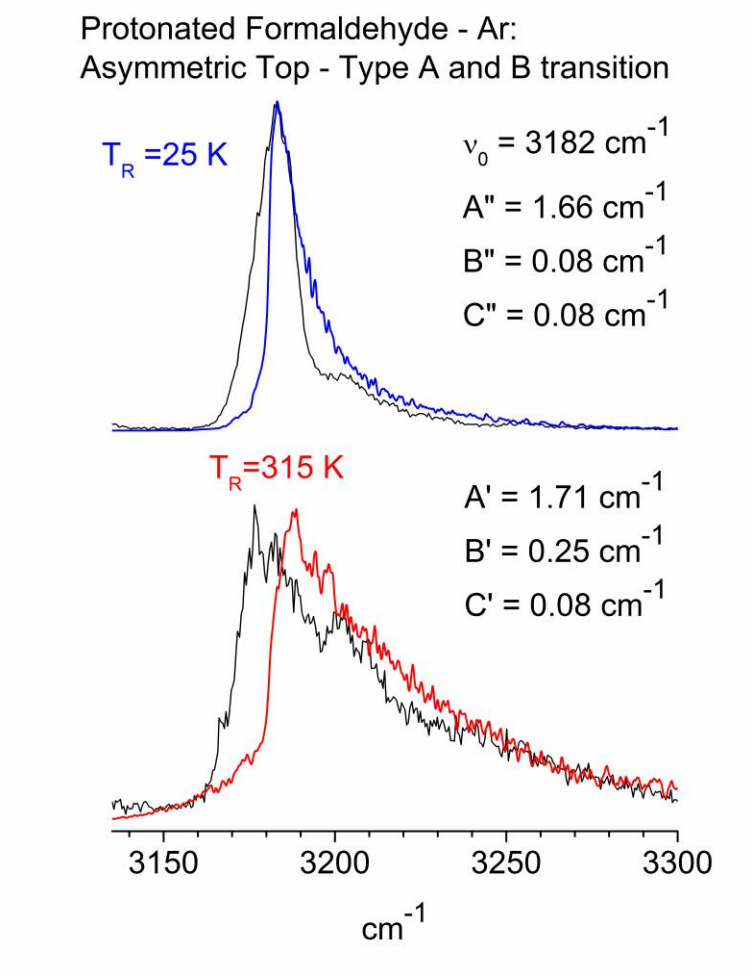

Figure 5.9. Comparison of the observed O–H stretch of CH_2OH^+-Ar (black) at two different source conditions with simulated ro-vibrational spectra for an asymmetric top using the PGOPHER program.

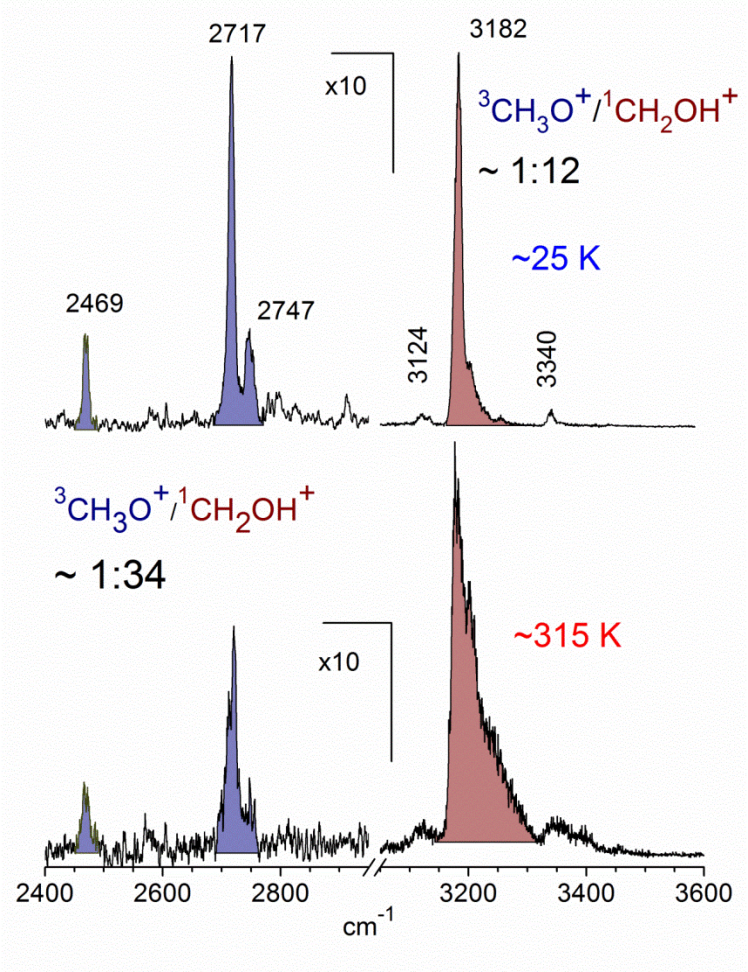

Figure 5.10. The variation in the bands attributed to methoxy (blue) versus protonated formaldehyde (red) when ions are produced under cold versus hot discharge conditions. Temperatures are estimated from the rotational contour of the O–H stretch of protonated formaldehyde (see Figure 5.9).

shaded to the blue, with a temperature of roughly 315K. Vibrations are not likely to be equilibrated to this same temperature, but this confirms that the plasma is heated to a significant degree. Furthermore, the bands attributed to methoxy decrease in intensity, corresponding to these hotter conditions. Again, comparing the integrated areas and computed IR intensities, we arrive at a CH_3O^+:CH_2OH^+ ratio of 1:34. Less methoxy survives at higher temperature, consistent with inefficient trapping behind the singlet/triplet curve crossing barrier. Overall, the dependence on precursor and discharge conditions are consistent with the assignment of the 2469, 2717 and 2747 cm^{-1} bands to an isomer other than protonated formaldehyde. The vibrational analysis indicates that this isomer is methoxy. Its production efficiency changes with different precursors and conditions, consistent with expectations for a metastable species. Because we have been able to capture this ion, the qualitative aspects of the potential energy surface and singlet/triplet curve crossings proposed previously[20] must be valid, i.e., there must be a significant local well on the methoxy surface.

The oxonio-methylene cation has been suggested as a possible structural isomer by theory,[8] but there is no experimental evidence for this ion to our knowledge. We find a stable minimum for this structure, whose predicted spectrum is shown in the third trace from the top in Figure 5.4. Vibrations are predicted at 2970 cm^{-1} and 3328 cm^{-1}, near experimental bands, but the relative intensities do not match the experiment. Because the IR laser power is steady in this region, measured intensities should resemble those computed. As noted above, the 2967 cm^{-1} band can also be assigned to the weak symmetric CH_2 stretch of protonated formaldehyde. This band is not evident in the theory trace for this ion because it is so much weaker than the O–H stretch. As discussed below, the 3340 cm^{-1} can be assigned to a combination band. Considering all this, it is not possible to completely exclude the presence of a small amount of oxonio-methylene cation, but we conclude that there is no compelling evidence for it.

Unassigned vibrational bands remain at 2058 and 3340 cm^{-1} that are not close to predicted fundamentals of protonated formaldehyde or methoxy cation. Therefore, we investigate assignments for these features involving overtones or combination bands, guided by past experience with similar systems (the following results were obtained by our collaborator Anne McCoy at the Ohio State University). Such

bands can be quite prominent in ion spectra because of the effects of charge on vibrational couplings and IR intensities. The 2058 cm^{-1} band is at frequency roughly twice that of the harmonic mode corresponding to the (H_2)COH out-of-plane torsion for protonated formaldehyde, which is calculated to be 1101 cm^{-1}. If anharmonicity is included in the calculation of the energy of this overtone using second order vibrational perturbation theory, as implemented in Gaussian03[34] at the MP2/6-311+G(d,p) level of theory, the overtone is reduced to 2090 cm^{-1}, close to the position of the unassigned band. To evaluate the feasibility of the assignment of this band to the overtone in the torsion, we performed a one-dimensional scan of the (H_2)COH torsion mode, while requiring that the argon atom remain coplanar with the CH_2 group. As expected, this motion induces a change in the component of the dipole moment along the axis perpendicular to the molecular plane (the c-axis) varying linearly with displacement of the O-H hydrogen atom off of the molecular plane (see Figure 5.11). The dipole moment along the a-axis, which lies nearly parallel to the OH bond in the equilibrium geometry, varies quadratically with the displacement along the (H_2)COH torsion angle. The calculated potential and dipole functions are fit to quadratic polynomials in the displacement of the torsion angle from its value at the minimum energy geometry. These curves are used to evaluate the vibrational wave functions (1-d) and with these the intensities of the fundamental and first overtone in the torsion. This analysis yields an intensity for the overtone transition that is roughly 25% of the fundamental excitation, or comparable in intensity to the three low-frequency fundamentals in the spectrum (Figures 5.3 and 5.4). We therefore assign the 2058 cm^{-1} band to the overtone of this out-of-plane torsional band.

The origin of the overtone intensity in the (H_2)COH torsion comes from the response of the charge distribution in protonated formaldehyde when the interaction between the charged OH group and the argon is broken. Similar behavior has been reported previously in halide-water clusters.[41, 42] In both systems the fundamental transition arises from the displacement of a hydrogen atom that carries a large part of the excess charge away from the molecular plane. The overtone comes from the fact that as the

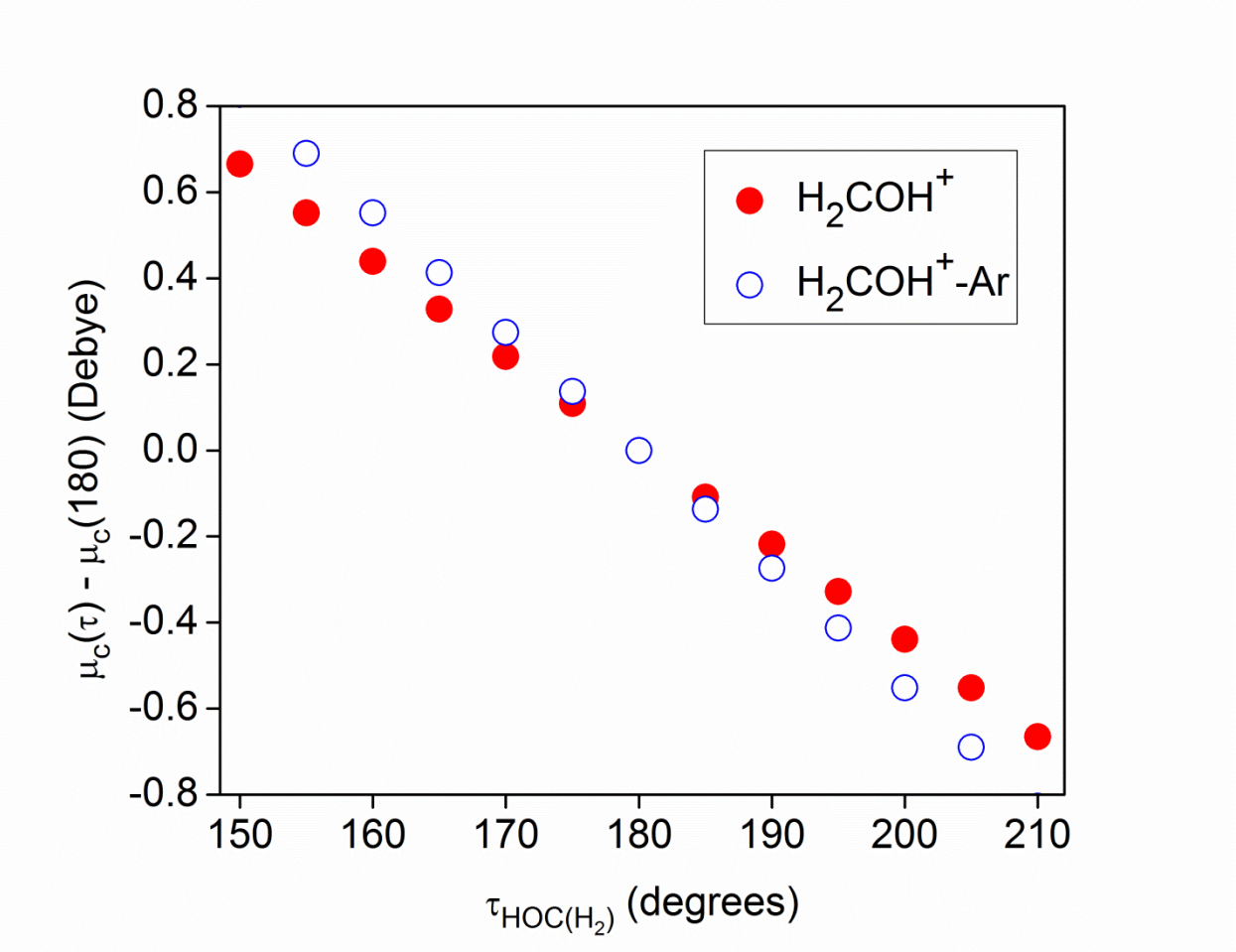

Figure 5.11. The variation in the component of the dipole moment along the *c*-axis, plotted as a function of the HOC(H_2) torsion angle (τ). The blue open circles are for the complex with argon present, while the red solid ones are for the complex without argon.

interaction between the argon atom and protonated formaldehyde is weakened by displacement of the hydrogen atom off of the molecular plane, the partial charge on argon becomes closer to zero, and the excess charge becomes localized on protonated formaldehyde. The charge redistribution is primarily in the molecular plane and these changes will be the same if the hydrogen is displaced above or below this plane. The angular dependence of the *a*-component of the dipole moment for bare protonated formaldehyde (red circles) and the complex of protonated formaldehyde with an argon atom (blue circles) are plotted in Figure 5.12. The intensities of the overtone transitions in these systems are proportional to the squares of the second derivatives of these curves. Because the bend dependence of the *a*-component of the dipole moment is only seen when the argon atom is present, this overtone is not likely to have strong IR intensity in the bare protonated formaldehyde. Thus, the occurrence of this overtone is a result of vibrational dynamics induced by argon.

The second unexpected feature in our spectrum at 3340 cm^{-1} lies 158 cm^{-1} to the blue of the shared proton O–H stretch. This interval is comparable to the harmonic frequency of the Ar–H stretch. Analogous bands have been seen in the spectra of halide-water systems[42] and protonated CO_2.[43] Again, we present here the results obtained by Anne McCoy at the Ohio State University. To analyze the origins of this band, particularly with respect to the source of its intensity, we develop an adiabatic model similar to one developed by Myshakin et al.[44] (see Appendix). Using the harmonic frequencies of the O–H and Ar–H stretches along with the cubic force constant that is quadratic in the O–H stretch displacement and linear in the Ar–H stretch displacement, we predict an intensity of the combination band that is roughly 4% that of the O−H stretching mode. The physical origins of the intensity comes from the fact that when the vibrational Hamiltonian is averaged over the probability amplitude for the ground and first excited states in the O–H stretch, the minimum in the resulting effective potential shifts to slightly larger values of the Ar–H distance.

Therefore, we have assigned all the bands measured in the photodissociation spectrum of the mass 31 cation. The most prominent features are the fundamentals of protonated formaldehyde;

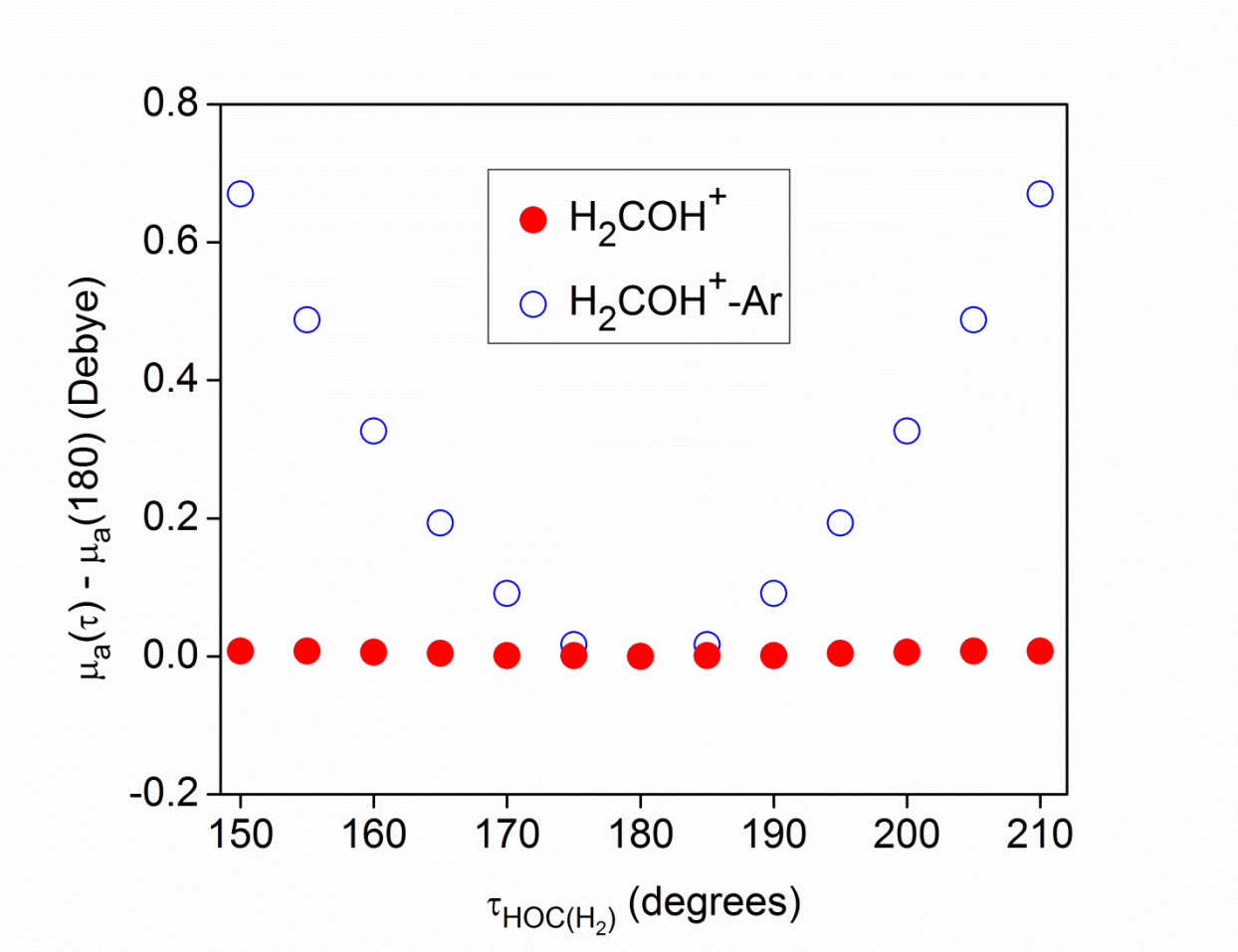

Figure 5.12. The variation in the component of the dipole moment along the *a*-axis, plotted -as a function of the HOC(H_2) torsion angle (τ). The blue open circles are for the complex with argon present, while the red solid ones are for the complex without argon. The large second derivative of this curve when the argon atom is present is responsible for the intensity of the overtone in the out-of-plane bend.

additional bands are assigned to an overtone of its out-of-plane torsional mode and a combination of its O–H stretch with an argon stretch. Protonated formaldehyde has long been recognized as the most stable form of this ion, and it is therefore no surprise that it would be present. Except for the strong O–H stretch, however, none of its vibrations have been reported previously. The O–H stretch here is strongly shifted because argon attaches on the proton, but the other five fundamentals are expected to have frequencies quite close (within 5-10 cm^{-1}) to their free-ion values. The torsional overtone (2058 cm^{-1}) and O–H/H–Ar combination (3340 cm^{-1}) band arise from the unusual vibrational dynamics resulting from attachment of argon to a cation. Our data here are also provide the first spectroscopic evidence for the metastable (triplet) methoxy cation. Methoxy is present at 2-10% of the amount of protonated formaldehyde, depending on the conditions. Its survival is heavily dependent on the efficient collisional cooling in our discharge/supersonic expansion source that makes it possible to stabilize this ion behind the barriers for curve crossing to protonated formaldehyde or dissociation to $HCO^+ + H_2$. It is therefore understandable that it has been difficult to isolate this isomer in the past. Like the O–H stretch of protonated formaldehyde, the C–H stretches of methoxy are perturbed significantly by the attachment of argon.

These data show that IR spectroscopy with a supersonic expansion source is useful to capture metastable ion structures resulting from complex reaction pathways and to reveal their spectral signatures. The rapid excitation followed by highly efficient collisional cooling provides a unique opportunity to sample structural configurations that are otherwise inaccessible. We have reported this behavior previously for $C_7H_9^+$ cations, which had co-existing isomeric structures (protonated toluene vs 1,3-dimethylcyclopentadienyl). Previous results from this laboratory also show similar behavior for $C_3H_3^+$ and $C_3H_5^+$ cations (cyclopropenyl vs propargyl; allyl vs 2-propenyl).[30] However, the present case is the most extreme example of this behavior yet, with triplet methoxy lying 96 kcal/mol higher in energy than protonated formaldehyde.

Conclusions

The m/z=31 cation, i.e., $[C,H_3,O]^+$, has been investigated with mass-selected ion infrared photodissociation spectroscopy using the method of argon tagging. The infrared spectrum contains sharp resonances from 1300 to 3500 cm^{-1}. Spectral analysis confirms the presence of both the protonated formaldehyde and methoxy structures; there is no clear evidence for the oxonio-methylene structure suggested previously by theory. Six fundamentals are detected for protonated formaldehyde; five of these are new. The O–H stretch detected with argon tagging is strongly red-shifted compared to this vibration in the isolated cation that was reported previously, and in the spectrum from neon tagging. The other vibrations are believed to be less perturbed by argon and to have frequencies close to their isolated ion values. Unusual vibrational dynamics arising from attachment of argon induces activity in the overtone of the torsion and in an argon combination with the O–H stretch. The methoxy detected is the triplet species which is metastable with respect to protonated formaldehyde. It lies far higher in energy (computed to be +96.0 kcal/mol), but can be stabilized behind a significant barrier. Rapid collisional cooling in the present experiment allows this species to be captured and studied. Ion production in our pulsed discharge/supersonic expansion source provides a convenient method with which to produce metastable ion structures and to document the IR spectra of these transient species.

References

(1) NIST Mass Spec Data Center, Stein, S.E., director, "Mass Spectra" in NIST Chemistry WebBook, NIST Standard Reference Database Number 69, Eds. Lindstrom, P.J. and Mallard, W.G., National Institute of Standards and Technology, Gaithersburg, MD, 20899, http://webbook.nist.gov, (retrieved May 14, 2012).

(2) Munson, M. S. B.; Franklin, J. L., Energetics of some gaseous oxygenated organic ions. *J. Phys. Chem.* **1964**, *68* (11), 3191-3196.

(3) Haney, M. A.; Patel, J. C.; Hayes, E. F., Nonempirical LCAO MO SCF and CI studies of the isomers of CH_3O^+. *J. Chem. Phys.* **1970**, *53* (10), 4105-4106.

(4) Bowen, R. D.; Williams, D. H., CH_3O^+ and $C_2H_5O^+$: high barriers to isomerisation and low barriers to symmetry-allowed 1,1-elimination. *J. Chem. Soc., Chem. Commun.* **1977**, (11), 378-380.

(5) Schleyer, P. V. R.; Jemmis, E. D.; Pople, J. A., 'CH_3O^+' and CH_2OH^+: High barriers to isomerization. *J. Chem. Soc., Chem. Commun.* **1978**, (5), 190-191.

(6) Dill, J. D.; Fischer, C. L.; McLafferty, F. W., Collisional activation and theoretical studies of gaseous COH_3^+ ions. *J. Am. Chem. Soc.* **1979**, *101* (22), 6531-6534.

(7) Bursey, M. M.; Hass, J. R.; Harvan, D. J.; Parker, C. E., Consequences of charge reversal in gaseous alkoxide ions. Oxenium ions. *J. Am. Chem. Soc.* **1979**, *101* (19), 5485-5489.

(8) Nobes, R. H.; Radom, L.; Rodwell, W. R., Influence of basis set and electron correlation on calculated barriers to 1,2-hydrogen shifts. The oxoniomethylene cation: A new CH_3O^+ isomer? *Chem. Phys. Lett.* **1980**, *74* (2), 269-272.

(9) Hoffmann, M. R.; Schaefer, H. F., Hydroxycarbene (HCOH) and protonated formaldehyde - 2 potentially observable inter-stellar molecules. *Astrophys. J.* **1981**, *249* (2), 563-565.

(10) Bouma, W. J.; Nobes, R. H.; Radom, L., On the nature of the 'methoxy' cation. *Org. Mass Spectrom.* **1982**, *17* (7), 315-317.

(11) Gilman, J. P.; Hsieh, T.; Meisels, G. G., The unimolecular decomposition rates of energy selected methylnitrite and deuterated methylnitrite ions. *J. Chem. Phys.* **1983**, *78* (6), 3767-3773.

(12) Burgers, P. C.; Holmes, J. L., The generation of triplet methoxy cations. *Org. Mass Spectrom.* **1984**, *19* (9), 452-456.

(13) Holmes, J. L.; Hop, C. E. C. A.; Terlouw, J. K., Does the unimolecular dissociation of ionized methyl acetate produce $CH_3O^{\cdot}$ or CH_2OH radicals? *Org. Mass Spectrom.* **1986**, *21* (11), 776-778.

(14) Zappey, H.; Ingemann, S.; Nibbering, N. M., Gas-phase ion-molecule reactions of the CH_3O^+ cation. *J. Am. Soc. Mass. Spectrom.* **1992**, *3* (5), 515-517.

(15) Uggerud, E.; Helgaker, T., Dynamics of the reaction $CH_2OH^+ \rightarrow CHO^+ + H_2$. Translational energy release from ab initio trajectory calculations. *J. Am. Chem. Soc.* **1992**, *114* (11), 4265-4268.

(16) Yarkony, D. R., Theoretical studies of spin-forbidden radiationless decay in polyatomic systems: Insights from recently developed computational methods. *J. Am. Chem. Soc.* **1992**, *114* (13), 5406-5411.

(17) Kuo, S.-C.; Zhang, Z.; Klemm, R. B.; Liebman, J. F.; Stief, L. J.; Nesbitt, F. L., Photoionization of hydroxymethyl (CD_2OH and CD_2OD) and methoxy (CD_3O) radicals: Photoion efficiency spectra, ionization energies, and thermochemistry. *J. Phys. Chem.* **1994**, *98* (15), 4026-4033.

(18) Lee, T. G.; Park, S. C.; Kim, M. S., Reaction dynamics of the four-centered elimination $CH_2OH^+ \rightarrow CHO^+ + H_2$: Measurement of kinetic energy release distribution and classical trajectory calculation. *J. Chem. Phys.* **1996**, *104* (12), 4517-4529.

(19) Suárez, D.; Sordo, T. L., Ab initio study of the H_2 elimination from CH_2OH^+, $CH_2NH_2^+$, and CH_2SH^+. *J. Phys. Chem. A* **1997**, *101* (8), 1561-1566.

(20) Aschi, M.; N. Harvey, J.; A. Schalley, C.; Schroder, D.; Schwarz, H., Reappraisal of the spin-forbidden unimolecular decay of the methoxy cation. *Chem. Commun.* **1998**, (5), 531-533.

(21) Harvey, J. N.; Aschi, M., Spin-forbidden dehydrogenation of methoxy cation: a statistical view. *Phys. Chem. Chem. Phys.* **1999**, *1* (24), 5555-5563.

(22) Zhu, X. J.; Ge, M. F.; Wang, J.; Sun, Z.; Wang, D. X., First experimental observation on different ionic states of both methylthio ($CH_3S^{\cdot}$) and methoxy ($CH_3O^{\cdot}$) radicals. *Angew. Chem. Int. Ed.* **2000**, *39* (11), 1940-1943.

(23) Amano, T.; Warner, H. E., Laboratory detection of protonated formaldehyde (H_2COH^+). *Astrophys. J.* **1989**, *342* (2), L99-L101.

(24) Dore, L.; Cazzoli, G.; Civis, S.; Scappini, F., Extended measurements of the millimeter-wave spectrum of H_2COH^+. *Chem. Phys. Lett.* **1995**, *244* (1-2), 145-148.

(25) Ohishi, M.; Ishikawa, S.; Amano, T.; Oka, H.; Irvine, W. M.; Dickens, J. E.; Ziurys, L. M.; Apponi, A. J., Detection of a new interstellar molecular ion, H_2COH^+ (protonated formaldehyde). *Astrophys. J.* **1996**, *471* (1), L61-L64.

(26) Del Bene, J. E.; Gwaltney, S. R.; Bartlett, R. J., Base Properties of H_2CO in the Excited $1n\rightarrow\pi^*$ State. *J. Phys. Chem. A* **1998**, *102* (26), 5124-5127.

(27) Blowers, P.; Masel, R. I., Calculated vibrational spectra for CH_nOH_m species. *J. Phys. Chem. A* **1999**, *104* (1), 34-44.

(28) Castro, M. E.; Nino, A.; Munoz-Caro, C., Structural and vibrational theoretical analysis of protonated formaldehyde in its (X) ^{1}Ã' ground electronic state. *Theor. Chem. Acc.* **2008**, *119* (4), 343-354.

(29) Sears, K. C.; Ferguson, J. W.; Dudley, T. J.; Houk, R. S.; Gordon, M. S., Theoretical investigation of small polyatomic ions observed in inductively coupled plasma mass spectrometry: H_xCO^+ and $H_xN_2^+$ (x=1, 2, 3). *J. Phys. Chem. A* **2008**, *112* (12), 2610-2617.

(30) Duncan, M. A., Infrared laser spectroscopy of mass-selected carbocations. *J. Phys. Chem. A* **2012**, *116* (47), 11477-11491.

(31) Cornett, D. S.; Peschke, M.; LaiHing, K.; Cheng, P. Y.; Willey, K. F.; Duncan, M. A., Reflectron time-of-flight mass spectrometer for laser photodissociation. *Rev. Sci. Instrum.* **1992**, *63* (4), 2177-2186.

(32) Bosenberg, W. R.; Guyer, D. R., Broadly tunable, single-frequency optical parametric frequency-conversion system. *J. Opt. Soc. Am. B* **1993**, *10* (9), 1716-1722.

(33) Gerhards, M.; Unterberg, C.; Gerlach, A., Structure of a b-sheet model system in the gas phase: Analysis of the C=O stretching vibrations. *Phys. Chem. Chem. Phys.* **2002**, *4* (22), 5563-5565.

(34) Frisch, M. J., et al., Gaussian 03 (Revision B.02). Gaussian, Inc.: Pittsburgh, PA, 2003.

(35) Merrick, J. P.; Moran, D.; Radom, L., An evaluation of harmonic vibrational frequency scale factors. *J. Phys. Chem. A* **2007**, *111* (45), 11683-11700.

(36) Shimanouchi, T., Molecular Vibrational Frequencies. In *NIST Chemistry WebBook: NIST Standard Reference Database Number 69* [Online] Linstrom, P. J.; Mallard, W. G., Eds. National Institute of Standards, Technology: Gaitherbburg, MD 20899, 1972. http://webbook.nist.gov.

(37) Dulcey, C. S.; Hudgens, J. W., Multiphoton ionization spectroscopy and vibrational analysis of a 3p Rydberg state of the hydroxymethyl radical. *J. Chem. Phys.* **1986**, *84* (10), 5262-5270.

(38) Johnson, R. D.; Hudgens, J. W., Structural and thermochemical properties of hydroxymethyl (CH_2OH) radicals and cations derived from observations of $\tilde{B}\ ^2A'(3p) \leftarrow \tilde{X}\ ^2A''$ electronic spectra and from ab initio calculations. *J. Phys. Chem.* **1996**, *100* (51), 19874-19890.

(39) Dyke, J. M.; Ellis, A. R.; Jonathan, N.; Keddar, N.; Morris, A., Observation of the CH_2OH radical in the gas phase by vacuum ultraviolet photoelectron spectroscopy. *Chem. Phys. Lett.* **1984**, *111* (3), 207-210.

(40) Botschwina, P.; Oswald, R., On the equilibrium structures of the complexes $H_2C_3H^+\cdot$Ar and c-$C_3H_3^+\cdot$Ar: Results of explicitly correlated coupled cluster calculations. *J. Chem. Phys.* **2011**, *134* (4), 044305.

(41) Roscioli, J. R.; Diken, E. G.; Johnson, M. A.; Horvath, S.; McCoy, A. B., Prying apart a water molecule with anionic H-bonding: A comparative spectroscopic study of the $X^-\cdot$H2O (X = OH, O, F, Cl, and Br) binary complexes in the 600−3800 cm^{-1} region. *J. Phys. Chem. A* **2006**, *110* (15), 4943-4952.

(42) Horvath, S.; McCoy, A. B.; Elliott, B. M.; Weddle, G. H.; Roscioli, J. R.; Johnson, M. A., Anharmonicities and isotopic effects in the vibrational spectra of $X^-\cdot H_2O$, ·HDO, and $\cdot D_2O$ [X = Cl, Br, and I] binary complexes. *J. Phys. Chem. A* **2010**, *114* (3), 1556-1568.

(43) Douberly, G. E.; Ricks, A. M.; Ticknor, B. W.; Duncan, M. A., Structure of protonated carbon dioxide clusters: Infrared photodissociation spectroscopy and ab initio calculations. *J. Phys. Chem. A* **2008**, *112* (5), 950-959.

(44) Myshakin, E. M.; Jordan, K. D.; Sibert, E. L.; Johnson, M. A., Large anharmonic effects in the infrared spectra of the symmetrical CH3NO2−·(H2O) and CH3CO2−·(H2O) complexes. *J. Chem. Phys.* **2003**, *119* (19), 10138-10145.

CHAPTER 6

UBIQUITOUS INTERSTELLAR MOLECULES WITH RADICALLY DIFFERENT CATION STRUCTURES: INFRARED SPECTROSCOPY OF FORMALDEHYDE AND METHANOL CATIONS

Introduction

Ions play a vital role in astrochemistry, and their structures underlie the significance of their chemical reactivity in the low densities of interstellar space.[1-6] Several organic molecules have been detected in interstellar space, including the well-known neutral formaldehyde and methanol molecules.[7-10] In fact, the discovery of formaldehyde marked the start of the study of interstellar organic chemistry.[11] Since their first recorded observations, these molecules have been found in nearly every type of interstellar environment,[11-19] and their astrochemical roles vary richly by environment.[12, 20-23] They can exist in their neutral or ionic forms, depending on the environment.[3-6] This work investigates the structure and bonding of the cationic forms of formaldehyde $[C,H_2,O]^+$and methanol $[C,H_4,O]^+$ via infrared spectroscopy.

$[C,H_2,O]^+$ has been the subject of mass spectrometric studies for many years.[24-34] Two important structures are recognized, the formaldehyde cation (CH_2O^+) and hydroxymethylene cation ($CHOH^+$). The oxonium ion (COH_2^+) was proposed on the basis of computational studies,[35] but there is apparently no experimental evidence for this structure. Photoionization/fragmentation studies of methanol and its isotopologues reveal that two fragments at m/z = 30 with roughly equal importance are observed, suggesting that two structural isomers exist with comparable stabilities.[29, 30] The collisional dissociation of a variety of ions

having m/z = 30 produces fragmentation with relatively abundant CH_2^+ and O^+ ions (from formaldehyde), or CH^+ and OH^+ ions (from methanol and cyclopropanol), suggesting that CH_2O^+ and $CHOH^+$ are indeed the structures formed for this ion. Holmes and coworkers also suggested a barrier to interconversion between these two structures of at least 34 kcal/mol, based on appearance energies for metastable decay of m/z = 30 ions to HCO^+ and H.[32] Numerous theoretical studies have been employed for this system.[35-38] The best theoretical results from the literature place $HCOH^+$ higher in energy than the global minimum structure, H_2CO^+, by 5.5 kcal/mol.[36] These results are completely consistent with the thermochemical data.[30, 32] Theoretical studies also predict a substantial barrier (+49 kcal/mol)[36] to rearrangement between these similarly energetic isomers, again consistent with the experimental data.[32] Interestingly, the energetics computed at the MP2 level of theory are incorrect not only in terms of the relative energies but also for the correct energy *ordering* of formaldehyde and hydroxymethylene ions.[37] Formaldehyde cation has also been studied with electron spin resonance (ESR) spectroscopy[39] and photoelectron spectroscopy.[40-44] To our knowledge, the infrared spectrum for hydroxymethylene cation has never been observed, although it has been predicted before.[45] The present work provides spectroscopic evidence for CH_2O^+ and $CHOH^+$ with infrared photodissociation spectroscopy.

The $[C,H_4,O]^+$ ion has been the subject of numerous mass spectrometric studies.[46-50] Two isomers are known, the methanol cation (CH_3OH^+) and the methyleneoxonium ion ($CH_2OH_2^+$), and it is not generally appreciated that the conventional structure is <u>not</u> the more stable ion. The collision dissociation of ionized methanol having m/z = 32 produces fragmentation with an intense m/z = 15/14 peak ratio, as is expected for the conventional radical cation structure. However, when a variety of ions having m/z = 32 are produced from other methods (e.g.,

ionization of ethylene glycol), fragmentation with an intense m/z = 14 peak, and a virtually absent m/z = 15 peak is observed.[46] These results are consistent with the two structures of methanol cation and the methyleneoxonium ion. Ion mobility measurements confirm the presence of two isomers.[50] Thermochemical data suggests that the latter structure is more stable by about 7 kcal/mol.[47] Several theoretical studies confirm that $CH_2OH_2^+$, rather than CH_3OH^+, is the global minimum structure.[51-56] The more stable $CH_2OH_2^+$ is one of the simplest examples of a distonic isomer, a phrase coined by Radom and coworkers[57, 58] describing a radical cation structure with separated charge and radical sites. Isomerization to these more stable structures has been demonstrated for several conventional radical cations.[59-62] Furthermore, Holmes et. al. determined that a barrier to rearrangement between the isomers occurs as the rate-limiting step for dissociation of $CH_2OH_2^+$ to CH_2OH^+ + H, based on kinetic isotope effects.[48] Theoretical predictions agree that a large barrier to interconversion exists;[55, 56] interestingly, interactions with water, noble gases, and methanol itself are predicted to substantially lower this barrier.[63, 64] The conventional radical cation has been studied via ESR spectroscopy.[65] The infrared spectra has been predicted for methanol cation,[45] but no spectroscopy of any kind has been reported for the methyleneoxonium ion. Here we describe the infrared spectroscopy of $[C,H_4,O]^+$, produced via discharge of methanol or ethylene glycol, which shows that both methanol cation and methyleneoxonium ion structures are present.

Experimental Details

$[C,H_2,O]^+$ and $[C,H_4,O]^+$ ions are produced in a pulsed discharge/supersonic expansion of Ar, and/or He containing the ambient vapor pressure of methanol or ethylene glycol at room temperature. The ions are mass-selected in a reflectron time-of-flight mass spectrometer and

observed with infrared photodissociation spectroscopy.[66] Since a single IR photon does not contain enough energy to break a bond, we employ rare gas tagging. Thus, $[C,H_2,O]^+Ar$ ions are mass-selected, and IR absorption eliminates Ar. The fragment ion intensity is recorded versus the frequency of the photodissociation laser (OPO/OPA, LaserVision). CCSD(T) calculations are carried out as implemented in the CFOUR programming package.[67] The atomic natural orbital (ANO) basis of Almlöf and Taylor is used for C, H and O atoms. The Roos augmented double ζ ANO basis is used for Ar atoms. Smaller and larger contractions of the Taylor ANO basis are designated by ANO0 and ANO1, respectively. Theoretical computations are carried out at the B3LYP/6-311+G** and MP2/aug-cc-pVTZ levels of theory using the GAMESS software package.[68]

Results and Discussion

A typical mass spectrum is shown in Figure 6.1 for the ambient vapor pressure of methanol at room temperature seeded in an expansion of Ar. Clearly, a very rich mass spectrum is obtained from methanol in our ion source. Several peaks are observed in the low mass region (m/z > 100) corresponding to ionization/fragmentation products, and their clusters with neutral methanol and argon. Peaks from the m/z = 14 – 19 range correspond to CH_2^+, CH_3^+, O^+, OH_2^+ and OH_3^+ fragment ions. Carbocations of the form $C_2H_x^+$ (x = 1−3) are observed from m/z = 25−27, while (x = 4−7) could potentially coincide with CH_mO^+ carboxonium ions (m = 0−3) in the m/z = 28−31 range. Peaks at m/z = 32 and 33 correspond to $[C,H_4,O]^+$ and $[C,H_5,O]^+$. Reaction products are seen at higher mass-to-charge ratios, as are their clusters with methanol and argon.

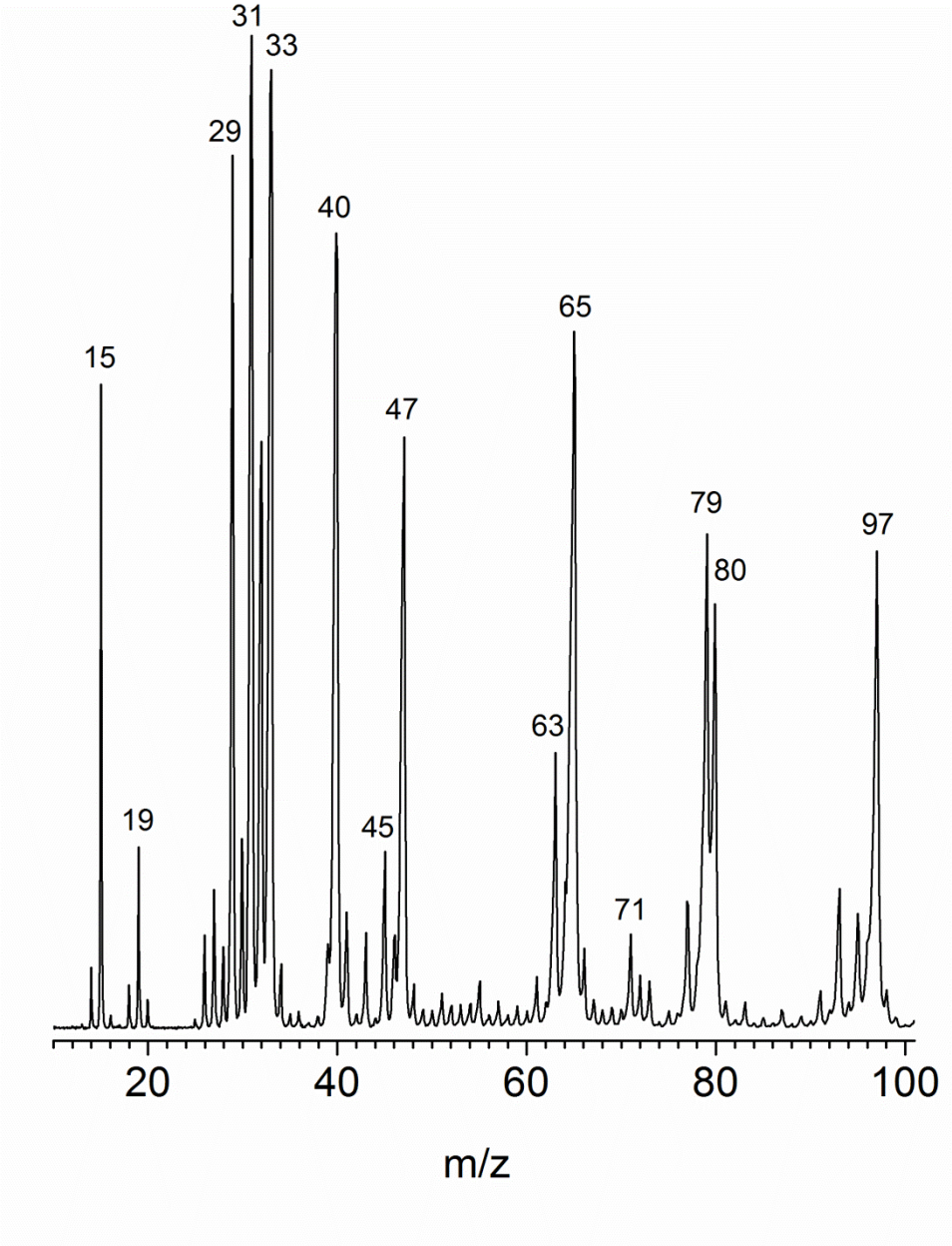

Figure 6.1. The mass spectrum of methanol in argon.

The infrared spectrum from 2600 − 3200 cm^{-1} for $[C,H_2,O]^+Ar$ observed by loss of Ar is presented in Figure 6.2. Two intense bands at 2757 and 2804 cm^{-1} dominate the spectrum. Two partially resolved doublets with moderate intensity are observed at 2892 and 3003 cm^{-1}, while three weaker bands are observed at 2835, 2925 and 2953 cm^{-1}. Seven bands are observed therefore in the C−H and O−H stretching region; clearly there are too many peaks to be assigned to just one structure. We also searched for signal in the fingerprint region; however, no bands were observed in the 600-2600 cm^{-1} range.

We use computational chemistry to determine the possible structures of $[C,H_2,O]^+$. Results obtained at the CCSD(T)/ANO1 level of theory are presented in Table 6.1. Three stable minima are found, with the global minimum structure being CH_2O^+. More energetic isomers are $CHOH^+$ and COH_2^+, with energies of +6.1 and +57.8 kcal/mol relative to the global minimum, respectively. These results are fully consistent with previous theoretical results.[35-38] The COH_2^+ isomer is much higher in energy and is not considered further here. We also find a first-order saddle point which lies 43.0 kcal/mol higher than CH_2O^+. Intrinsic reaction calculations at the B3LYP/6-311+G** of theory confirm this to be a transition state corresponding to a 1,2 hydrogen transfer reaction between hydroxymethylene and formaldehyde cations (see Figure 6.3). B3LYP overestimates the relative energies between the isomers (+8.2 kcal/mol) and the barrier height for reaction (+45.7 kcal/mol), compared to the CCSD(T) results; however, it does succeed in correctly predicting the relative energy ordering of the two structures, whereas the MP2 level of theory does not.[37] Thus, the B3LYP results should give qualitatively accurate results for such an IRC calculation. The structures of CH_2O^+ and $CHOH^+$ with argon were also investigated (see Table 6.1). Two binding sites for argon were found on each structure. We consider the CH_2O^+ ion first. The global minimum structure for CH_2O^+−Ar corresponds to

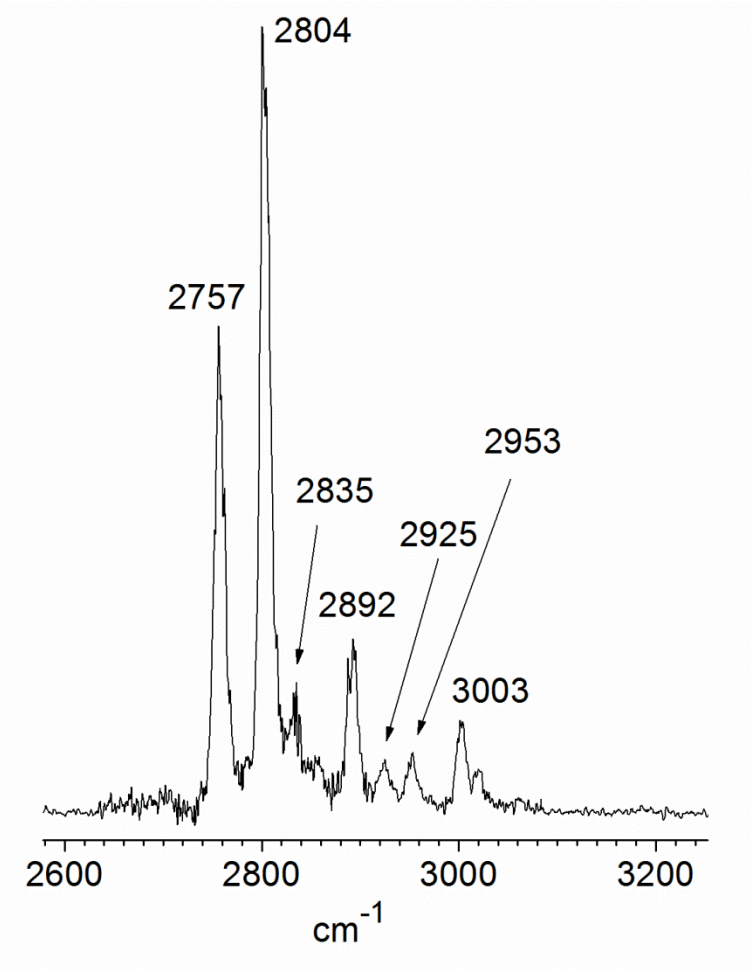

Figure 6.2. The infrared spectrum from 2600 – 3200 cm^{-1} of $[C,H_2,O]^+Ar$ recorded by loss of Ar.

Table 6.1. The relative energies for isomers of $[C,H_2,O]^+$ with and without argon. Relative energies and binding energies (B.E.) are corrected for zero-point vibrational energy.

Isomer	CCSD(T) [hartree]	ΔE (CCSD(T)) [kcal mol^{-1}]	B.E. [cm^{-1}]
H_2CO^+	-113.949160	0.0	
$CHOH^+$	-113.941522	+6.1	
COH_2^+	-113.857940	+57.8	
T.S.	-113.876515	+43.0	
CH_2O^+−Ar1	-640.961230	0.0	925
CH_2O^+−Ar2	-640.960992	+0.4	778
$CHOH^+$−Ar1	-640.958140	+3.3	1879
$CHOH^+$−Ar2	-640.952654	+7.0	606

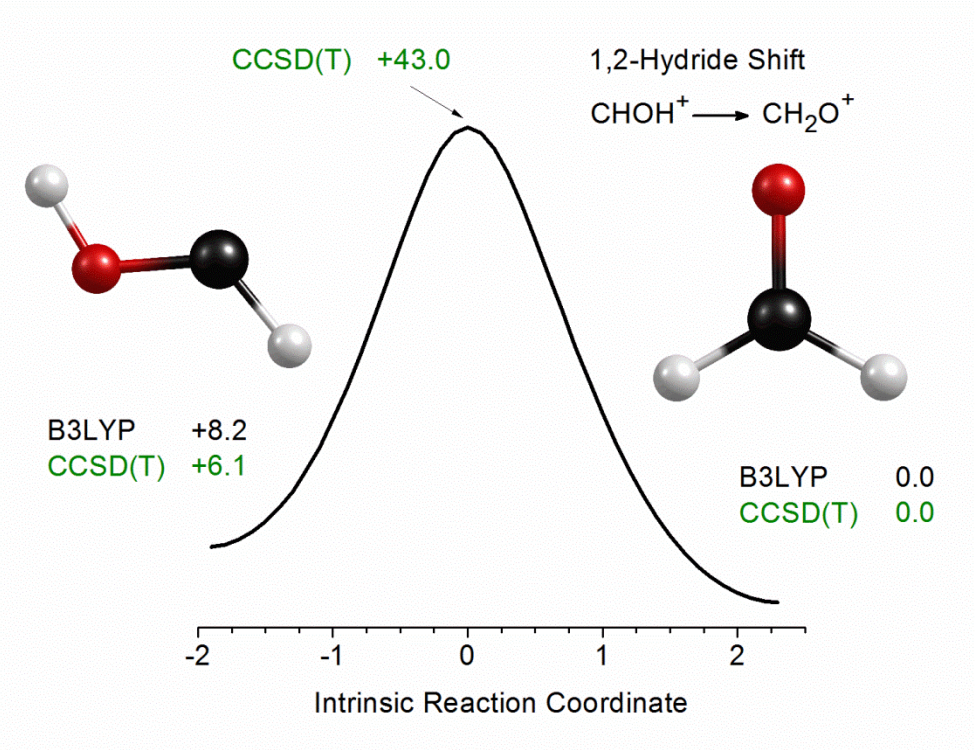

Figure 6.3. Results of an intrinsic reaction pathway calculation corresponding to the 1,2 hydride shift reaction $CHOH^+ \rightarrow CH_2O^+$ computed at the B3LYP/6-311+G** level of theory. Relative energies computed at the CCSD(T)/ANO1 level of theory are shown for comparison. Relative energies are corrected for zero-point vibrational energy effects.

argon binding to a CH group. An argon isomer corresponding to a binding site out of the molecular plane above the carbon, is found at essentially the same energy, only +0.4 kcal/mol higher in energy. The global minimum for $CHOH^+$−Ar corresponds to argon binding to the OH group. An argon isomer exists, with argon binding above the carbon out of the molecular plane. These structures have energies +3.3 and +7.0 kcal/mol relative to the global minimum for CH_2O^+−Ar.

We use computational chemistry to predict vibrational spectra for the $[C,H_2,O]^+$Ar ions to aid spectral assignment. We consider first the possibility that argon isomers may be responsible for the spectral complexity observed in our experiment. Vibrations for the two structures predicted by theory at the CCSD(T) level for CH_2O^+−Ar are presented in Table 6.2 and Figure 6.4 for comparison to our infrared spectrum (black trace, top). Frequencies are scaled by a factor of 0.951 to correct for vibrational anharmonicity. The scaling factor was derived from the predicted ν_1 frequency values for HCO^+ and HCO^+Rg (Rg=Ar,Ne), which are known experimentally.[69-71] Predicted frequencies for the untagged formaldehyde cation, corresponding to the symmetric and asymmetric C−H stretching modes, are represented as dashed red lines. Two bands are also predicted for CH_2O^+−Ar. If argon attaches to a CH group, it interacts strongly with one hydrogen, and induces a large red shift in both C−H stretching frequencies (blue trace, second from top). Similar effects are seen in the predicted spectra at the B3LYP level of theory (dark cyan trace, fourth from top). On the other hand, if argon attaches above the molecular plane, it weakly interacts with both hydrogens, and only a slight blue shift is observed for both bands (wine trace, third from top). Similar small shifts to higher frequency are observed at the B3LYP level (olive trace, bottom). Remarkably, the agreement between theory and experiment with respect to frequencies is poor. Preliminary results with collaborator John

Table 6.2. Predicted infrared bands (in cm^{-1}) for three isomers of $[C,H_2,O]^+Ar$. Intensities are given in km/mol.

CCSD(T) (Int)[a]	B3LYP (Int)[b]	Description
2551 (728.6)	2453 (957.8)	C−H_2 sym str CH_2O^+−Ar1
2688 (148.5)	2692 (143.7)	C−H_2 sym str CH_2O^+−Ar2
2737 (214.2)	2728 (313.1)	C−H_2 asym str CH_2O^+−Ar1
2790 (143.4)	2773 (186.4)	C−H_2 asym str CH_2O^+−Ar2
2896 (1902.2)	2894 (1834.8)	O−H str $CHOH^+$−Ar
2924 (361.2)	2930 (255.3)	C−H str $CHOH^+$−Ar

[a]scaled by 0.95. [b]scaled by 0.97. [c]This work.

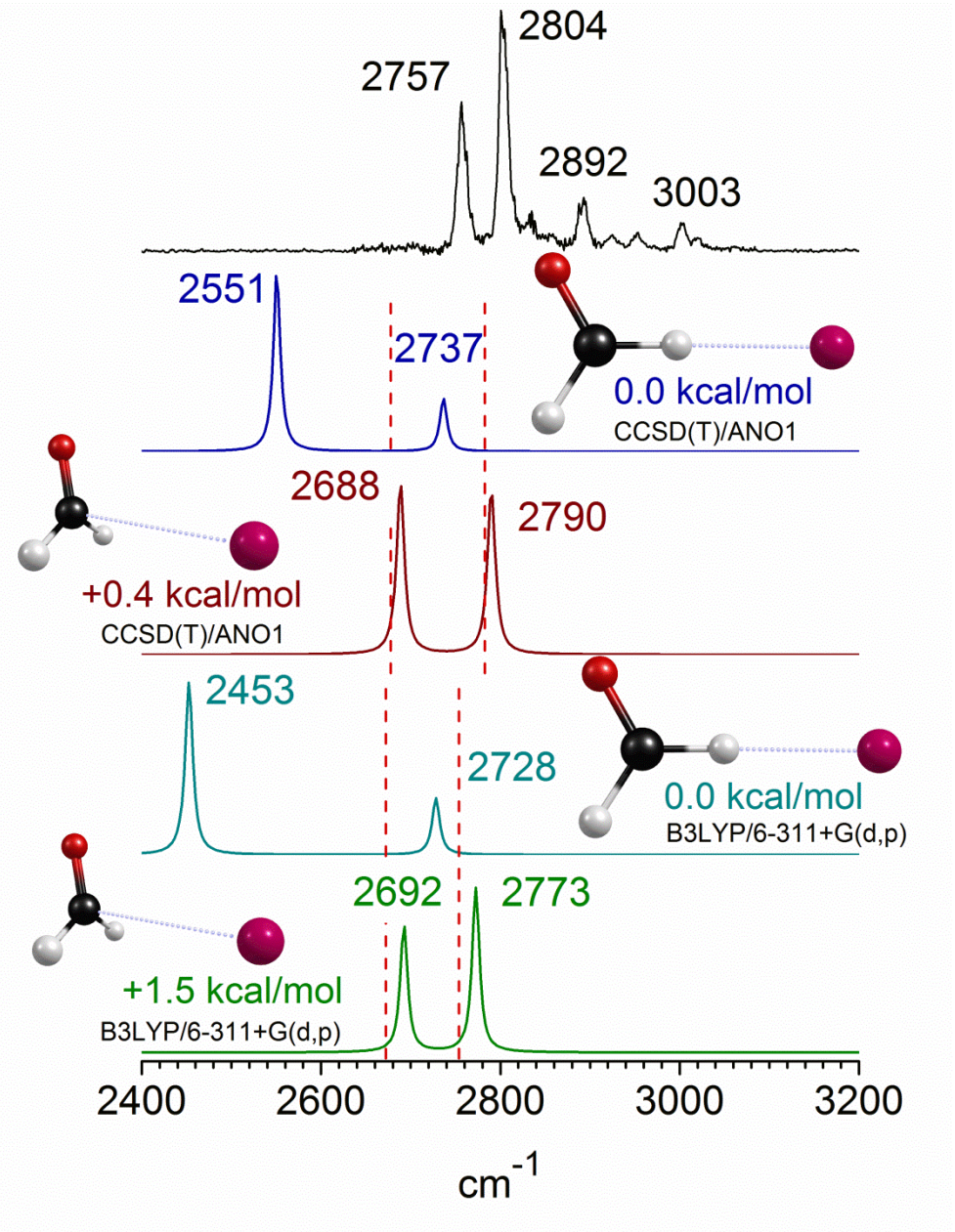

Figure 6.4. Comparison of the infrared spectrum of $[C,H_2,O]^+Ar$ to predicted spectra for Ar isomers of formaldehyde cation at two different levels of theory. Predicted vibrations corresponding to the isolated ion are shown as dashed red lines. Relative energies are corrected for zero-point vibrational energy effects.

Stanton at the University of Texas, Austin, have been obtained which use anharmonic corrections to the predicted frequencies of untagged formaldehyde cation. These results predict the symmetric and asymmetric C−H stretches at 2636 and 2722 cm^{-1}, respectively. It seems that the scaling factor used here produces artificially high values for these bands (2678 and 2781 cm^{-1} for the untagged species), suggesting that agreement for the tagged species is likely to be worse if similar anharmonic corrections are employed here! While there are stark discrepancies between experimental and theoretical values, there is agreement between the different levels of theory, specifically with the ordering of vibrations between the argon isomers, and the shifts induced by argon attachment.

Next, we consider the possibility that structural isomers may be responsible for the infrared spectrum. Predicted vibrations at the CCSD(T) level for the lowest energy structure of $CHOH^{+}$−Ar are presented in Table 6.2 and Figure 6.5 (wine trace, third from top). The higher energy isomer does not have any obvious bands predicted from 2400 to 3200 cm^{-1}, and is not considered further. Two bands are predicted for $CHOH^{+}$−Ar at 2896 and 2924 cm^{-1}, corresponding to the O−H and C−H stretching modes, respectively. Predicted frequencies at the B3LYP level (olive trace, bottom) are in good agreement with the higher level theory for this structure. The 2892 and 2925 cm^{-1} peaks appear to correspond to the $CHOH^{+}$−Ar vibrational bands both in band position and relative intensity. However, given the poor agreement between theory and experiment for CH_2O^{+}−Ar, it is impossible to definitively assign these peaks to hydroxymethylene cation.

We have also considered the possibility of rotational structure in our spectrum. Perpendicular-type transitions can have widely spaced rotational structure, and the peak separation is roughly equal to four times the A" rotational constant. For $CHOH^{+}$, we expect two

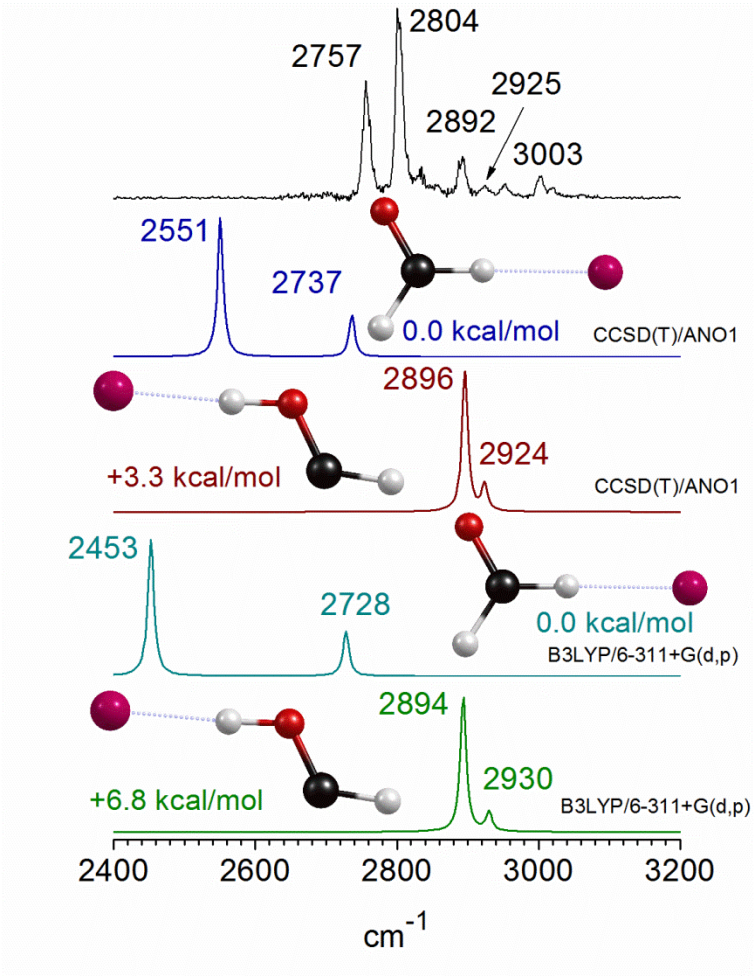

Figure 6.5. Comparison of the infrared spectrum of $[C,H_2,O]^+Ar$ to predicted spectra of two structures at two different levels of theory. Relative energies are corrected for zero-point vibrational energy effects.

parallel-type transitions, and thus do not expect to see rotational structure from this species. For formaldehyde cation, we expect one parallel-type and one perpendicular-type transition in the C−H stretching region. The same transitions are expected for the global minimum CH_2O^+−Ar complex, only with a reduced rotational constant. The global minimum structure of CH_2O^+−Ar has a ground state rotational constant, A", of 2.0 cm^{-1}, computed at the CCSD(T)/ANO1 level of theory (that of CH_2O^+ is 8.9 cm^{-1}). The observed spacings between the main peaks in our spectrum are roughly 100 cm^{-1}, which are too large to be explained by this type of rotational structure.

What is the source of the discrepancies between theory and experiment? And, how can this be sorted out? Being confident in the accuracy of our infrared spectrum, we have tried other experiments to aid the spectral assignment. Unfortunately, attempts to use other precursors to generate $[C,H_2,O]^+$ ions have been unsuccessful, in part due to insufficient signal levels produced at m/z = 30. Additionally, the infrared spectrum in the fingerprint region would provide additional support in assigning the spectrum, especially when more than one structure may be present. However, no signal is observed in this region, presumably due to inefficient photodissociation from high argon binding energies (see Table 6.1). Attempts to use other tag species (such as Ne or N_2) or multiple Ar tags, that would have lower binding energies, have also proved unsuccessful, due to low signal levels. Deuteration could also provide definitive evidence needed to assign the spectrum. We endeavored to obtain the spectrum for $[C,D_2,O]^+$, but initial attempts were unsuccessful in producing this ion from perdeuterated methanol. Nevertheless, we plan to persevere.

Let us now consider the infrared spectrum of $[C,H_4,O]^+$Ar obtained by loss of Ar. Figure 6.6 presents the spectrum from 2000 – 3800 cm^{-1} for the mass-selected ion obtained from

methanol. This spectrum is quite unusual in appearance. An intense peak at 3156 cm^{-1} dominates the spectrum, where an O−H stretch might be expected. Three strong bands are observed at 2473, 2573, and 2654 cm^{-1} in the C−H stretching region, as part of a larger progression of seven peaks which span the 2400 – 3000 cm^{-1} range. Lastly, a weaker band is observed at 3317 cm^{-1}, about 150 cm^{-1} to the blue of the largest peak. The spectrum was measured in the fingerprint region as well; however, no signal was observed there. We also recorded the spectrum of $[C,H_4,O]^+$Ne obtained by loss of Ne, as shown in Figure 6.7. Notably, much lower signal levels were achieved with Ne tagging; the spectrum is much simpler, however, with only a single strong band observed at 3373 cm^{-1}. No other signal is distinguishable from the noise in this spectrum.

As for the previous ion, we use theory to predict structures and energies of $[C,H_4,O]^+$ ions. We find two isomers that are stable minima on the potential energy surface. Their structures and relative energies are presented in Table 6.3 and Figure 6.8. The conventional radical cation of methanol is found to be +6.4 kcal/mol above its distonic isomer, methyleneoxonium ion, at the CCSD(T)/cc-pVTZ level of theory. The relative energies are completely consistent with previous theoretical[51-56] and experimental[47] results. We also find a first-order saddle point which lies +30.8 kcal/mol higher in energy than $CH_2OH_2^+$ at the B3LYP level of theory. This is confirmed to be a transition state for the 1,2-hydride shift between the two predicted isomers, consistent with previous results.[48, 55, 56] The structures of $[C,H_4,O]^+$ ions tagged with Ar and Ne were also investigated at the B3LYP level of theory (computations at the

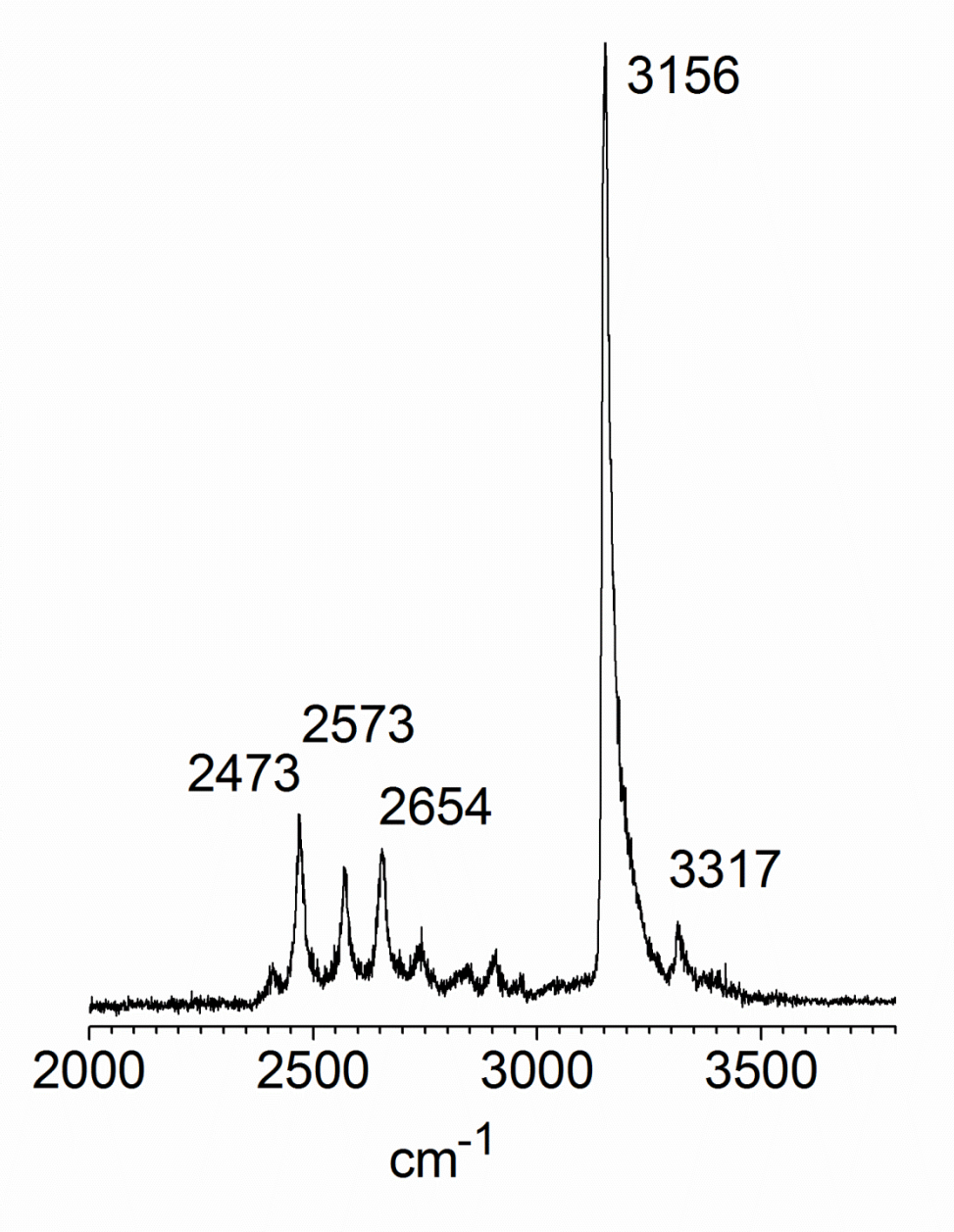

Figure 6.6. The infrared spectrum from 2000 – 3800 cm^{-1} of $[C,H_4,O]^+$AR recorded by loss of Ar.

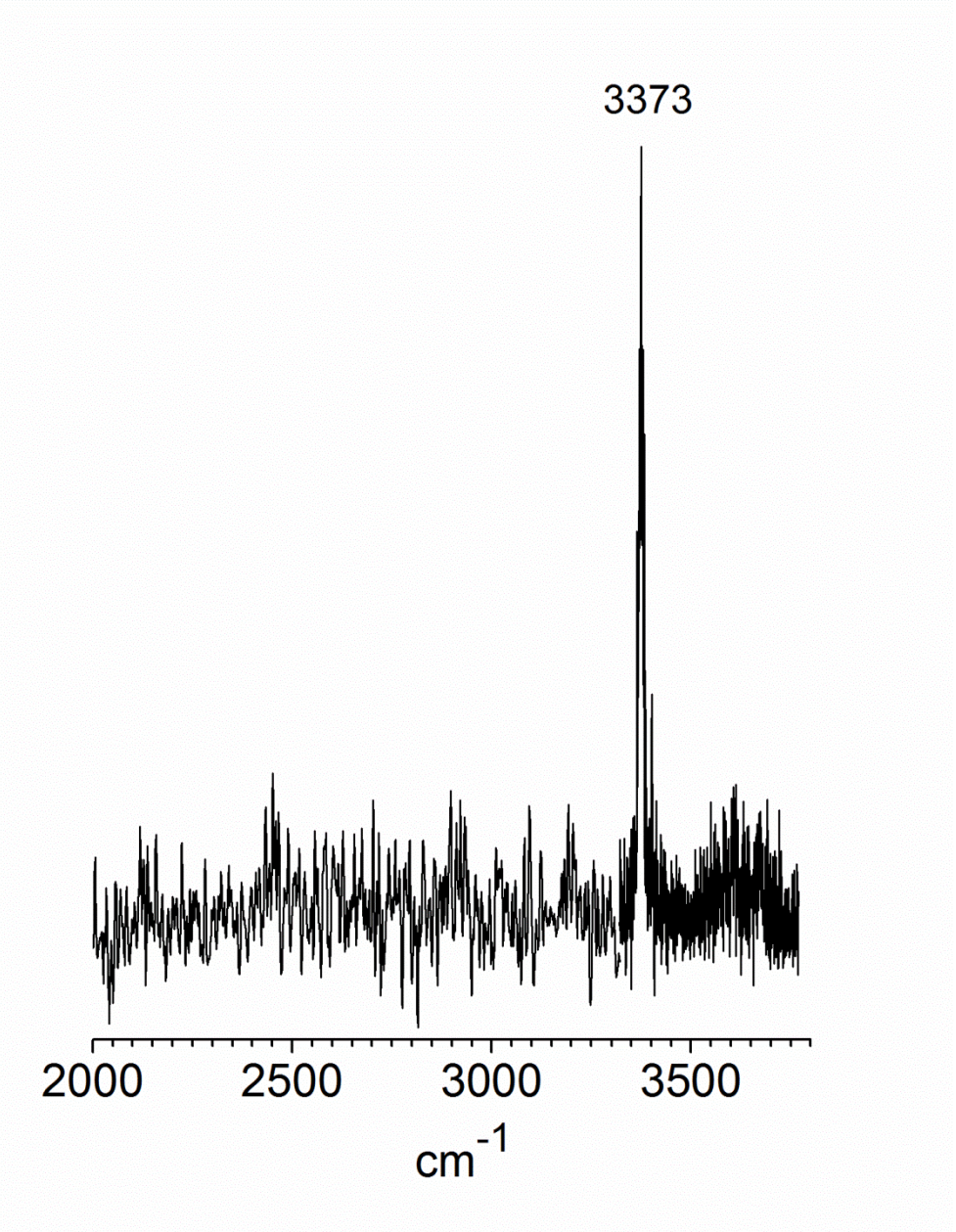

Figure 6.7. The infrared spectrum from 2000 – 3800 cm^{-1} of $[C,H_4,O]^+Ne$ recorded by loss of Ne.

Table 6.3. The relative energies for isomers of $[C,H_4,O]^+$ with and without argon. Relative energies and binding energies (B.E.) are corrected for zero-point vibrational energy.

Isomer	Description	CCSD(T) [hartree]	ΔE (CCSD(T)) [kcal/mol]	B3LYP [hartree]	ΔE (B3LYP) [kcal/mol]
$CH_2OH_2^+$	Methyleneoxonium ion	-115.167726	0.0	-115.325054	0.0
CH_3OH^+	Methanol radical cation	-115.154492	+6.4	-115.320783	+1.3
T.S.				-115.271529	+30.8
$CH_2OH_2^+$−Ar	Ar on OH			-642.822924	0.0
CH_3OH^+−Ar1	Ar on OH			-642.818067	+1.6
CH_3OH^+−Ar2	Ar on CH			-642.816198	+2.8
$CH_2OH_2^+$−Ne1	Ne on OH			-244.255697	0.0
$CH_2OH_2^+$−Ne2	Ne in CH_2 pocket			-244.253374	+1.1
$CH_2OH_2^+$−Ne3	Ne above CO			-244.253367	+1.1
CH_3OH^+−Ne1	Ne on OH			-244.251098	+1.4
CH_3OH^+−Ne2	Ne on CH (trans OH)			-244.249680	+2.2
CH_3OH^+−Ne3	Ne in CH_3 pocket			-244.249387	+2.3
CH_3OH^+−Ne4	Ne on CH (cis OH)			-244.249397	+2.3

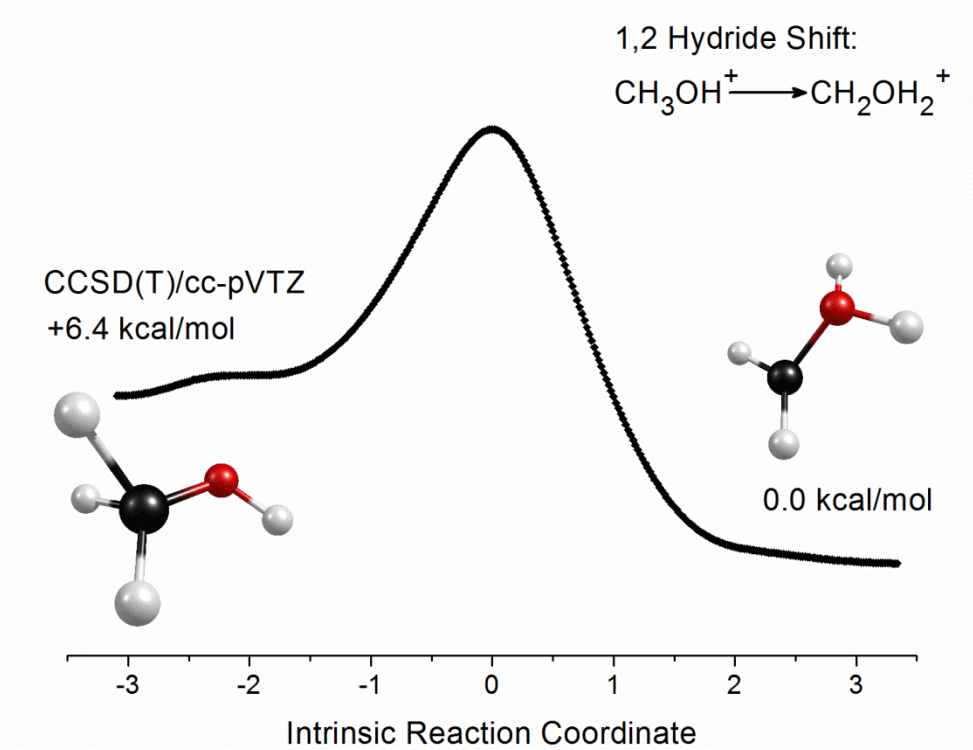

Figure 6.8. Results of an intrinsic reaction pathway calculation at the MP2/aug-cc-pVTZ level of theory corresponding to a 1,2-hydride shift from methanol cation (left inset) to methyleneoxonium ion (right inset). Relative energies are corrected for zero-point vibrational energy effects.

CCSD(T) level for the tagged species are prohibitively time consuming). These structures and their relative energies are presented in Table 6.3.

Figure 6.9 shows an expanded view of the infrared spectrum of $[CH_3OH^+]Ar$ compared to the predictions of theory for the methanol and methyleneoxonium ions with attached argon. It is immediately apparent that the main spectral feature can be assigned to the methanol cation with argon attached to the proton site (Figure 6.9, wine trace inset, second from top). The strong 3156 cm^{-1} band is reproduced reasonably well in position and intensity for the O−H stretch vibration. This feature is observed at 3373 cm^{-1} for CH_3OH^+ Ne tagging (see Figure 6.7). The different positions of this band result from the tag atoms binding to the proton, which induces a strong red shift compared to the vibration in the isolated ion (predicted at 3430 cm^{-1}). This is reproduced by theory (see Table 6.4), and has been observed for other ions where the tag attaches to a proton site.[66, 70, 71] Additionally, the shift induced by Ne is much smaller, consistent with previous results.[70, 71] Two bands are predicted in the C−H stretching region, at 2585 and 2673 cm^{-1}, corresponding to the symmetric and asymmetric C−H stretches of methanol cation. A third C−H stretch, corresponding to the CH bond with a cis configuration relative to the OH group, is predicted with much weaker intensity at 3073 cm^{-1}, and is not distinguishable in the predicted spectrum due to the strong intensity of the O−H stretch. As noted above, a progression of seven bands is observed in the C−H stretching region, with band positions at 2413, 2473, 2573, 2643, 2738, 2832, and 2902 cm^{-1}. One other isomer for CH_3OH^+Ar is predicted by theory, corresponding to Ar binding on a CH group, but its spectrum does not match any of these bands (see Figure 6.9, olive trace, third from top). Clearly, this region cannot be assigned based on these results alone.

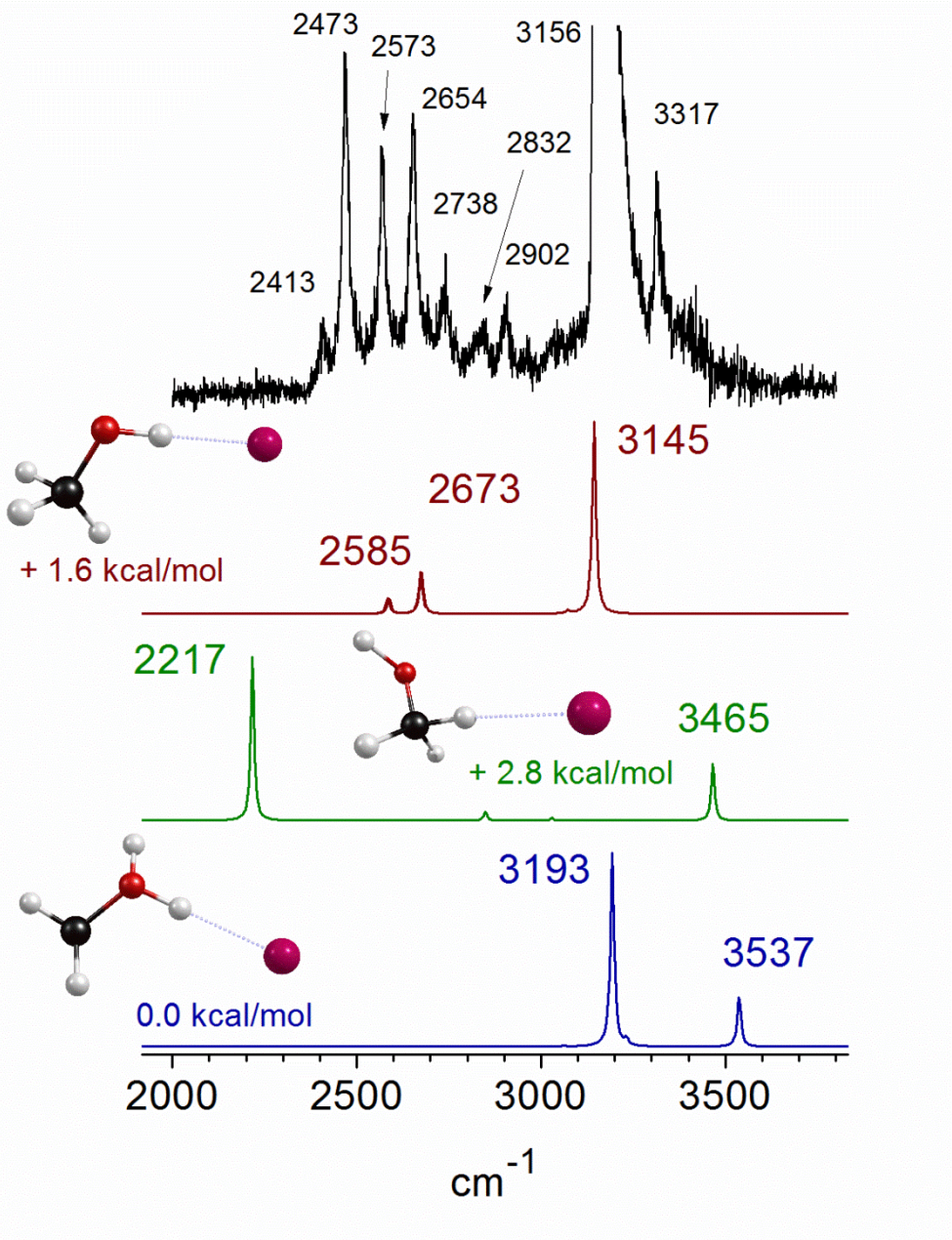

Figure 6.9. Comparison of the infrared spectrum of $[C,H_4,O]^+Ar$ to the predicted spectra for different isomers at the B3LYP/aug-cc-pVTZ level of theory. Relative energies are corrected for zero-point vibrational energy effects.

Table 6.4. Infrared bands (in cm^{-1}) assigned for three isomers of $[C,H_2,O]^+Ar$. Intensities are given in km/mol.

Exp	B3LYP (Int)[d] (CH_3OH^+)	B3LYP (Int)[d] ($CH_2OH_2^+$)	Assignment
2413			
2473			
2573			
2654			
2738			
2832			
2902			
3156	3145 (1251.7)		O−H str of CH_3OH^+Ar
3182[b]		3193 (1264.4)	symm O−H str of $CH_2OH_2^+Ar$
3317	3301 (52.5)		$\nu_{O-Hstr} + \nu_{Ar-Hstr}$ of CH_3OH^+Ar
3373[a]	3368 (590.4)		O−H str of CH_3OH^+Ne
3523[b,c]		3537 (326.5)	asymm O−H str of $CH_2OH_2^+Ar$

[a]From the spectrum of $[C,H_4,O]^+Ne$. [b]From the spectrum of $[C,H_4,O]^+Ar$ using an ethylene glycol precursor. [c]From the spectrum of $[C,H_4,O]^+Ar$ using a methanol precursor and hotter plasma conditions. [d]Scaled by a factor of 0.9682.

To investigate this further, we investigate assignments for these features involving overtones or combination bands, guided by past experience with similar systems. Such bands can be quite prominent in ion spectra because of the effects of charge on vibrational couplings and IR intensities. The peak at 2473 cm^{-1} is at a frequency roughly twice that of the harmonic mode corresponding to the OH bend towards the cis CH bond, predicted at 1307 cm^{-1}. If anharmonicity is included in the calculation of the energy of this overtone using second order vibrational perturbation theory, as implemented in Gaussian09[72] at the B3LYP/aug-cc-pVTZ level of theory, the overtone is reduced to 2469 cm^{-1}, close to the observed band position. Its predicted infrared intensity is 12.4 km/mol. It is possible that this overtone borrows intensity from one or both of the C−H stretches via vibrational coupling. A combination band is predicted at 2855 cm^{-1} (19.2 km/mol), corresponding to one quantum each of the symmetric C−H stretch and the OH torsional mode. Another overtone is predicted close to the 2832 cm^{-1} band at 2843 cm^{-1} (7.8 km/mol intensity), which corresponds to the CH_3 umbrella motion. Extra bands associated with a C−H stretch/bend overtone Fermi resonance have been observed before in the formate dimer anion.[73] The case of methanol cation is more complex, because of the possibility of two C−H stretches involved in Fermi resonances with the OH bend overtone, the CH_3 umbrella overtone, and the C−H stretch/OH torsion combination band. In collaboration with Anne McCoy, at the Ohio State University, we are currently investigating the vibrational dynamics associated with the band progression.

We now consider the unexpected feature at 3317 cm^{-1}, which lies 161 cm^{-1} to the blue of the shared proton O−H stretch. This interval is comparable to the harmonic frequency of the Ar−H stretch, and could results from a combination of this vibration with the O−H stretch. Analogous bands have been seen in the spectra of halide-water systems[74] and protonated CO_2,[75]

as well as our recent work on protonated formaldehyde.[76] We follow a similar approach here as utilized by Anne McCoy in the protonated formaldehyde system.[76] Using the harmonic frequencies of the O−H and Ar−H stretches along with the cubic force constant that is linear in the Ar−H stretch displacement and quadratic in the OH stretch displacement, we predict an intensity of the combination band that is roughly 4% that of the O−H stretching mode, and a frequency that is 156 cm^{-1} blue shifted from the O−H stretching band position. The intensity arises from a slight lengthening of the Ar−H bond distance due to vibrational averaging in the ground and first excited vibrational potentials. Thus, we assign the 3317 cm^{-1} band to this combination band.

We have assigned all of the obvious bands predicted for the lowest energy structure of CH_3OH^+Ar, and none of the methyleneoxonium bands appear in our spectrum. It would appear that the methanol cation is initially produced following the energetic ionization and fragmentation processes, and rapid, efficient cooling prevents any structural rearrangement from occurring. To estimate the temperature of the ions, we use the computed rotational constants of methanol cation tagged with argon to simulate a rotational contour for the O−H stretching band, and adjust its linewidth (FWHM) to match that in the experiment (see Figure 6.10, blue trace, bottom). This procedure is not perfect; the linewidth may also have contributions from predissociation. However, it is good enough for a rough estimate. Our normal cold discharge/expansion conditions using methanol give a rotational temperature of about 100 K, consistent with ion temperatures measured previously with this source.[66]

To investigate other structures on the potential surface, we first varied the precursor used to produce the m/z = 32 ion. Figure 6.11 presents the spectrum in the O−H stretching region of $[CH_3OH^+]Ar$ obtained by loss of Ar, using ethylene glycol as a precursor (black trace, top). The

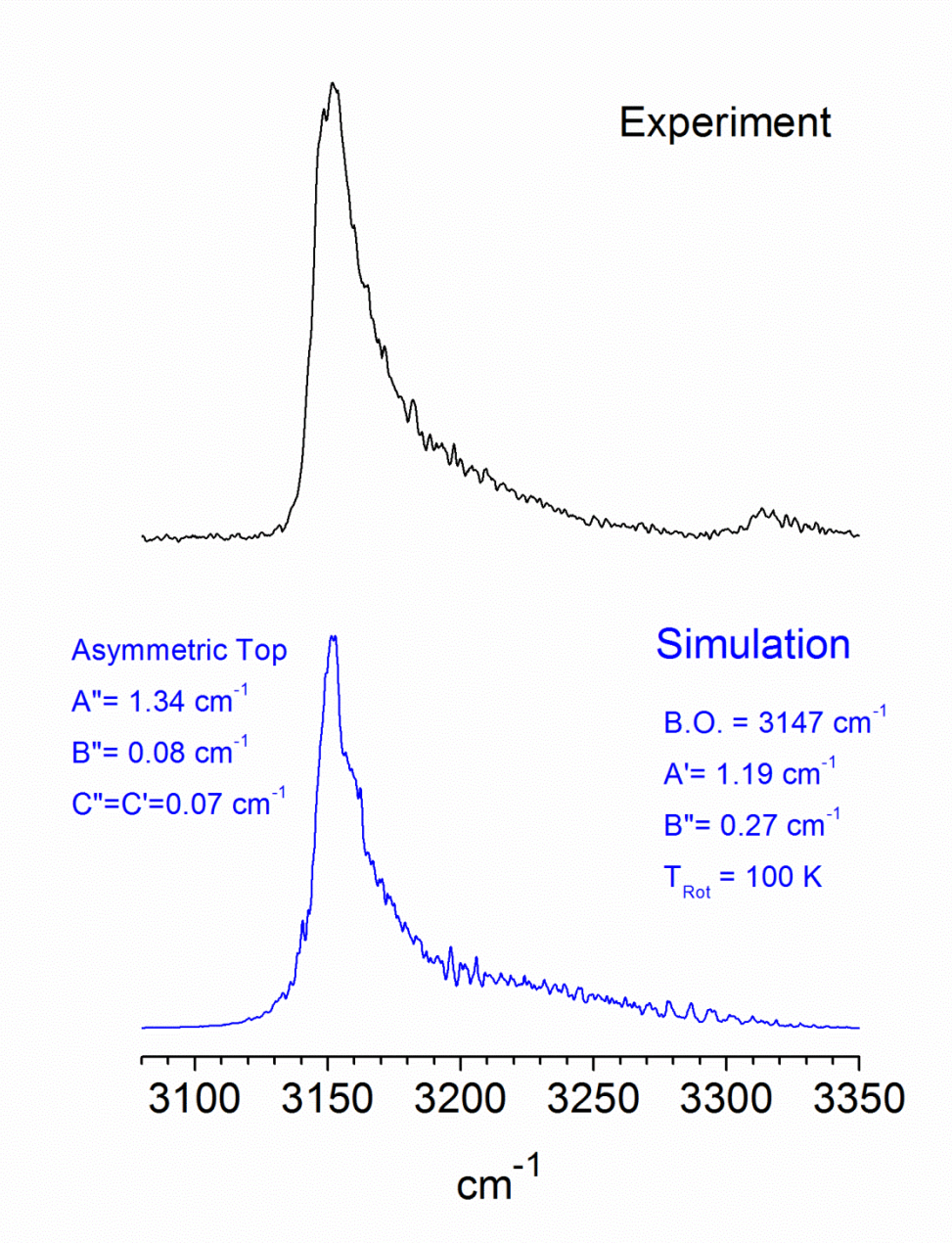

Figure 6.10. Comparison of the infrared spectrum of $[C,H_4,O]^+Ar$ to a rovibrational simulation using pGOPHER.

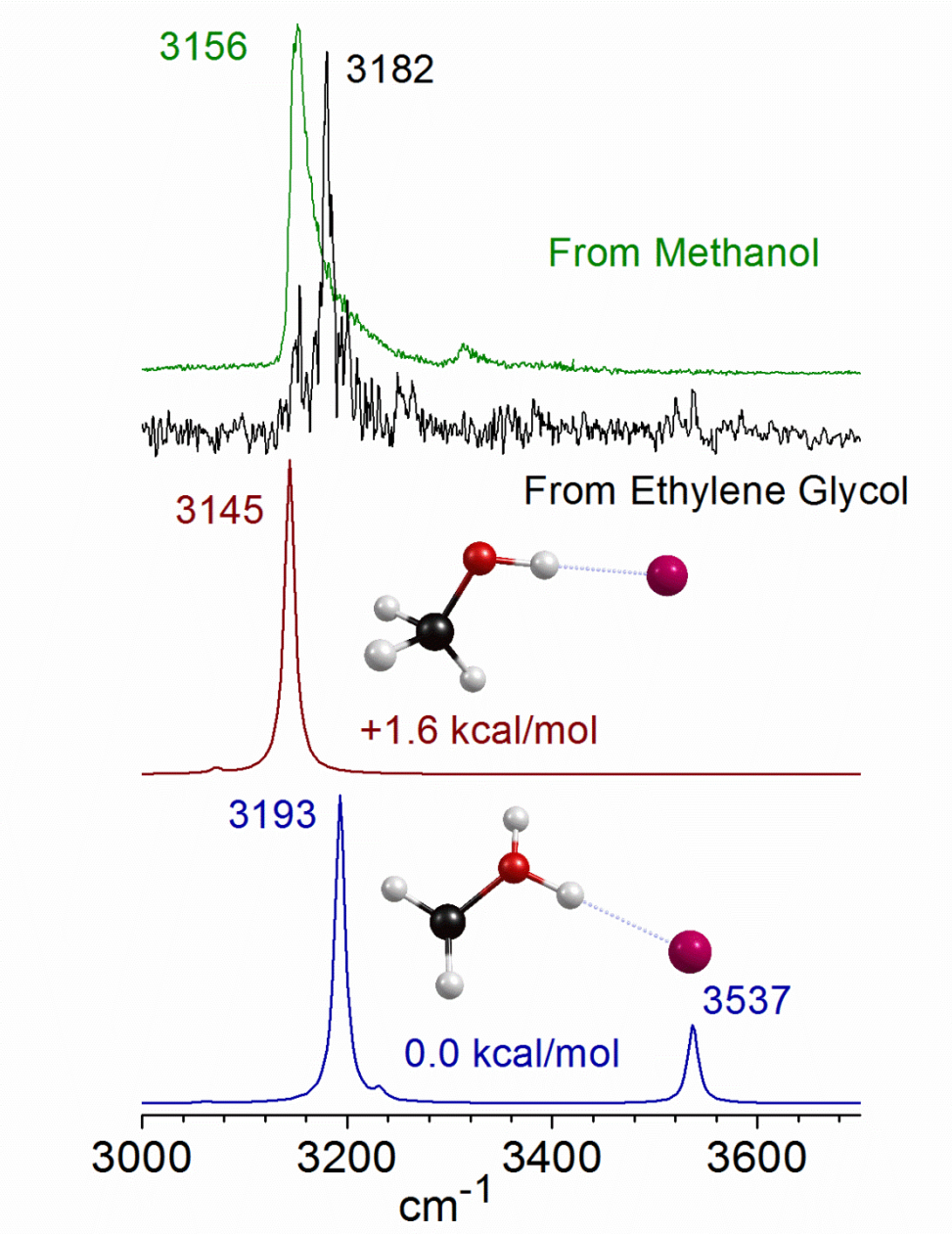

Figure 6.11. The infrared spectra of $[C,H_4,O]^+Ar$ generated using different precursors compared to the predictions from theory at the B3LYP/aug-cc-pVTZ level. Relative energies are corrected for zero-point vibrational energy effects.

original spectrum, obtained with methanol in the ion source, is shown in comparison (green trace, top). The new spectrum suffers from low signal levels, but one new peak appears at 3182 cm^{-1}. This band is clearly at a different position from that corresponding to the O−H stretch of CH_3OH^+Ar. The predicted spectrum for $CH_2OH_2^+Ar$ aids in the assignment of this band (royal trace, bottom). The new band corresponds to the symmetric O−H stretch of the methyleneoxonium ion. Due to the low signal levels, we cannot clearly distinguish the higher energy asymmetric stretch from the baseline. However, the appearance of the O−H stretch at 3182 cm^{-1} provides strong evidence that the lower energy structure is produced.

To investigate $CH_2OH_2^+Ar$ further, we varied the discharge conditions used to produce the ions, using methanol as the precursor. Given the barrier to rearrangement between the global minimum structure and the conventional radical cation,[48, 55, 56] the latter's survival depends on its cooling rate and efficiency in our source. The temperature of the plasma should therefore affect the trapping efficiency. To change the temperature of the ions, we increase the discharge voltage level and move its pulse timing relative to the center of the gas pulse. This simultaneously increases the heating of the plasma and spoils the collisional cooling. The comparison of the spectrum obtained with these hotter conditions to that with the normal cold plasma is shown in Figure 6.12. The rotational simulation under cold conditions is reproduced here and is vertically offset for clarity (blue trace, top). Based on the observed linewidths for the O−H stretching band, methanol cations have approximately the same temperature under both conditions, but a new band appears at 3523 cm^{-1}, where no signal is observed under the cold conditions. This peak corresponds to the asymmetric O−H stretch of methyleneoxonium. The lower frequency stretch observed at 3182 cm^{-1} (see Figure 6.11), overlaps significantly with the rotational tail of methanol cation's O−H stretch, and is not clearly distinguishable from the shoulder of this peak.

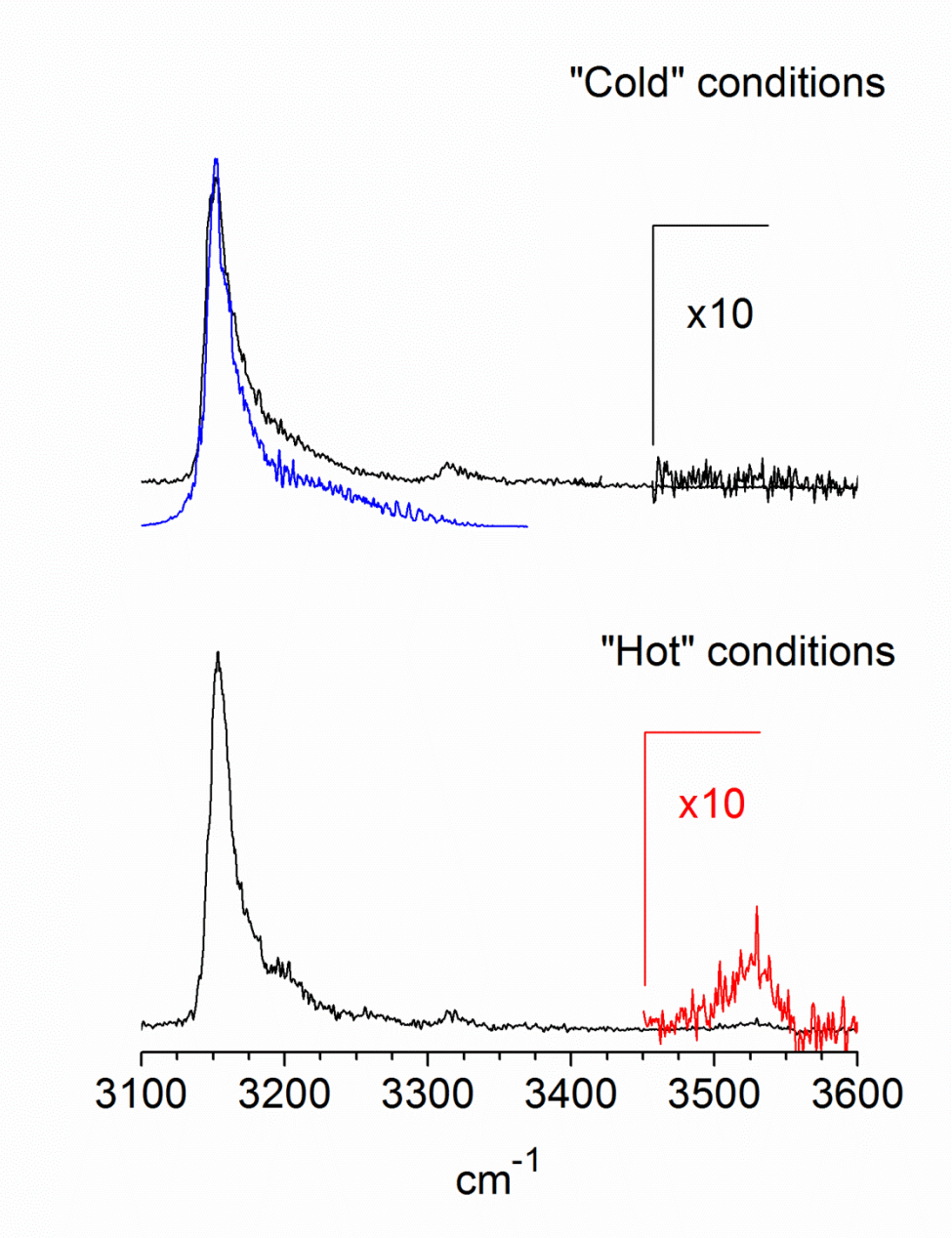

Figure 6.12. Comparison of infrared spectra for $[C,H_4,O]^+Ar$ using different discharge conditions. The ions are generated from methanol in the source.

Apparently, changing the discharge conditions activates new chemistry in the plasma, leading to production of the global minimum structure. Interestingly, the methanol cations are not heated to a significant degree. This is consistent with the qualitative aspects of the potential energy surface predicted previously;[48,55,56] the barrier(s) to interconversion (or dissociation) allow only the coldest subset of ions to survive in our experiment.

Conclusion

$[C,H_2,O]^+$ and $[C,H_4,O]^+$ were produced with the discharge/expansion source and the mass-selected ions were investigated with infrared spectroscopy. The infrared spectrum of $[C,H_2,O]^+$ contains several sharp resonances from 2750 to 3050 cm^{-1}. Spectral analysis is unable to definitively assign the bands to either the formaldehyde or hydroxymethylene cations, but more bands are observed than can be accounted for by either structure alone. Further investigations are therefore needed into the apparent discrepancies between experiment and theory. The spectrum of $[C,H_4,O]^+$ contains sharp features from 2400 cm^{-1} to 3500 cm^{-1}, when the ion is made using methanol in our source. A seven band progression is observed in the C−H stretching region and two peaks are seen in the O−H stretching region. Spectral analysis confirms the structure is that of the conventional methanol cation; there is no clear evidence for the lower energy methyleneoxonium structure in this spectrum. Three bands are assigned to fundamental vibrations of CH_3OH^+; all of these are new. The O−H stretch detected with argon tagging is strongly red-shifted compared to the same vibration detected with neon tagging and to the prediction for that of the isolated cation. The other vibrations have frequencies much closer to their isolated values. The lower energy methyleneoxonium ion is detected only when the precursor or source conditions are varied, suggesting that the conventional ion is indeed higher in

energy and can be stabilized behind a barrier to interconversion. Rapid collisional cooling in the present experiment allows this species to be captured and studied. Ion production in our pulsed discharge/supersonic expansion source provides a convenient method with which to produce and characterize transient ion species.

References

(1) Hartquist, T. W.; Williams, D. A., eds., *The Molecular Astrophysics of Stars and Galaxies*. Clarendon Press: Oxford, 1998.

(2) Tielens, A. G. G. M., *The Physics and Chemistry of the Interstellar Medium*. Cambridge University Press: Cambridge, U.K., 2005.

(3) Ziurys, L. M., The chemistry in circumstellar envelopes of evolved stars: Following the origin of the elements to the origin of life. *Proc. Natl. Acad. Sci.* **2006**, *103* (33), 12274-12279.

(4) Petrie, S.; Bohme, D. K., Ions in space. *Mass Spectrom. Rev.* **2007**, *26* (2), 258-280.

(5) Snow, T. P.; Bierbaum, V. M., Ion chemistry in the interstellar medium. *Annu. Rev. Anal. Chem.* **2008**, *1* (1), 229-259.

(6) Klemperer, W., Astronomical chemistry. *Annu. Rev. Phys. Chem.* **2011**, *62*, 173-184.

(7) Palmer, P.; Zuckerma.B; Buhl, D.; Snyder, L. E., Formaldehyde absorption in dark nebulae. *Astrophys. J.* **1969**, *156* (3P2), L147-&.

(8) Snyder, L. E.; Buhl, D.; Zuckerma, B.; Palmer, P., Microwave detection of interstellar formaldehyde. *Phys. Rev. Lett.* **1969**, *22* (13), 679-&.

(9) Ball, J. A.; Gottlieb, C. A.; Lilley, A. E.; Radford, H. E., Detection of methyl alcohol in Sagittarius. *Astrophys. J.* **1970**, *162* (3), L203-&.

(10) Zuckerma.B; Buhl, D.; Palmer, P.; Snyder, L. W., Observations of interstellar formaldehyde. *Astrophys. J.* **1970**, *160* (2), 485-&.

(11) Snyder, L. E., Interferometric observations of large biologically interesting interstellar and cometary molecules. *Proc. Natl. Acad. Sci.* **2006**, *103* (33), 12243-12248.

(12) Herbst, E.; Klemperer, W., Formation and depletion of molecules in dense interstellar clouds. *Astrophys. J.* **1973**, *185* (2), 505-533.

(13) Mutel, R. L.; Broderic.Jj; Carr, T. D.; Lynch, M.; Desch, M.; Warnock, W. W.; Klempere.Wk, Vlb observations of crab-nebula and wavelength dependence of interstellar scattering. *Astrophys. J.* **1974**, *193* (1), 279-282.

(14) Johansson, L. E. B.; Andersson, C.; Ellder, J.; Friberg, P.; Hjalmarson, A.; Hoglund, B.; Irvine, W. M.; Olofsson, H.; Rydbeck, G., Spectral scan of Orion-a and IRC + 10216 from 72 to 91 GHz. *Astron. Astrophys.* **1984**, *130* (2), 227-256.

(15) Tielens, A.; Hagen, W., Model-calculations of the molecular composition of inter-stellar grain mantles. *Astron. Astrophys.* **1982**, *114* (2), 245-260.

(16) Danks, A. C.; Encrenaz, T.; Bouchet, P.; Lebertre, T.; Chalabaev, A., The spectrum of comet P/Halley from 3.0 to 4.0 μm. *Astron. Astrophys.* **1987**, *184* (1-2), 329-332.

(17) Allamandola, L. J.; Sandford, S. A.; Valero, G. J., Photochemical and thermal evolution of interstellar precometary ice analogs. *Icar.* **1988**, *76* (2), 225-252.

(18) Mumma, M. J.; Reuter, D. C., On the identification of formaldehyde in Halleys comet. *Astrophys. J.* **1989**, *344* (2), 940-948.

(19) Snyder, L. E.; Palmer, P.; Depater, I., Radio detection of formaldehyde emission from comet halley. *Astron. J.* **1989**, *97* (1), 246-253.

(20) Smith, D.; Adams, N. G., Molecular synthesis in inter-stellar clouds - radiative association reactions of CH_3^+ ions. *Astrophys. J.* **1978**, *220* (3), L87-L92.

(21) Huntress, W. T.; Mitchell, G. F., Synthesis of complex-molecules in inter-stellar clouds. *Astrophys. J.* **1979**, *231* (2), 456-467.

(22) Javahery, G.; Petrie, S.; Wincel, H.; Wang, J.; Bohme, D. K., Gas-phase reactions of the buckminsterfullerene cations C_{60}^+, C_{60}^{2+}, and C_{60}^{3+} with water, alcohols, and ethers. *J. Am. Chem. Soc.* **1993**, *115* (14), 6295-6301.

(23) Schutte, W.; Allamandola, L.; Sandford, S., Formaldehyde and organic molecule production in astrophysical ices at cryogenic temperatures. *Science* **1993**, *259* (5098), 1143-1145.

(24) Brand, J. C. D.; Reed, R. I., 457. The electronic spectrum of formaldehyde. Part II. Mechanisms of dissociation of formaldehyde and the formaldehyde molecular ion. *J. Chem. Soc.* **1957**, (0), 2386-2392.

(25) Kanomata, I., Mass-spectrometric study on ionization and dissociation of formaldehyde, acetaldehyde, acetone and ethyl methyl ketone by electron impact. *Bull. Chem. Soc. Jap.* **1961**, *34* (12), 1864-1871.

(26) Baer, T.; Ng, C.; Powis, I., *The Structure, Energetics, and Dynamics of Organic Ions*. Wiley: New York, 1996.

(27) Holmes, J. L.; Aubrey, C.; Mayer, P. M., *Assigning Structures to Ions in Mass Spectrometry*. CRC: Boca Raton, 2007.

(28) Olah, G. A.; Laali, K. K.; Wang, Q.; Prakash, G. K. S., *Onium Ions*. John Wiley & Sons: New York, 1998.

(29) Beynon, J. H.; Fontaine, A. E.; Lester, G. R., Mass spectrometry: the mass spectrum of methanol. Part I. Thermochemical information. *Intl. J. Mass. Spectrom. Ion Phys.* **1968**, *1* (1), 1-24.

(30) Berkowitz, J., Photoionization of CH_3OH, CD_3OH, and CH_3OD: Dissociative ionization mechanisms and ionic structures. *J. Chem. Phys.* **1978**, *69* (7), 3044-3054.

(31) Wesdemiotis, C.; McLafferty, F. W., Mass spectral evidence for the hydroxymethylene radical cation. *Tetra. Lett.* **1981**, *22* (36), 3479-3480.

(32) Burgers, P. C.; Mommers, A. A.; Holmes, J. L., Ionized oxycarbenes: hydroxymethylidyne cation ($[COH]^+$), hydroxymethylene cation ($[HCOH]^+$), dihydroxymethylene cation ($[C(OH)_2]^+$), formoxylium cation ($[HCO_2]^+$) and carboxyl cation ($[COOH]^+$), their generation, identification, heat of formation, and dissociation characteristics. *J. Am. Chem. Soc.* **1983**, *105* (19), 5976-5979.

(33) Reed, R. I., Studies in electron impact methods. Part 1.-Formaldehyde, deuteroformaldehyde and some related compounds. *Trans. Farad. Soc.* **1956**, *52* (0), 1195-1200.

(34) Guyon, P. M.; Chupka, W. A.; Berkowitz, J., Photoionization mass spectrometric study of formaldehyde H_2CO, HDCO and D_2CO. *J. Chem. Phys.* **1976**, *64* (4), 1419-1436.

(35) Bouma, W. J.; Macleod, J. K.; Radom, L., Ab initio molecular-orbital study of the CH_2O^+ isomers - stability of the hydroxymethylene radical cation. *Int. J. Mass Spectrom. Ion Process.* **1980**, *33* (1), 87-93.

(36) Osamura, Y.; Goddard, J. D.; III, H. F. S.; Kim, K. S., Near degenerate rearrangement between the radical cations of formaldehyde and hydroxymethylene. *J. Chem. Phys.* **1981**, *74* (1), 617-621.

(37) Ma, N. L.; Smith, B. J.; Radom, L., The energy difference between formaldehyde and hydroxymethylene radical cations: Failure of unrestricted (UMP2) and restricted (RMP2) Møller—Plesset procedures. *Chem. Phys. Lett.* **1992**, *193* (5), 386-394.

(38) Wiest, O., Density functional theory studies of the methanol radical cation hypersurface. *J. Mol. Struct.: THEOCHEM* **1996**, *368* (0), 39-48.

(39) Lon B. Knight, J.; Steadman, J., An ESR investigation of the formaldehyde cation radicals ($H_2{}^{12}CO^+$ and $H_2{}^{13}CO^+$) in neon matrices at 4 K. *J. Chem. Phys.* **1984**, *80* (3), 1018-1025.

(40) Baker, A. D.; Baker, C.; Brundle, C. R.; Turner, D. W., The electronic structures of methane, ethane, ethylene and formaldehyde studied by high-resolution molecular photoelectron spectroscopy. *Intl. J. Mass. Spectrom. Ion Phys.* **1968**, *1* (4–5), 285-301.

(41) Niu, B.; Shirley, D. A.; Bai, Y., High resolution photoelectron spectroscopy and femtosecond intramolecular dynamics of $H_2CO^+$and D_2CO^+. *J. Chem. Phys.* **1993**, *98* (6), 4377-4390.

(42) Wiedmann, R. T.; White, M. G.; Wang, K.; McKoy, V., Rotationally resolved photoionization of polyatomic hydrides: CH_3, H_2O, H_2S, H_2CO. *J. Chem. Phys.* **1994**, *100* (7), 4738-4746.

(43) Liu, J.; Kim, H.-T.; Anderson, S. L., Multiphoton ionization and photoelectron spectroscopy of formaldehyde via its 3p Rydberg states. *J. Chem. Phys.* **2001**, *114* (22), 9797-9806.

(44) Schulenburg, A. M.; Meisinger, M.; Radi, P. P.; Merkt, F., The formaldehyde cation: Rovibrational energy level structure and Coriolis interaction near the adiabatic ionization threshold. *J. Mol. Spectrosc.* **2008**, *250* (1), 44-50.

(45) Blowers, P.; Masel, R. I., Calculated Vibrational Spectra for CH_nOH_m Species. *J. Phys. Chem. A* **1999**, *104* (1), 34-44.

(46) Bouma, W. J.; MacLeod, J. K.; Radom, L., Experimental evidence for the existence of a stable isomer of CH_3OH^+: the methylenoxonium radical cation, $CH_2OH_2^+$. *J. Am. Chem. Soc.* **1982**, *104* (10), 2930-2931.

(47) Holmes, J. L.; Lossing, F. P.; Terlouw, J. K.; Burgers, P. C., The radical cation $[CH_2OH_2]^+$ and related stable gas-phase ion-dipole complexes. *J. Am. Chem. Soc.* **1982**, *104* (10), 2931-2932.

(48) Holmes, J. L.; Lossing, F. P.; Terlouw, J. K.; Burgers, P. C., Novel gas-phase ions. The radical cations $[CH_2XH]^{+\bullet}$ (X=F, Cl, Br, I, OH, NH_2, SH) and $[CH_2CH_2NH_3]^{+\bullet}$. *Can. J. Chem.* **1983**, *61* (10), 2305-2309.

(49) Bramer, E. M.; Weger, E.; Ischtwan, J.; Brand, W. A.; Levsen, K., Photodissociation of some small heteroatom-containing organic ions. *Intl. J. Mass Spectrom. Ion Proc.* **1983**, *55* (1), 83-91.

(50) Verbeck, G. F.; Gillig, K. J.; Russell, D. H., Variable-temperature ion mobility time-of-flight mass spectrometry studies of electronic isomers of Kr^{2+} and CH_3OH^+ radical cations. *Eur. J. Mass Spectrom.* **2003**, *9* (6), 579-587.

(51) Bouma, W. J.; Nobes, R. H.; Radom, L., Methylenoxonium radical cation ($CH_2OH_2^+$): a surprisingly stable isomer of the methanol radical cation. *J. Am. Chem. Soc.* **1982**, *104* (10), 2929-2930.

(52) Yates, B. F.; Bouma, W. J.; Radom, L., Ylides and ylidions: A comparative study of unusual gas-phase structures. *J. Am. Chem. Soc.* **1987**, *109* (8), 2250-2263.

(53) Ma, N. L.; Smith, B. J.; Pople, J. A.; Radom, L., Rearrangement and dissociative reactions of the methanol radical cation (CH_3OH^+): a comparison of theory and experiment. *J. Am. Chem. Soc.* **1991**, *113* (21), 7903-7912.

(54) Ma, N. L.; Smith, B. J.; Radom, L., Refined thermochemistry for the methanol radical cation (CH_3OH^+) and its distonic isomer ($CH_2OH_2^+$). *J. Phys. Chem.* **1992**, *96* (14), 5804-5807.

(55) Radom, L., The chemistry of gas-phase ions: A theoretical approach. *Intl. J. Mass Spectrom. Ion Proc.* **1992**, *118–119* (0), 339-368.

(56) Gauld, J. W.; Radom, L., A reappraisal of the structures and stabilities of prototype distonic radical cations and their conventional isomers. *J. Phys. Chem.* **1994**, *98* (3), 777-784.

(57) Yates, B. F.; Bouma, W. J.; Radom, L., Detection of the prototype phosphonium (CH_2PH_3), sulfonium (CH_2SH_2), and chloronium (CH_2ClH) ylides by neutralization reionization mass-spectrometry - a theoretical prediction. *J. Am. Chem. Soc.* **1984**, *106* (20), 5805-5808.

(58) Yates, B. F.; Bouma, W. J.; Radom, L., Distonic radical cations : Guidelines for the assessment of their stability. *Tetrahedron* **1986**, *42* (22), 6225-6234.

(59) Hammerum, S., Distonic radical cations in gaseous and condensed phase. *Mass Spectrom. Rev.* **1988**, *7* (2), 123-202.

(60) Zeller, L.; Farrell, J.; Vainiotalo, P.; Kenttamaa, H. I., Long-lived radical cations of simple organophosphates isomerize spontaneously to distonic structures in the gas-phase. *J. Am. Chem. Soc.* **1992**, *114* (4), 1205-1214.

(61) Leeck, D. T.; Stirk, K. M.; Zeller, L. C.; Kiminkinen, L. K. M.; Castro, L. M.; Vainiotalo, P.; Kenttamaa, H. I., The long-lived radical cations of simple carbon esters isomerize to the lowest-energy structure. *J. Am. Chem. Soc.* **1994**, *116* (7), 3028-3038.

(62) Bjoernholm, T.; Hammerum, S.; Kuck, D., Distonic ions as reacting species. *J. Am. Chem. Soc.* **1988**, *110* (12), 3862-3869.

(63) Gauld, J. W.; Audier, H.; Fossey, J.; Radom, L., Water-catalyzed interconversion of conventional and distonic radical cations: Methanol and methyleneoxonium radical cations. *J. Am. Chem. Soc.* **1996**, *118* (26), 6299-6300.

(64) Gauld, J. W.; Radom, L., Effects of neutral bases on the isomerization of conventional radical cations CH_3X^+ to their distonic isomers (CH_2X^+H)-C-(X = F, OH, NH_2): Proton-transport catalysis and other mechanisms. *J. Am. Chem. Soc.* **1997**, *119* (41), 9831-9839.

(65) Knight, L. B.; Kerr, K.; Villanueva, M.; McKinley, A. J.; Feller, D., Theoretical and neon matrix electron spin resonance studies of the methanol cation: CH_3OH^+, CH_3OD^+, CH_2DOH^+, and $^{13}CH_3OH^+$. *J. Chem. Phys.* **1992**, *97* (8), 5363-5376.

(66) Duncan, M. A., Infrared laser spectroscopy of mass-selected carbocations. *J. Phys. Chem. A* **2012**, *116* (47), 11477-11491.

(67) CFOUR, a quantum chemical program package written by J. F. Stanton, J. Gauss, M. E. Harding, and P. G. Szalay with contributions from A. A. Auer, R. J. Bartlett, U. Benedikt, C. Berger, D. E. Bernholdt, Y. J. Bomble, L. Cheng, O. Christiansen, M. Heckert, O. Heun, C. Huber, T.-C. Jagau, D. Jonsson, J. Jusélius, K. Klein, W. J. Lauderdale, D. A. Matthews, T. Metzroth, L. A. Mück, D. P. O'Neill, D. R. Price, E. Prochnow, C. Puzzarini, K. Ruud, F. Schiffmann, W. Schwalbach, S. Stopkowicz, A. Tajti, J. Vázquez, F. Wang, J. D. Watts and the integral packages MOLECULE (J. Almlöf and P. R. Taylor), PROPS (P. R. Taylor), ABACUS (T. Helgaker, H. J. Aa. Jensen, P. Jørgensen, and J. Olsen), and ECP routines by A. V. Mitin and C. van Wüllen. For the current version, see http://www.cfour.de.

(68) Schmidt, M. W.; Baldridge, K. K.; Boatz, J. A.; Elbert, S. T.; Gordon, M. S.; Jensen, J. H.; Koseki, S.; Matsunaga, N.; Nguyen, K. A.; Su, S.; Windus, T. L.; Dupuis, M.; Montgomery, J. A., General atomic and molecular electronic structure system. *J. Comput. Chem.* **1993**, *14* (11), 1347-1363.

(69) Gudeman, C. S.; Begemann, M. H.; Pfaff, J.; Saykally, R. J., Velocity-modulated infrared laser spectroscopy of molecular ions: The ν_1 band of HCO^+. *Phys. Rev. Lett.* **1983**, *50* (10), 727-731.

(70) Nizkorodov, S. A.; Dopfer, O.; Ruchti, T.; Meuwly, M.; Maier, J. P.; Bieske, E. J., Size effects in cluster infrared spectra: The ν_1 band of Ar_n-HCO^+ (n = 1-13). *J. Phys. Chem.* **1995**, *99* (47), 17118-17129.

(71) Nizkorodov, S. A.; Dopfer, O.; Meuwly, M.; Maier, J. P.; Bieske, E. J., Mid-infrared spectra of the proton-bound complexes Ne_n–HCO^+ (n=1,2). *J. Chem. Phys.* **1996**, *105* (5), 1770-1777.

(72) Frisch, M. J., et al., Gaussian 09 (Revision D.01). Gaussian, Inc.: Wallingford CT, 2003.

(73) Gerardi, H. K.; DeBlase, A. F.; Leavitt, C. M.; Su, X.; Jordan, K. D.; McCoy, A. B.; Johnson, M. A., Structural characterization of electron-induced proton transfer in the formic acid dimer anion, $(HCOOH)_2^-$, with vibrational and photoelectron spectroscopies. *J. Chem. Phys.* **2012**, *136* (13), 134318.

(74) Horvath, S.; McCoy, A. B.; Elliott, B. M.; Weddle, G. H.; Roscioli, J. R.; Johnson, M. A., Anharmonicities and isotopic effects in the vibrational spectra of $X^-\cdot H_2O$, $\cdot HDO$, and $\cdot D_2O$ [X = Cl, Br, and I] binary complexes. *J. Phys. Chem. A* **2010**, *114* (3), 1556-1568.

(75) Douberly, G. E.; Ricks, A. M.; Ticknor, B. W.; Duncan, M. A., Structure of protonated carbon dioxide clusters: Infrared photodissociation spectroscopy and ab initio calculations. *J. Phys. Chem. A* **2008**, *112* (5), 950-959.

(76) Mosley, J. D.; Cheng, T. C.; McCoy, A. B.; Duncan, M. A., Infrared spectroscopy of the mass 31 cation: Protonated formaldehyde vs methoxy. *J. Phys. Chem. A* **2012**, *116* (37), 9287-9294.

CHAPTER 7

INFRARED PHOTODISSOCIATION SPECTROSCOPY OF THE ACETYL CATION AND ITS PROTONATED KETENE ISOMER

Introduction

The structures of ions have been of particular interest in mass spectrometry[1-3] and astrochemistry.[4-7] Ion reactivity studies and collisional dissociation dynamics can indicate the presence of more than one isomer, though spectroscopy can give more direct structural information.[1-3] Additionally, the observation of ions in space requires spectroscopy in the laboratory to confirm their presence in interstellar environments. However, ion spectroscopy is difficult due to the high internal temperatures and low densities per quantum state resulting from standard ion production methods.[1] On the other hand, quantum chemistry can provide structural information of ions as well as the relative energetics of isomers. Indeed, theory and spectroscopy are both needed to corroborate which isomers exist, in nature or the laboratory environment.[1-3] Recent developments in ion production methods and infrared laser technology make it possible to obtain the spectra of mass-selected ions via laser photodissociation.[8-10] This work investigates the $[C_2,H_3,O]^+$ organic ion with infrared photodissociation spectroscopy.

$[C_2,H_3,O]^+$ has been studied extensively with mass spectrometry, mainly because ions of this mass to charge ratio (m/e = 43) are prevalent among the mass spectra produced from oxygen-containing precursors.[1-3, 11-15] Ion/molecule reactions and collisional dissociation studies suggest that the structure(s) could be that of the acetyl cation (CH_3CO^+), protonated ketene (CH_2COH^+) and/or oxiranyl cation (H_2COCH^+).[3, 11-13] Mass spectrometric and thermochemical studies indicate that the lowest energy structure is CH_3CO^+.[12-15] The infrared spectrum and

crystal structure of acetyl have been measured before in superacid matrices.[16-18] To our knowledge, no spectroscopy has been reported for other isomers of $[C_2,H_3,O]^+$. Previous theoretical results indicate that a few of the more energetic structures lie behind large barriers to interconversion, and that the acetyl cation is the global minimum structure.[19, 20] $[C_2,H_3,O]^+$ is also important in astrochemical models,[7, 21-23] though it has not yet been detected in space, in part due to a lack of laboratory gas phase spectra. Therefore, $[C_2,H_3,O]^+$ is a compelling target for study with infrared laser spectroscopy.

Experimental Section

The infrared spectrum of $[C_2,H_3,O]^+$ is obtained via infrared photodissociation spectroscopy, which has been described before.[24] Briefly, ions are produced in a pulsed electrical discharge with typical pulse widths of 5−10 microseconds through a supersonic expansion with typical pulse widths of 250−300 microseconds. The expansion is backed by 15-17 atm of a mixture of He and Ar seeded with the ambient vapor pressure of methyl acetate (99%, Alfa Aesar) or acetone (>99.5%, Fisher Scientific) at room temperature. The expansion is skimmed into a second differentially pumped chamber which houses a home-made reflectron time-of-flight mass spectrometer (RTOF). The resulting molecular beam contains neutrals, positive and negative ions and their Ar complexes. Positive ions are pulse-extracted perpendicular to the molecular beam. $[C_2,H_3,O]^+Ar$ is mass selected with pulsed deflection plates in the first flight tube of the RTOF and intersected with a tunable infrared laser (Laservision OPO/OPA system) in the turning region of the reflectron.[24] The complex loses an Ar atom through resonant photodissociation, and parent and daughter ions are separated in the RTOF's second flight tube. Fragment ion signal is integrated while tuning the laser to obtain an infrared spectrum.

CCSD(T)/cc-pVTZ calculations with zero point vibrational energy (ZPE) corrections are used to accurately predict the structures and relative energetics of $[C_2,H_3,O]^+$, and frequencies are predicted at the CCSD(T) level using a comparably sized atomic natural orbital basis set (ANO1), playing to the strengths of each basis set for predicting molecular properties.[25] Anharmonic corrections are obtained at the CCSD(T)/ANO1 level of theory in conjunction with second order vibrational perturbation theory (VPT2).[26, 27] It is generally not feasible to run calculations of structures with the Ar tag atom at this level when performing anharmonic vibrational analyses. Therefore, harmonic frequencies are computed at the MP2/cc-pVTZ level for the Ar tagged species and are scaled by standard scaling factors to account for vibrational anharmonicity.[28] MP2 computations are performed using the GAMESS-US computational chemistry package.[29] CCSD(T) computations are performed using the CFOUR programming package (public release version 1.0).[30]

Results and Discussion

Of the several oxygen containing molecules tested, methyl acetate produces the greatest ion intensity at m/e = 43, corresponding to $[C_2,H_3,O]^+$ (see Figure 7.1). Several other fragment ions are observed in the mass spectrum as well. CH_3^+ is observed at m/z = 15, and the peak at m/z = 29 could be $C_2H_5^+$ or HCO^+. The peak at m/z = 41 is most likely ArH^+. A smaller fragment peak is detected at m/z = 59, which is likely to be $[C_3,H_7,O]^+$.[3] The protonated form of methyl acetate is produced in relatively high abundance as evidenced by the peak at m/z = 75. Signal at larger mass to charge ratios corresponds to clusters of ions and neutrals. Due to the high ion intensities, particularly at m/z = 43, this precursor is used to generate the ion for investigation with infrared spectroscopy.

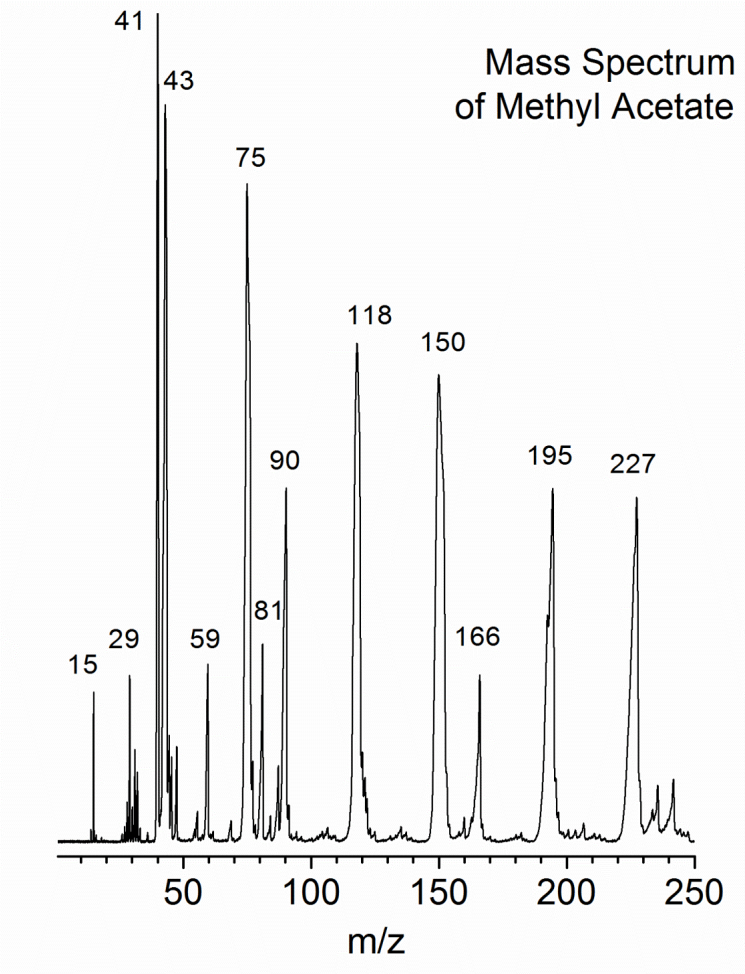

Figure 7.1. The mass spectrum of methyl acetate produced by needle electrical discharge in an expansion of 10% Ar/ 90% He.

The infrared spectrum from 750 – 3500 cm^{-1} for $[C_2,H_3,O]^+Ar$ obtained by loss of Ar is presented in Figure 7.2 (black, top trace). Three sharp bands are observed in the fingerprint region of the spectrum at 1025, 1344 and 1378 cm^{-1}, where stretching and bending vibrations unique to the molecular structure are typically found. No signal is measured between 1750 and 2150 cm^{-1}. One sharp band is seen at 2307 cm^{-1}, which falls close to the frequency typical of CO stretches. Three bands appear in the C−H and O−H stretching region of the spectrum. Two intense bands with noticeably different linewidths are seen at 2903 and 2985 cm^{-1}, and a weaker sharp band exists at 3200 cm^{-1}.

To determine the possible structures of $[C_2,H_3,O]^+$, we performed an extensive search of the potential energy surface (PES) at the MP2/cc-pVTZ level of theory. This led to the optimization of nine different structures, six of which were confirmed to be stable minima by calculating their harmonic frequencies and verifying only positive frequency values. These structures and their relative energies at the MP2/cc-pVTZ level are presented in Table 7.1 and Figure 7.3. The lowest energy structure is the acetyl cation (**A**). Previous theoretical results confirm that **A** is the global minimum of the PES.[19, 20] The next lowest energy structure is that of protonated ketene (herein referred to as **B**). We computed the relative energetics at the CCSD(T)/cc-pVTZ level for **A** and **B** and obtained a value of $\Delta E = +176.2$ kJ/mol, as presented in Table 7.1. This value is corrected for zero point vibrational energy (ZPE) effects at the same level, and is consistent with previous results.[16, 20] Other computed structures include the oxiranyl cation (**C**), oxygen-methylated CO (**D**), ethynyloxonium cation (**E**), and protonated oxirene (**F**).

We use quantum chemistry to assign the bands in our spectrum to molecular vibrations. Figure 7.2 (red, bottom trace) shows the results of fundamental vibrations (with VPT2 anharmonic corrections) predicted at the CCSD(T)/ANO1 level of theory for **A** without Ar, which has C_{3v} symmetry. Predicted frequencies and their computed intensities are given in

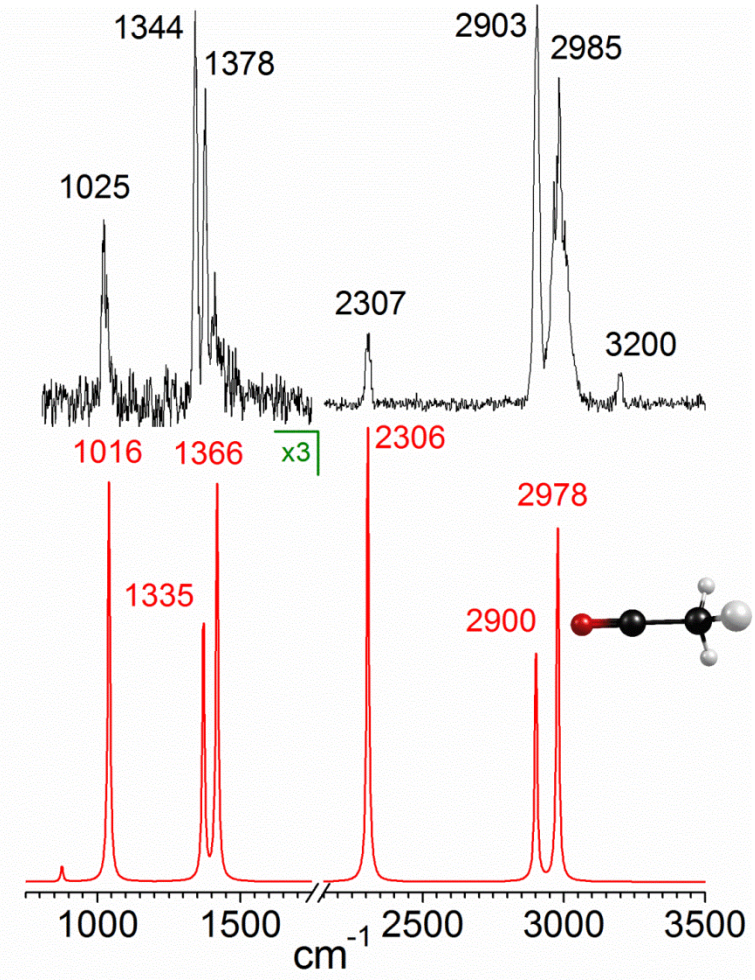

Figure 7.2. The infrared spectrum (black trace, top) of $[C_2,H_3,O]^+$ from methyl acetate versus predicted fundamentals at the CCSD(T)/ANO1 level (red trace, bottom) for the acetyl cation. Anharmonic corrections are obtained at the CCSD(T)/ANO1 level combined with second order vibrational perturbation theory (VPT2).

Table 7.1. CCSD(T) and MP2 energies for the acetyl cation, protonated ketene and their Ar complexes. All relative energies (in kJ/mol) are corrected for zero-point vibrational energy (ZPE) effects. Double dagger(‡) indicates a transition state (TS) with exactly one negative frequency.

Isomer	Description	CCSD(T) Energy	ΔE (CCSD(T))	MP2 Energy	ΔE(MP2)
CH_3CO^+ (**A**)	Acetyl cation	-152.686199[a]	0.0	-152.650784	0.0
CH_2COH^+ (**B**)	Protonated ketene	-152.617482[a]	+176.2	-152.574465	+196.1
TS1‡	1,3−hydride transfer	−−	−−	-152.484499	+417.2
CH_3CO^+−Ar	Acetyl cation Ar complex				
1	Ar above C (staggered)	-679.712606[b]	0.0	-679.674102	0.0
2	Ar above C (eclipsed)	-679.712274[b]	+0.3	-679.673717	+0.4
3	Ar in CH_3 pocket	-679.711428[b]	+2.4	-679.672956	+2.3
CH_2COH^+−Ar	Protonated ketene Ar complex				
4	Ar on OH	-679.649219[b]	0.0	-679.602266	0.0
5	Ar on CH	−−	−−	-679.596627	+14.2

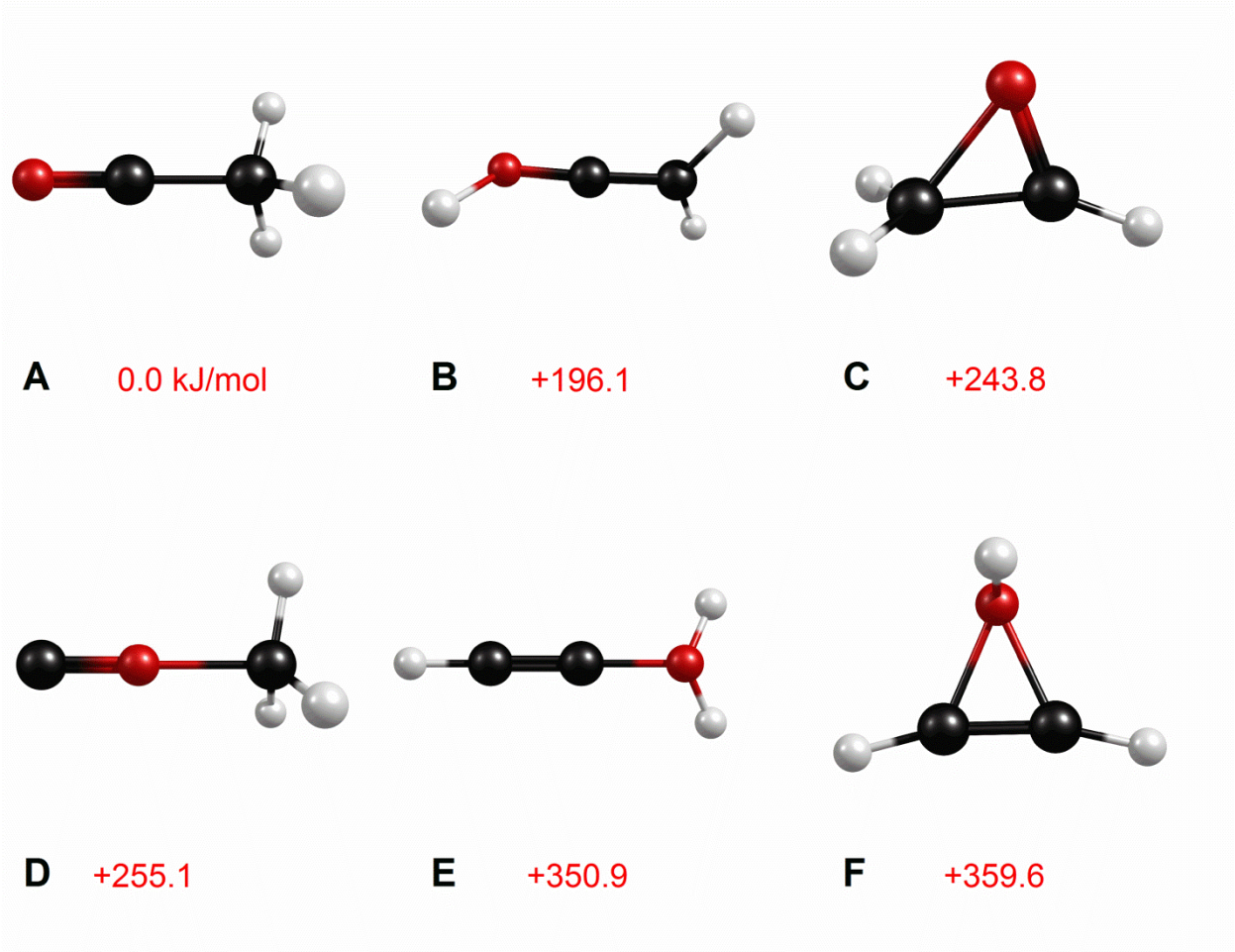

Figure 7.3. Six isomers of $[C_2,H_3,O]^+$ calculated at the MP2/cc-pVTZ level of theory. Relative energies (in kJ/mol) are corrected for zero-point vibrational energy effects.

Table 7.2. The 1025 cm^{-1} band corresponds to the CCO bend predicted at 1016 cm^{-1}. The 1344 and 1378 cm^{-1} bands correspond to the s-CH_3 deformation (umbrella) and d-CH_3 deformation modes predicted at 1335 and 1366 cm^{-1}, respectively. The 2307 cm^{-1} band corresponds to the C−O stretch predicted at 2306 cm^{-1}. The methyl stretches are predicted at 2900 cm^{-1} (symmetric stretch) and 2978 cm^{-1} (degenerate stretch). The bands at 2903 and 2985 cm^{-1} match these predicted vibrations. No fundamental vibrations are predicted near 3200 cm^{-1}. However, a combination band with modest infrared intensity (~5 km/mol) is predicted at 3182 cm^{-1}, corresponding to one quantum each of the C−O and C−C stretches. Infrared spectroscopy is sensitive to combination bands and overtones, and ion spectra are particularly prone to these because of the effects of charge on vibrational couplings and infrared intensities. Thus, we tentatively assign the 3200 cm^{-1} peak to this combination band. All of the observed bands are reproduced remarkably well by theory ($\Delta\nu \leq 11$ cm^{-1}), and no fundamental vibrations are predicted that are not observed. The excellent agreement between theory and experiment may be surprising, considering the fact that we have not accounted for the presence of the Ar tag. However, the inclusion of Ar at the MP2 level of theory in the harmonic approximation minimally ($\Delta\nu$(Ar) < 4 cm^{-1}) perturbs the predicted frequencies for **A** (see discussion below). Thus, we tentatively assign our spectrum to this structure.

The gas phase infrared bands can be compared to previously measured vibrations for **A** in the condensed phase (see Table 7.2).[16, 17] There is good agreement between all of our observed fundamental vibrations and those measured by Olah in a superacid matrix, indicating that the frequencies are insensitive to the environment.[17] Of particular interest is the C−O stretch, observed here at 2307 cm^{-1}. Cook measured the infrared spectrum of a Friedel-Crafts catalyst in solution and obtained a band around 2307 cm^{-1}, which he attributed to CH_3CO^+.[16] Olah measured the C−O stretch at 2294 cm^{-1}.[17] This band has an unusually high frequency for a

Table 7.2. Infrared bands (in cm^{-1}) assigned to two isomers of $[C_2,H_3,O]^+$. Predicted fundamental frequencies (in cm^{-1}) are given for the bare cation structures at the CCSD(T) level of theory. Predicted (scaled) frequencies (in cm-1) are given for the Ar complex at the MP2 level of theory. Infrared intensities are given in km/mol.

Exp.	CCSD(T) (Int)[a]	MP2 (Int)[b]	Previous Work[c]	Assignment[e]
Acetyl				
1025	1017 (40.0)	1037 (46.0)	1022	CH_3 rock
1344	1335 (25.5)	1374 (29.8)	1344	s-CH_3 deform
1378	1367 (38.9)	1425 (44.4)	1379	d-CH_3 deform
2307	2306 (128.6)	2281 (80.2)	2294,~2307[d]	CO stretch
2903	2901 (67.2)	2925 (76.6)	2924	CH_3 symm stretch
2985	2978 (102.3)	3029 (114.3)	3030	CH_3 asymm stretch
3200	3182 (5.3)			CO stretch + CC stretch
Protonated Ketene				
2049	2043 (256.5)	2041 (367.6)		CO stretch
2727	––			Combination band
2982	2978 (170.1)	3001 (673.7)		CH_2 symm stretch
3045	3365 (404.0)	3053 (1467.7)		OH stretch

[a]anharmonic corrections are obtained at the CCSD(T)/ANO1 level combined with second order vibrational perturbation theory (VPT2). [b]harmonic frequencies are scaled by 0.956 (high frequency scaling factor) and 0.996 (low frequency scaling factor), obtained from Ref[31]. [c]from Ref[21], unless otherwise noted. [d]from Ref[20].[e]symm=symmetric, asymm=anti-symmetric.

carbonyl stretch. For reference, the vibration of CO is at 2143 cm^{-1}.[31] Ionization (CO^+; $\upsilon_{CO} = 2184$ cm^{-1})[31] and protonation (HCO^+; $\upsilon_{CO} = 2184$ cm^{-1})[32] both induce a 41 cm^{-1} blue shift in the carbonyl stretch relative to neutral CO. We observe a 164 cm^{-1} blue shift for CH_3CO^+. Apparently, the effect observed here is significantly greater than that of protonation and ionization. Nevertheless, the agreement with previous work confirms that the assignment of our spectrum to **A**−**Ar** is unambiguous. Remarkably, it also appears to be the only structure present when $[C_2,H_3,O]^+$ is made from methyl acetate, given the lack of any other signal in our spectrum.

A closer inspection of the C−H stretching region of the infrared spectrum reveals unusual behavior in the observed linewidths of the bands at 2903 and 2985 cm^{-1}. Figure 7.4 (black trace, top) reveals that the band at 2903 cm^{-1} has a linewidth of 24 cm^{-1}, and that of the 2985 cm^{-1} band is 43 cm^{-1}, when measured at the full width-half maximum (FWHM). The different linewidths are further investigated using pGOPHER.[33] Two rovibrational bands are computed for a prolate symmetric top, representing the two methyl stretches of **A** (C_{3v} symmetry). The band origins (B.O.) and infrared intensities for the simulation are obtained from theory at the CCSD(T) level (see Table 7.2). The equilibrium ground state rotational constants of **A**, computed at the CCSD(T)/cc-pVTZ level of theory, are 5.13 and 0.30 cm^{-1} for A_e and C_e, respectively. These values are used as the upper and lower level constants in the simulation. Figure 7.4 presents the rovibrational simulation (navy trace, middle) obtained at a 100 K rotational temperature and a Lorentzian linewidth (Γ_{IR}) of 1.2 cm^{-1}, corresponding to the linewidth of the infrared laser. Clearly, more structure is evident in the predicted spectrum than is observed experimentally. When the linewidth parameter is increased to 6 cm^{-1} without changing the rotational temperature, a simulation is obtained that closely resembles the experimental spectrum, in terms of peak linewidth (wine trace, bottom). This linewidth (Γ_{VP}) presumably corresponds to homogeneous

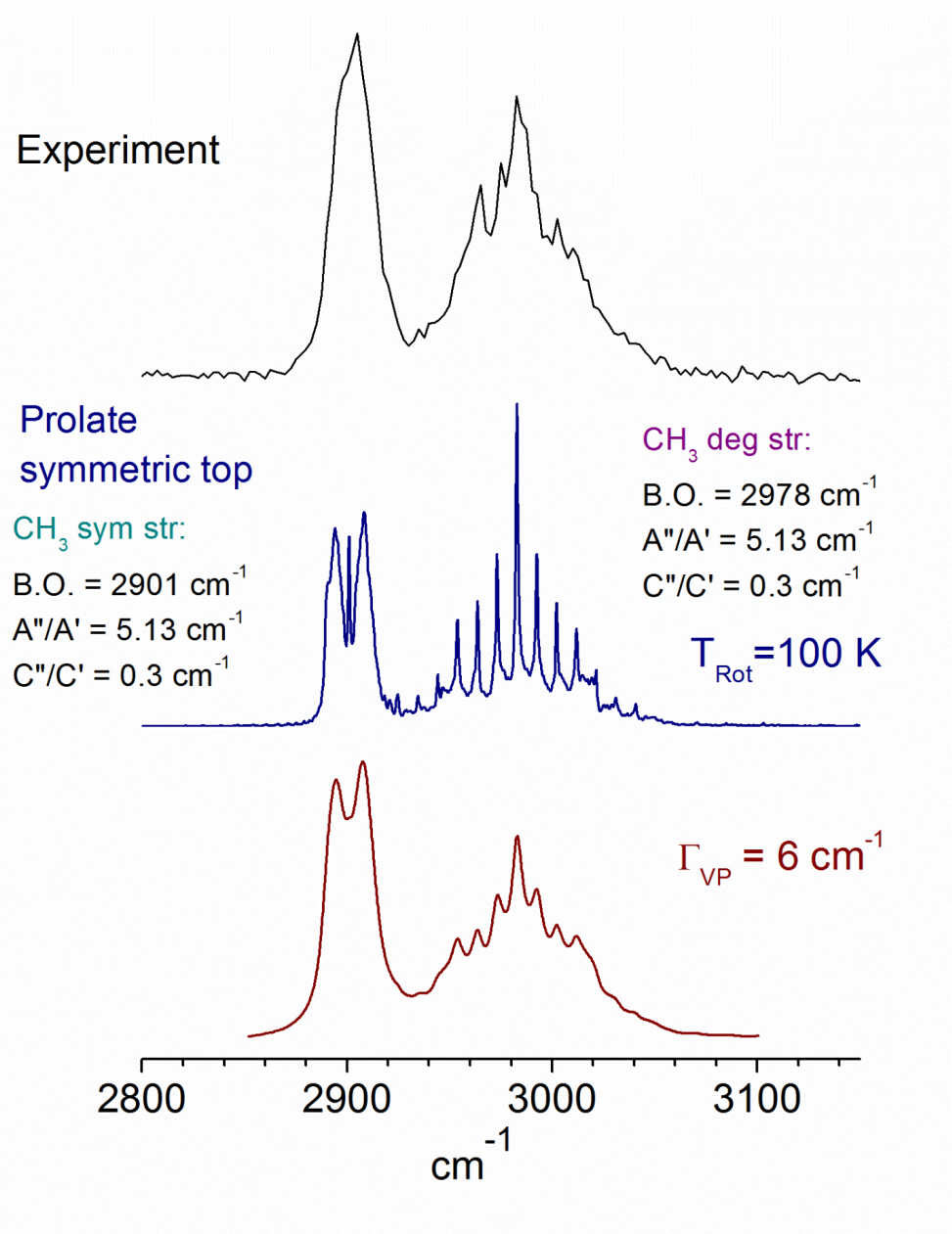

Figure 7.4. Close-up view of the C−H stretching region of acetyl's infrared spectrum (black trace, top) compared with rovibrational simulations of a prolate symmetric top using pGOPHER at the laser linewidth (navy trace, middle) and the vibrational predissociation linewidth (wine trace, bottom). Band origins (B.O.), rotational constants (A, C) and the rotational temperature (T_{Rot}) are identical for both simulations.

broadening due to the fast (picoseconds) vibrational predissociation lifetime present in the **A**−Ar complex, and is what limits the resolution of our experiment. Due to the low resolution of the experimental data, it is impossible to obtain a perfect contour fit. However, the simulation does serve to reproduce the different linewidths observed for a parallel (25 cm^{-1}) versus perpendicular (43 cm^{-1}) type bands of a prolate symmetric top at a rotational temperature of 100 K. We believe this is a reasonable approximation to the rotational temperature. Indeed, varying the temperature by ± 20 K changes the simulated linewidth of the perpendicular type transition at 2978 cm^{-1} by ± 18 cm^{-1}. The band at 2901 cm^{-1} is much less sensitive (±1 cm^{-1}) to similar changes, as is expected for a parallel type transition. Thus, we estimate the temperature of **A**−Ar to be 100 K. This value lies within the optimal temperature range of collisionally cooled ions observed in our ion source.[24, 34, 35]

The rovibrational simulation suggests that the C_{3v} structure and rotational constants of **A** are preserved in the **A**−Ar complex, within the resolution of our experiment. Quantum chemical calculations at the MP2 level of theory reveal the presence of multiple Ar isomers whose relative energetics vary by only 2.3 kJ/mol (see Table 7.1). They are designated isomers **1**, **2**, and **3**. Isomers **1** and **2** correspond to Ar attachment sites above the central carbon with staggered (**1**) and eclipsed (**2**) orientations of Ar with respect to the methyl group. These isomers are essentially isoenergetic (ΔE=+0.4 kJ/mol including ZPE effects). However, **2** is found to have a small negative frequency (−43 cm^{-1}) and is thus not considered a stable minimum. Isomer **3** (ΔE=+2.3 kJ/mol) corresponds to Ar binding on the principal axis in the methyl "pocket", preserving the symmetry of the bare cation. For reference, the rotational energy of the complex at a temperature of 100 K is 1.2 kJ/mol. Distinguishing between the different binding sites at the resolution of our experiment is impossible. Based on past experience, it is likely that the lowest energy Ar binding site is present, while dynamic sampling of other binding sites could possibly

occur as well. Nevertheless, the spectral analysis confirms that free methyl rotation occurs, strengthening the conclusion that the Ar tag does not perturb the symmetry of acetyl.

Prompted by previous mass spectrometric studies,[1-3, 11-15] we wanted to see what other oxygen-containing precursors produce $[C_2,H_3,O]^+$. Figure 7.5 presents the mass spectrum of acetone generated in an expansion of 10% Ar / 90% He under optimal conditions in our ion source. Many similar fragment peaks are seen compared to the mass spectrum from methyl acetate (see Figure 7.1). CH_3^+ (m/z = 15) and $C_2H_5^+$/HCO^+ (m/z = 29) are present, as well as $[C_3,H_7,O]^+$ (m/z = 59). The higher relative intensity of the m/z = 59 peak in the mass spectrum of acetone suggests the structure is that of protonated acetone, which has been studied before.[36] As Figure 7.5 shows, Ar^+ is generated in high abundance, with only a small amount of ArH^+, in contrast to the large amount of ArH^+ in the mass spectrum of methyl acetate in a similar expansion. This observation suggests that different plasma chemistry occurs when using acetone as a precursor. As seen in the previous mass spectrum, signal at larger mass to charge ratios correspond to clusters of ions with neutral precursor molecules and argon, which are common in our ion source. Acetone was found to produce the second most intense ion signal at m/z = 43 in our mass spectrometer. Previous ion reactivity studies suggested that more than one structure for $[C_2,H_3,O]^+$ is formed when using acetone as a precursor.[12]

To investigate this possibility, we measured a second infrared spectrum of $[C_2,H_3,O]^+$ using acetone as a precursor. The spectrum is presented in Figure 7.6 from 2000-3400 cm^{-1} (black trace, second from top) compared to the spectrum of **A** obtained using methyl acetate as a precursor (black trace, top). At first glance, we note that the new spectrum contains bands similar to those already observed for **A**. These features at 2307, 2903, 2982 and 3200 cm^{-1} are almost identical in appearance to those from the acetyl spectrum, with the exception of the 2903 and 2982 cm^{-1} bands. The linewidths appear sharper (15 and 13 cm^{-1}, respectively) than those

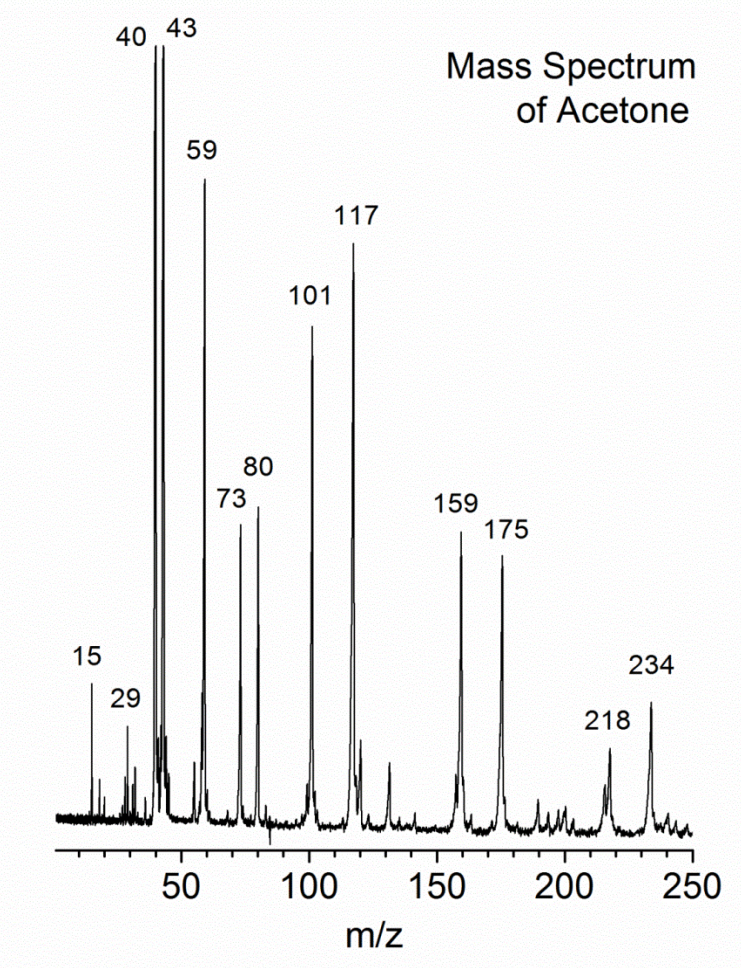

Figure 7.5. The mass spectrum of acetone produced by needle electrical discharge in an expansion of 10% Ar/ 90% He.

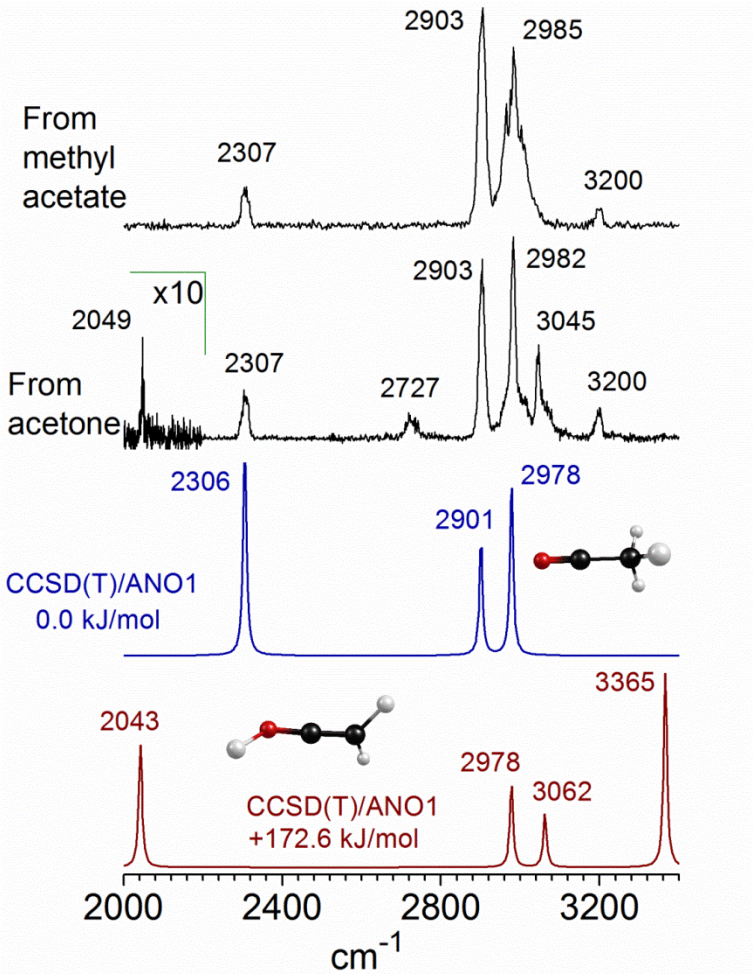

Figure 7.6. Infrared spectra of $[C_2,H_3,O]^+Ar$, obtained by loss of Ar with the ion produced from methyl acetate (black trace, top) and acetone (black trace, second from top) versus fundamental frequencies of acetyl cation (blue trace, third from top) and O−protonated ketene (red trace, bottom), calculated at the CCSD(T)/ANO1 level of theory. Relative energies (in kJ/mol) are corrected for zero-point vibrational energy effects.

of the corresponding bands at 2903 and 2985 cm^{-1} (see Figure 7.6, black trace, top), which is likely due to a lower rotational temperature for **A** made from acetone. In fact, when the rotational temperature in the pGOPHER simulation is reduced to 25 K, without changing any other variables, the linewidths of the symmetric and degenerate methyl stretches reduce to 16 and 14 cm^{-1}, respectively (see Figure 7.7). Similar to before, varying the temperature by ± 5K produces an average change of about 5 cm^{-1} in the linewidth of the 2978 cm^{-1} band. Apparently, discharge conditions using acetone as a precursor result in colder ions than those using methyl acetate.

As Figure 7.6 shows, new bands appear in the second spectrum at 2049, 2727 and 3045 cm^{-1}, which must be due to another structural isomer. For other isomers to survive on the timescale of our experiment, there must be a barrier to interconversion on the PES. Therefore, we investigated the PES using intrinsic reaction coordinate (IRC) calculations at the MP2/cc-pVTZ level of theory. Three first-order saddle points were found by geometry optimization and subsequent frequency analysis. Each saddle point structure, designated **TS1**, **TS2** and **TS3**, has a single negative frequency corresponding to the normal mode of vibration along a unique reaction coordinate. IRC calculations confirm that these structures are transition states, linking structure **A** with structures **B**, **C** and **D**, respectively. Of particular note are the IRC results which show a large barrier to interconversion (+221 kJ/mol at the MP2 level) between **B** and **A**, as shown in Figure 7.8. **TS1** therefore corresponds to the transition state in a [1,3]-hydride shift reaction between terminal atoms. Radom et al previously found a barrier between **B** and **A** which corresponds to two consecutive [1,2]-hydride shifts through an intermediate.[20] Their computed barrier was ~65 kJ/mol higher than the direct shift computed here.[20] Previous results from similar experiments suggest that the current barrier is sufficiently high for observation of a more

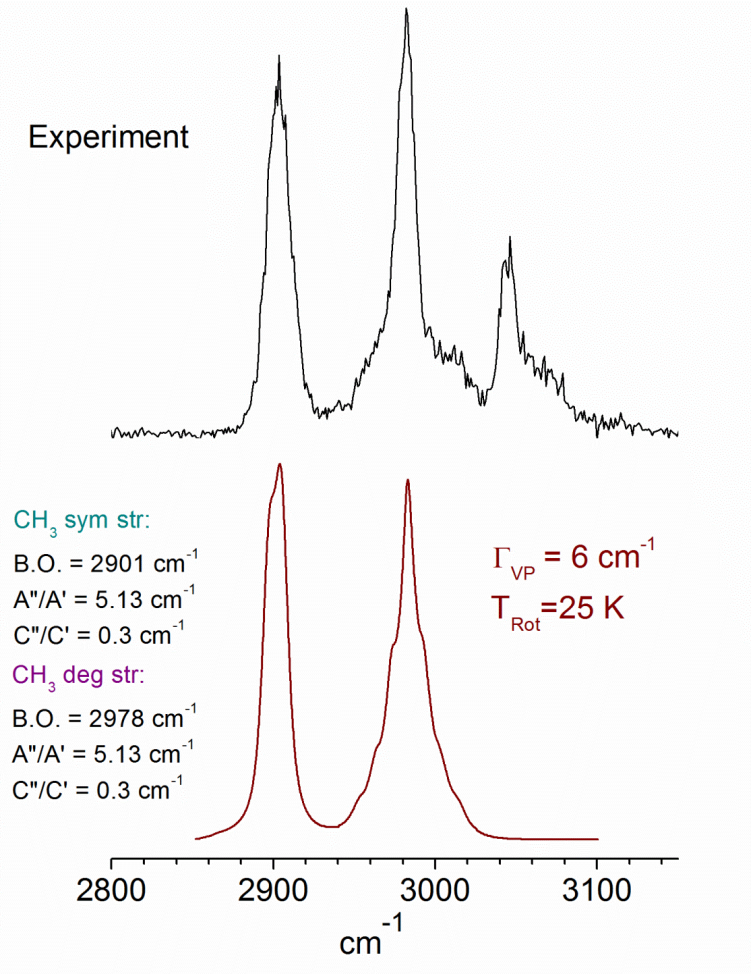

Figure 7.7. Close-up view of the C−H stretching region of acetyl's infrared spectrum (black trace, top) for the ion obtained from acetone, compared to a rovibrational simulation of a prolate symmetric top using pGOPHER (wine trace, bottom) at a linewidth of 6 cm^{-1} and a rotational temperature of 25 K. The linewidth is presumably due to vibrational predissociation (VP).

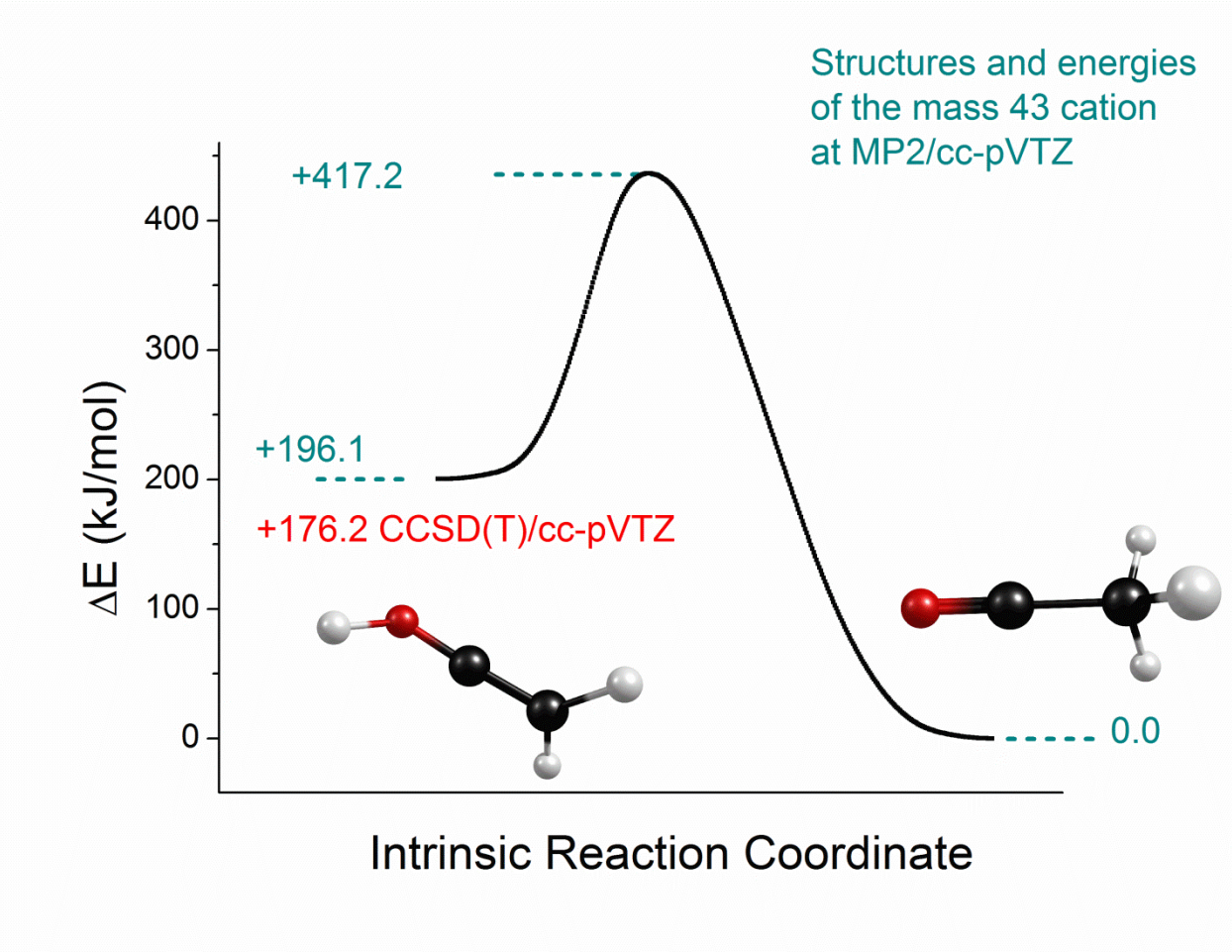

Figure 7.8. Results of an intrinsic reaction pathway calculation at the MP2/cc-pVTZ level of theory. Relative energies (in kJ/mol) are corrected for zero-point vibrational energy effects.

energetic isomer.[24, 35] Indeed, when frequencies predicted at the MP2/cc-pVTZ level for isomers **B**-**F** are compared to the spectrum obtained from acetone, only isomer **B** matches the new bands.

To assign the bands at 2049, 2727 and 3045 cm^{-1}, we first computed the frequencies of **B** without Ar at the CCSD(T)ANO1 level for comparison to the infrared spectrum. The results are presented in Table 7.2 and in Figure 7.6. We see good agreement between the band at 2049 cm^{-1} and the predicted C−O stretch at 2043 cm^{-1}. No fundamental frequency is predicted in the vicinity of the 2727 cm^{-1} band. The symmetric methylene stretch, predicted at 2978 cm^{-1}, overlaps exactly with **A**'s degenerate methyl stretch, predicted at 2978 cm^{-1} and observed at 2982 cm^{-1} in the second spectrum. The anti-symmetric methylene stretch is predicted at 3062 cm^{-1}, which coincides with the shoulder of the 3045 cm^{-1} band. The O−H stretch is predicted at 3365 cm^{-1}, where no signal is observed. Clearly, this indicates that the high level of theory without Ar cannot be used to definitively assign these new bands.

To investigate the spectral assignment further, we performed theory for **B**−Ar at the MP2/cc-pVTZ level of theory to compare to our spectrum. Predicted frequencies are presented in Table 7.2 and Figure 7.9 (bottom trace, wine). These values have been scaled by 0.956 to account for vibrational anharmonicity.[28] Four vibrations are predicted in the 2000-3400 cm^{-1} range. The 2049 cm^{-1} band corresponds to the C−O stretch of protonated ketene, predicted at 2041 cm^{-1} (2043 cm^{-1} at the CCSD(T) level for **B** without Ar). No fundamental vibration is predicted in the vicinity of the 2727 cm^{-1} band for CH_2COH^+Ar, and no other isomers have fundamental vibrations predicted in this region. The symmetric methylene stretch is predicted at 3001 cm^{-1}, and overlaps significantly with **A**'s degenerate methyl stretch at 2982 cm^{-1}. The 3045 cm^{-1} band corresponds to the O−H stretch, predicted at 3053 cm^{-1}. The inclusion of Ar at the MP2 level shifts the OH stretching vibration to 3053 cm^{-1} ($\Delta\nu(Ar) = -326$ cm^{-1}). A 308 cm^{-1} red

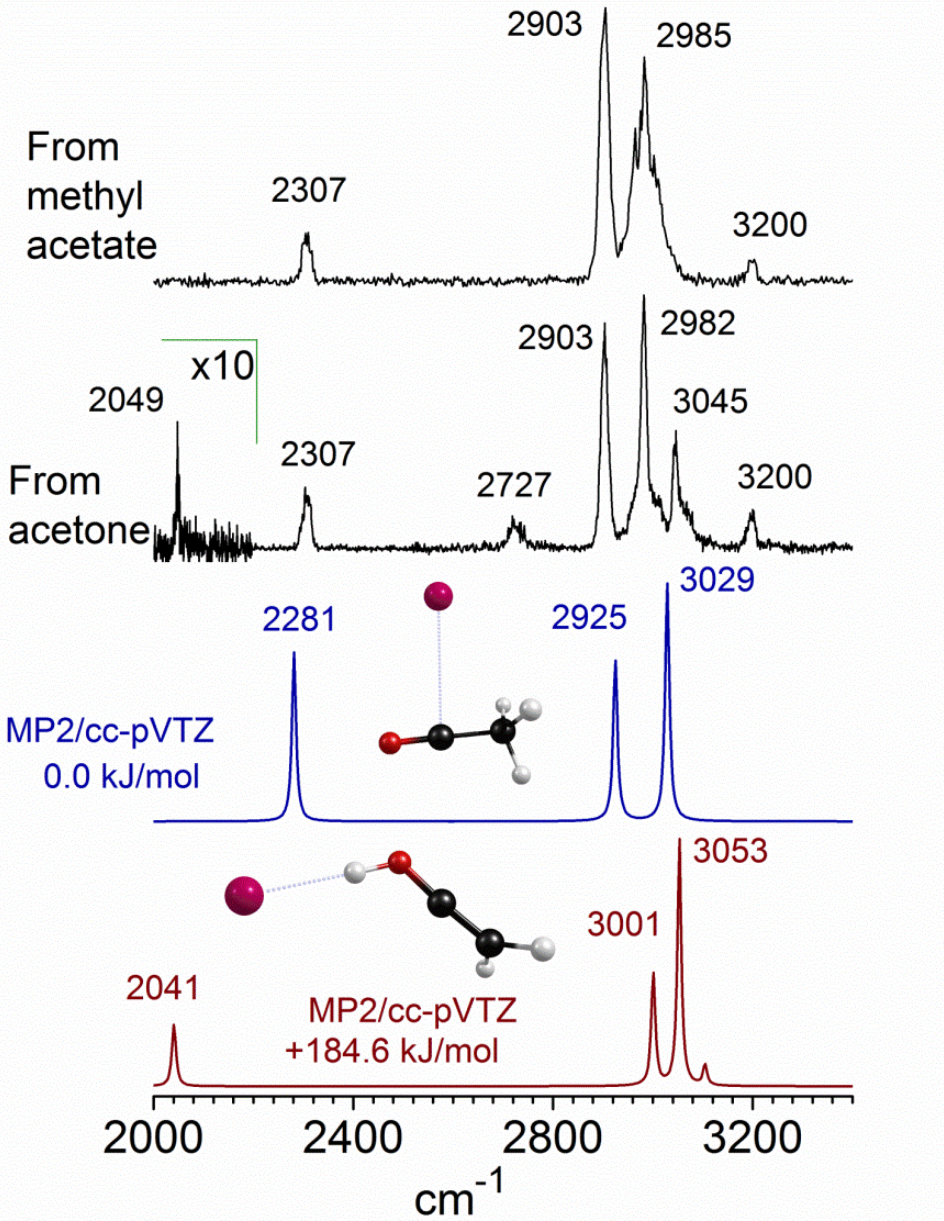

Figure 7.9. Infrared spectra of $[C_2,H_3,O]^+Ar$ obtained by loss of Ar with the ion produced from methyl acetate (black trace, top) and acetone (black trace, second from top). versus (scaled) predicted frequencies of acetyl cation−Ar (blue trace, third from top) and O−protonated ketene−Ar (red trace, bottom), calculated at the MP2/cc-pVTZ level of theory. Relative energies (in kJ/mol) are corrected for zero-point vibrational energy effects.

shift is predicted at the CCSD(T)/ANO1 level using the harmonic approximation. This red shift arises from the Ar attachment site on the OH group (Figure 7.9, bottom trace, inset), as observed for other ions where Ar attaches to a proton site.[24, 35-40] Additionally, the 3045 cm^{-1} band appears blue-shaded (see Figure 7.7, black trace, top), consistent with the proton stretches observed previously.[24, 35-40] This blue-shading is indicative of a shorter OH bond distance upon excitation as a result of vibrational averaging over the probability amplitude for the ground and excited states in the O−H stretch. Thus, we assign the 3045 cm^{-1} band with reasonable confidence to the O−H stretch of the **B**−Ar complex. The anti-symmetric methylene stretch, predicted at 3104 cm^{-1}, apparently overlaps with the tail of the O−H stretch, and thus is not directly observed in our spectrum.

We also present the predicted frequencies of **A**−Ar at the MP2/cc-pVTZ level in Table 7.2 and Figure 7.9 (blue trace, third from top). Three harmonic bands are predicted at 2281, 2925 and 3029 cm^{-1}, which correspond to **A**'s C−O stretch, symmetric and degenerate methyl stretches, respectively. These values have been scaled by 0.956 (methyl stretches) and by 0.996 (carbonyl stretch).[28] The agreement of the MP2 results with our experimental data is reasonable. As one would expect, agreement is better at the higher level of theory with anharmonic corrections than at the (scaled) lower MP2 level (see Table 7.2). The CCSD(T) fundamental frequencies differ on average by 6 cm^{-1} from experiment, and are systematically lower than the experimental values. On the other hand, the average absolute difference for scaled harmonic MP2 frequencies is 29 cm^{-1}. Additionally, these values are systematically higher than the observed bands, with the exception of the carbonyl stretch, which is predicted 17 cm^{-1} below the 2307 cm^{-1} band. When using the methyl stretch scaling factor for the C−O stretch, the discrepancy becomes much greater. This emphasizes an important principle, that when using scaling factors, one must consider that they can be mode-specific. Excellent agreement is

achieved without considering the Ar tag atom (*vide supra*). Moreover, the largest computed Ar shift at the MP2 level is $\Delta\nu(Ar) = +2.9$ cm^{-1} and +3.3 cm^{-1} for the degenerate methyl stretch ($\Delta\nu(Ar) = +3.2$ cm^{-1} and +3.7 cm^{-1} at the harmonic CCSD(T)/ANO1 level).

It is generally observed that tagging with an inert species, such as an Ar atom, minimally perturbs the infrared spectrum of the tagged molecule. However, a number of systems show large perturbations in vibrational frequencies as a result of Ar tagging.[24, 35-40] In these systems, the perturbed frequencies always correspond to proton stretching modes where Ar binds to a proton site. In a larger study on proton bound dimers, results obtained by Johnson and coworkers showed a correlation between the frequency of the shared proton stretch and the difference in proton affinity (ΔPA) between the corresponding neutral molecule and the Ar tag.[39]

To investigate this further, we made a similar comparison of proton bound argon complexes with the present system. Figure 7.10 presents the perturbed frequencies of a number of Ar-tagged species compared to ΔPA between Ar and the corresponding neutral. All of these systems contain Ar bound to a proton site. Data (open circles, black) obtained by Maier and coworkers[37, 38] and in this laboratory[35, 36, 40] show a very similar correlation to that presented by Johnson and coworkers for intermolecular proton stretches of PBD's, which is exponential in nature.[39] The dashed gray line represents an exponential function that is fitted to the data from previous systems. Interestingly, when the present data is included using the literature value for the proton affinity of ketene (PA = 825 kJ/mol; Figure 7.10, closed circle, red),[41] we see a deviation from the trend. The explanation for this anomalous result is simple; the experimental value for the proton affinity of ketene corresponds to protonation at the methylenic carbon site, and previous gas phase protonation studies in fact produced **A**.[11, 14, 15, 41] An extensive literature search failed to discover another experimental value for the proton affinity of ketene. However, we did find that the heat of formation of CH_2COH^+ has been calculated at the G2 level by

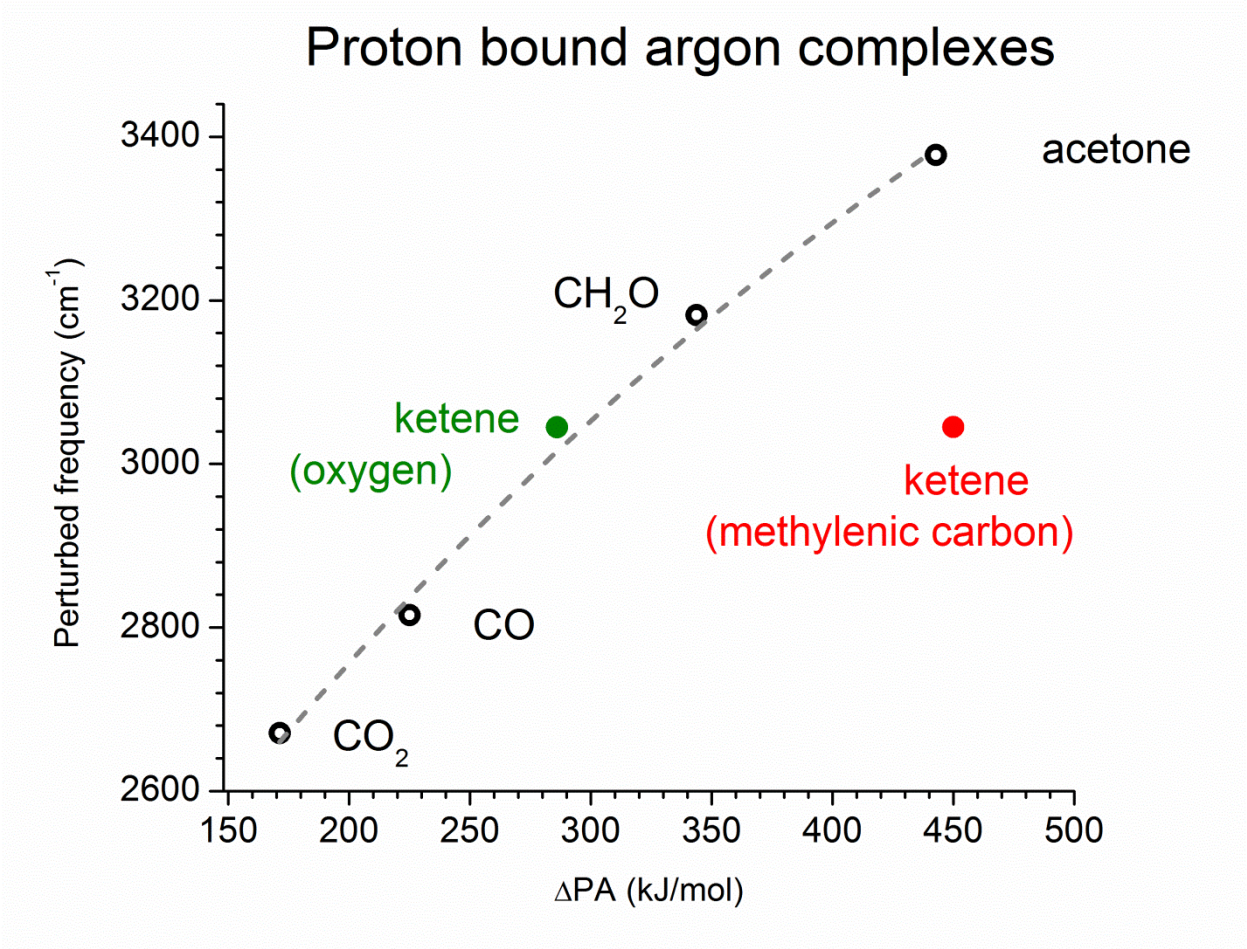

Figure 7.10. The difference in proton affinity (ΔPA, in kJ/mol) between Ar and the corresponding neutral molecule plotted against the perturbed frequency (in cm^{-1}) for proton bound argon complexes studied previously (open circles, black) and in the current work (closed circles, colored). The dashed gray line represents an exponential fit to the data. The colored dots correspond to proton affinities of ketene for different protonation sites.

Bouchoux and coworkers to be 833.0 ± 6 kJ/mol.[42] Using the method of Kebarle,[43] we find the proton affinity of ketene to be 655 ± 9 kJ/mol, corresponding to O−protonation. As shown in Figure 7.10 (PA = 655 kJ/mol; Figure 7.10, closed circle, green), this result gives excellent agreement with the data from previous proton bound Ar complexes. It is not surprising that ketene can have different proton affinities corresponding to C and O protonation sites. For example, CO is well known to have different proton affinities corresponding to the structures HCO^+ and HOC^+.[41] Interestingly, the relative proton affinities of C and O in ketene (ΔPA=170 kJ/mol) are very similar to those in CO (ΔPA=168 kJ/mol). These results confirm that we produce the proton bound Ar complex, CH_2COH^+Ar (see Figure 7.9, bottom trace, inset) in our source.

A and **B** have been identified as potential ions in space, and a variety of possible interstellar formation mechanisms have been discussed.[7, 21-23] $[C_2,H_3,O]^+$ is a product (branching ratio = 0.10) of the reaction of atomic oxygen with protonated acetylene, $C_2H_3^+$.[7] Ion molecule reactions of CH_3^+ with CO have been shown to form $[C_2,H_3,O]^+$, whose structure is likely to be **A**.[21] Huntress and Mitchell proposed that the likely electron recombination product of **A** is ketene, a known interstellar molecule.[22, 44] The same authors proposed that **A** is an ion intermediate in the production of acetaldehyde and acetic acid via ion molecule reactions with H_2 and H_2O, respectively.[22] Both of these products are known to be widespread interstellar compounds.[45, 46] **A** was proposed as the primary precursor for interstellar acetic acid, together with H_2O, and as the primary fragment produced by high energy photoionization of acetic acid.[22, 23] The latter result suggests that it could play a crucial role in decrease H_2O abundance in hot molecular cores.[23] **B** has also been proposed as the structure formed by interstellar reactions of acetylene cation and H_2O,[13] and **A** has been shown to be a minor product in the reaction of atomic oxygen with ethylene cation.[7] While **A** has been studied more extensively than **B**, in

terms of its role in astrochemistry, it is reasonable to expect significantly different chemical reaction pathways for these two isomers. Therefore, further study of these isomers, such as with high-resolution infrared spectroscopy, could conceivably lead to their identification in the interstellar environment.

These data show that infrared spectroscopy with a supersonic expansion source is useful to capture metastable ion structures resulting from complex reaction pathways and to reveal their spectral signatures. Prompt collisional cooling is able to efficiently quench excess energy from the ions as they are formed, allowing for a unique opportunity to sample structural configurations that are otherwise inaccessible. This so-called kinetic trapping concept is consistent with previous results in our laboratory and elsewhere.[24, 35, 47, 48] It is particularly important in the study of transient species, which could survive in the harsh environments of space that generally lack thermodynamic equilibrium.[4-7] We recently reported the most extreme case yet of kinetic trapping, with triplet methoxy cation lying ~400 kJ/mol higher in energy than protonated formaldehyde (a known interstellar ion).[35] Further investigations of $[C_2,H_3,O]^+$ could allow for the study of even more exotic structures, such as those investigated theoretically here (**C**-**F**). One exciting possibility is the capture of **C**, which together with **A**, can be thought of as the methylated analogs to interstellar HCO^+ and HOC^+.[4-7] These species could conceivably be two products of the known ion molecule reaction $CH_3^+ + CO \rightarrow CH_3CO^+$.[21] The use of other precursor molecules to obtain **C** will be attempted in future work to record its infrared spectrum.

Conclusion

Infrared spectra of $[C_2,H_3,O]^+$ in the gas phase are presented using mass-selected laser photodissociation spectroscopy of the argon tagged complex. Different spectra are obtained for the ion produced using methyl acetate or acetone as precursors, respectively. Spectral analysis

reveals that a single structure, that of **A**, is produced for the ion made from methyl acetate, whereas both **A** and **B** are produced for the ion made from acetone. An extensive study of the PES confirms that **A** is the global minimum structure, and that **B** lies 173 kJ/mol higher in energy. IRC results show that a large barrier to interconversion exists between **B** and **A**, and a direct [1,3]-hydride shift reaction mechanism connects the two structures. **A**−Ar's spectral signature is found to be identical to that of the bare (untagged) cation, whereas **B**−Ar is a PBD whose proton stretches are significantly red-shifted from those of the **B** monomer. The relevance of **A** and **B** to astrochemistry is discussed. Rapid collisional cooling in the present experiment allows these species to be captured and studied. Ion production in our pulsed discharge/supersonic expansion source provides a convenient method with which to produce metastable ion structures and to document their infrared spectra.

References

(1) Bowers, M. T., *Gas Phase Ion Chemistry*. Academic Press: New York, 1984; Vol. I-III.

(2) Baer, T.; Ng, C.; Powis, I., *The Structure, Energetics, and Dynamics of Organic Ions*. Wiley: New York, 1996.

(3) Holmes, J. L.; Aubrey, C.; Mayer, P. M., *Assigning Structures to Ions in Mass Spectrometry*. CRC Press: Boca Raton, FL, 2007.

(4) Hartquist, T. W.; Williams, D. A., eds., *The Molecular Astrophysics of Stars and Galaxies*. Clarendon Press: Oxford, 1998.

(5) Tielens, A. G. G. M., *The Physics and Chemistry of the Interstellar Medium*. Cambridge University Press: Cambridge, U.K., 2005.

(6) Petrie, S.; Bohme, D. K., Ions in space. *Mass Spectrom. Rev.* **2007**, *26* (2), 258-280.

(7) Snow, T. P.; Bierbaum, V. M., Ion chemistry in the interstellar medium. *Annu. Rev. Anal. Chem.* **2008**, *1* (1), 229-259.

(8) Boo, D. W.; Lee, Y. T., Infrared-spectra of CH_5^+ core in CH_5^+ (H_2). *Chem. Phys. Lett.* **1993**, *211* (4-5), 358-363.

(9) Bieske, E. J.; Dopfer, O., High-resolution spectroscopy of cluster ions. *Chem. Rev.* **2000**, *100*, 3963-3998.

(10) Duncan, M. A., Frontiers in the spectroscopy of mass-selected molecular ions. *Int. J. Mass Spectrom.* **2000**, *200*, 545-569.

(11) Vogt, J.; Williamson, A. D.; Beauchamp, J. L., Properties and reactions of ketene in the gas phase by ion cyclotron resonance spectroscopy and photoionization mass spectrometry. Proton affinity, site specificity of protonation, and heat of formation of ketene. *J. Am. Chem. Soc.* **1978**, *100* (11), 3478-3483.

(12) Eberlin, M. N.; Majumdar, T. K.; Cooks, R. G., Structures and mechanisms of reactions of isomeric $C_2H_3O^+$ and $C_2H_3S^+$ ions revealed through ion/molecule reactions in conjunction with 2D and 3D mass spectrometry. *J. Am. Chem. Soc.* **1992**, *114* (8), 2884-2896.

(13) Momoh, P. O.; Xie, E.; Abrash, S. A.; Meot-Ner, M.; El-Shall, M. S., Gas phase reactions between acetylene radical cation and water. Energies, structures and formation mechanism of $C_2H_3O^+$ and $C_2H_4O^+$ ions. *J. Phys. Chem. A* **2008**, *112* (27), 6066-6073.

(14) Fogleman, E. A.; Koizumi, H.; Kercher, J. P.; Sztáray, B.; Baer, T., Heats of formation of the acetyl radical and ion obtained by threshold photoelectron photoion coincidence. *J. Phys. Chem. A* **2004**, *108* (24), 5288-5294.

(15) Shuman, N. S.; Stevens, W. R.; Baer, T., Dissociation dynamics of energy-selected acetic acid ions: The gas phase heat of formation of the acetyl ion. *Intl. J. Mass Spectrom.* **2010**, *294* (2–3), 88-92.

(16) Cook, D., The interaction of Friedel-Crafts catalysts with organic molecules .1. The CH_3COCl-$AlCl_3$ system. *Can. J. Chem.* **1959**, *37* (1), 48-53.

(17) Olah, G. A.; Kuhn, S. J.; Tolgyesi, W. S.; Baker, E. B., Stable Carbonium Ions. II. Oxocarbonium (acylium) tetrafluoroborates, hexafluorophosphates, hexafluoroantimonates and hexafluoroarsenates. Structure and chemical reactivity of acyl fluoride: Lewis acid fluoride complexes. *J. Am. Chem. Soc.* **1962**, *84* (14), 2733-2740.

(18) Boer, F. P., Crystal structure of a Friedel-Crafts intermediate. Methyloxocarbonium hexafluoroantimonate. *J. Am. Chem. Soc.* **1968**, *90* (24), 6706-6710.

(19) Yarkony, D. R.; Schaefer III, H. F., The acetyl cation and its geometrical isomers. *J. Chem. Phys.* **1975**, *63* (10), 4317-4328.

(20) Nobes, R. H.; Bouma, W. J.; Radom, L., Structures and stabilities of gas-phase $C_2H_3O^+$ ions: An ab initio molecular orbital study. *J. Am. Chem. Soc.* **1983**, *105* (3), 309-314.

(21) Smith, D.; Adams, N. G., Molecular synthesis in inter-stellar clouds - radiative association reactions of CH_3^+ ions. *Astrophys. J.* **1978**, *220* (3), L87-L92.

(22) Huntress, W. T.; Mitchell, G. F., Synthesis of complex-molecules in inter-stellar clouds. *Astrophys. J.* **1979**, *231* (2), 456-467.

(23) Pilling, S.; Santos, A. C. F.; Boechat-Roberty, H. M., Photodissociation of organic molecules in star-forming regions - II. Acetic acid. *Astron. Astrophys.* **2006**, *449* (3), 1289-1296.

(24) Duncan, M. A., Infrared laser spectroscopy of mass-selected carbocations. *J. Phys. Chem. A* **2012**, *116* (47), 11477-11491.

(25) McCaslin, L.; Stanton, J., Calculation of fundamental frequencies for small polyatomic molecules: A comparison between correlation consistent and atomic natural orbital basis sets. *Mol. Phys.* **2013**, *111* (9-11), 1492-1496.

(26) Mills, I. M., In *Molecular Spectroscopy: Modern Research*, Rao, K. N.; Mathews, C. W., Eds. Academic Press: New York, 1972; Vol. 1.

(27) Clabo, D. A.; Allen, W. D.; Remington, R. B.; Yamaguchi, Y.; Schaefer, H. F., A systematic study of molecular vibrational anharmonicity and vibration-rotation interaction by self-consistent-field higher-derivative methods - asymmetric-top molecules. *Chem. Phys.* **1988**, *123* (2), 187-239.

(28) Merrick, J. P.; Moran, D.; Radom, L., An evaluation of harmonic vibrational frequency scale factors. *J. Phys. Chem. A* **2007**, *111* (45), 11683-11700.

(29) Schmidt, M. W.; Baldridge, K. K.; Boatz, J. A.; Elbert, S. T.; Gordon, M. S.; Jensen, J. H.; Koseki, S.; Matsunaga, N.; Nguyen, K. A.; Su, S.; Windus, T. L.; Dupuis, M.;

Montgomery, J. A., General atomic and molecular electronic structure system. *J. Comput. Chem.* **1993**, *14* (11), 1347-1363.

(30) CFOUR, a quantum chemical program package written by J. F. Stanton, J. Gauss, M. E. Harding, and P. G. Szalay with contributions from A. A. Auer, R. J. Bartlett, U. Benedikt, C. Berger, D. E. Bernholdt, Y. J. Bomble, L. Cheng, O. Christiansen, M. Heckert, O. Heun, C. Huber, T.-C. Jagau, D. Jonsson, J. Jusélius, K. Klein, W. J. Lauderdale, D. A. Matthews, T. Metzroth, L. A. Mück, D. P. O'Neill, D. R. Price, E. Prochnow, C. Puzzarini, K. Ruud, F. Schiffmann, W. Schwalbach, S. Stopkowicz, A. Tajti, J. Vázquez, F. Wang, J. D. Watts and the integral packages MOLECULE (J. Almlöf and P. R. Taylor), PROPS (P. R. Taylor), ABACUS (T. Helgaker, H. J. Aa. Jensen, P. Jørgensen, and J. Olsen), and ECP routines by A. V. Mitin and C. van Wüllen. For the current version, see http://www.cfour.de.

(31) Huber, K. P.; Herzberg, G., *Constants of Diatomic Molecules*. Van Nostrand-Reinhold: New York, 1979.

(32) Foster, S. C.; McKellar, A. R. W.; Sears, T. J., Observation of the ν_3 fundamental band of HCO^+. *J. Chem. Phys.* **1984**, *81* (1), 578-579.

(33) Western, C. M. *PGOPHER, a Program for Simulating Rotational Structure*, University of Bristol: 13 Sep 2010.

(34) Duncan, M. A., Spectroscopy of metal ion complexes: Gas phase models for solvation. *Ann. Rev. Phys. Chem.* **1997**, *48*.

(35) Mosley, J. D.; Cheng, T. C.; McCoy, A. B.; Duncan, M. A., Infrared spectroscopy of the mass 31 cation: Protonated formaldehyde vs methoxy. *J. Phys. Chem. A* **2012**, *116* (37), 9287-9294.

(36) Douberly, G. E.; Ricks, A. M.; Ticknor, B. W.; McKee, W. C.; Schleyer, P. V. R.; Duncan, M. A., Infrared photodissociation spectroscopy of protonated acetylene and its clusters. *J. Phys. Chem. A* **2008**, *112* (9), 1897-1906.

(37) Nizkorodov, S. A.; Dopfer, O.; Ruchti, T.; Meuwly, M.; Maier, J. P.; Bieske, E. J., Size effects in cluster infrared spectra: The ν_1 band of Ar_n-HCO^+ (n = 1-13). *J. Phys. Chem.* **1995**, *99* (47), 17118-17129.

(38) Dopfer, O.; Olkhov, R. V.; Roth, D.; Maier, J. P., Intermolecular interaction in proton-bound dimers.: Infrared photodissociation spectra of RG–$HOCO^+$ (RG=He, Ne, Ar) complexes. *Chem. Phys. Lett.* **1998**, *296* (5–6), 585-591.

(39) Roscioli, J. R.; McCunn, L. R.; Johnson, M. A., Quantum structure of the intermolecular proton bond. *Science* **2007**, *316* (5822), 249-254.

(40) Douberly, G. E.; Ricks, A. M.; Ticknor, B. W.; Duncan, M. A., Structure of protonated carbon dioxide clusters: Infrared photodissociation spectroscopy and ab initio calculations. *J. Phys. Chem. A* **2008**, *112* (5), 950-959.

(41) Hunter, E. P. L.; Lias, S. G., Evaluated gas phase basicities and proton affinities of molecules: An update. *J. Phys. Chem. Ref. Data* **1998**, *27* (3), 413-656.

(42) Bouchoux, G.; Penaud-Berruyer, F.; Bertrand, W., Structure, thermochemistry and reactivity of protonated glycolaldehyde. *Eur. J. Mass Spectrom.* **2001**, *7* (4-5), 351-357.

(43) Davidson, W. R.; Lau, Y. K.; Kebarle, P., Gas phase dissociation of protonated acetic acid to the acyl cation and water. Heat of formation of CH_3CO^+ and proton affinity of ketene. *Can. J. Chem.* **1978**, *56* (7), 1016-1019.

(44) Turner, B. E., Microwave detection of interstellar ketene. *Astrophys. J.* **1977**, *213* (2), L75-L79.

(45) David, M. M.; Lewis, E. S.; Yanti, M.; Frank, J. L., Detection and confirmation of interstellar acetic acid. *Astrophys. J. Lett.* **1997**, *480* (1), L71.

(46) Chengalur, J. N.; Kanekar, N., Widespread acetaldehyde near the galactic centre. *Astron. Astrophys.* **2003**, *403* (3), L43-L46.

(47) Dopfer, O.; Roth, D.; Maier, J. P., Infrared spectra of $C_3H_3^+$-N_2 dimers: Identification of proton-bound c-$C_3H_3^+$-N_2 and H_2CCCH^+-N_2 isomers. *J. Am. Chem. Soc.* **2002**, *124* (3), 494-502.

(48) Lorenz, U. J.; Solcà, N.; Lemaire, J.; Maître, P.; Dopfer, O., Infrared spectra of isolated protonated polycyclic aromatic hydrocarbons: Protonated naphthalene. *Angew. Chem. Int. Ed.* **2007**, *46* (35), 6714-6716.

CHAPTER 8

CONCLUSION

The structures of ions are important in mass spectrometry and astrochemistry. Multiple isomers are often present in ionic systems, and the actual structures formed depend on the energetics of the ion production methods, the precursor used to generate the ion, the inherent stability of the binding configurations, and their local environment. Infrared spectroscopy with a supersonic expansion source is useful to capture metastable ion structures resulting from complex reaction pathways and to reveal their spectral signatures. The rapid excitation followed by highly efficient collisional cooling provides a unique opportunity to sample structural configurations that are otherwise inaccessible.

In chapter 3, we studied the $C_7H_{11}^+$ carbocation system with this technique. The ion was produced with protonation of norbornene, a method that was used previously to generate the 2-norbornyl cation (2-NB) in the gas phase. Spectral analysis showed that the structure produced in our source was in fact not 2-NB. Computational chemistry was used to assign the spectrum to the global minimum structure, that of the 1,3-dimethylcyclopentenyl cation (DMCP). Apparently, the protonating agent used produced a highly excited ion, which undergoes rapid rearrangement to a much more stable configuration. Indeed, DMCP contains the carbocation stabilizing allyl resonance in a five-membered ring with optimally placed methyl groups. This study reveals completely unanticipated complex reaction pathways connecting these structures, some of which are starting to be investigated. Future studies of this ion will use softer production methods to attempt to isolate the authentic 2-NB.

We investigated the structure of $C_7H_9^+$, made from norbornene in our source. This ion was studied previously, and is known to exist as the global minimum structure, para-protonated toluene. The infrared spectrum shows the spectral signature of protonated toluene in addition to new bands from

another structural isomer. Predictions from theory showed that we had obtained a new structure, that of 1,3-dimethylcyclopentadienyl. This structure is very similar to that of DMCP, and the formation mechanisms remain unknown for this metastable species.

Switching to oxygen-containing ions, we studied the ubiquitious mass 31 cation of the form $[C,H_3,O]^+$. This ion is widely recognized to have two structural forms, those of protonated formaldehyde and the metastable methoxy cation. The latter species has eluded previous characterization attempts, and rapid rearrangements were postulated to explain this behavior. When we made the ion from ethanol in our source, we observed multiple bands in the infrared spectrum. Comparison to theory showed that spectral features could be assigned to both species. Upon switching precursors and discharge conditions, the spectra revealed that the relative amounts of the two structures could be varied and that methoxy was present in roughly one tenth the abundance of protonated formaldehyde. Methoxy, which has a triplet ground state and lies behind a substantial barrier to curve crossing to the singlet protonated formaldehyde surface, is the most extreme case yet of metastable ion trapping in our source.

We also investigated the $[C,H_2,O]^+$ and $[C,H_4,O]^+$ systems, which are analogous to the neutral molecules formaldehyde and methanol. These compounds are some of the most abundant polyatomic molecules in space, yet their cationic forms have not yet been characterized with infrared spectroscopy. There are two known structures for $[C,H_2,O]^+$, those of the formaldehyde (H_2CO) radical cation and the hydroxymethylene (HCOH) cation. The infrared spectrum of $[C,H_2,O]^+$ in the C−H and O−H stretching region contains more bands than can be assigned to one isomer. Unfortunately, there is strong disagreement between theory and experiment for the infrared bands of this system. Further experimental and/or theoretical analyses to definitively assign the spectrum are discussed. The $[C,H_4,O]^+$ system also has two known structures, that of the conventional methanol (CH_3OH) cation and its distonic isomer, the methyleneoxonium (CH_2OH_2) ion. It is not generally appreciated that the more stable species is $CH_2OH_2^+$, which is stabilized by separating the radical character and excess charge within the molecule. When the ion is made from methanol in our source, only the higher energy conventional structure is

formed. However, by changing the precursor and discharge conditions, the more stable structure is produced.

Finally we measured the spectrum from 1000−3800 cm^{-1} for the $[C_2,H_3,O]^+$ ion, made from methyl acetate, which contains relatively few peaks. Theory predicts several isomers, yet the spectrum can be completely assigned to just one structure, that of the acetyl cation, which is also the global minimum structure on the potential surface. Comparison of our gas phase spectrum to previous condensed phase results show that the ion's spectrum is insensitive to the local environment. Upon switching precursors to acetone, the spectral features of acetyl appear in the spectrum alongside new features. Theory for the next highest isomer, protonated ketene, confirms that this ion is also present when the ion is formed from acetone in our source. Thus, protonated ketene is observed spectroscopically for the first time. The implications of the different reaction pathways involving the two isomers for astrochemistry are discussed. All of the studies presented herein confirm that infrared spectroscopy in a supersonic expansion source is useful for the capture of transient species and characterization of their infrared spectra.

APPENDIX TO CHAPTER 5

ANALYSIS OF THE COMBINATION BAND AT 3340 CM^{-1}

We follow an approach that is similar to the one taken by Myshakin et al in their analysis of complexes of $CH_3NO_2^-$ and $CH_3CO_2^-$ with H_2O [J. Chem. Phys. **2003**, *119*, 10138]. In the present analysis, the Hamiltonian is reduced to the two normal coordinates, which are treated in the harmonic approximation. The two chosen coordinates are the OH stretch (q_1) and the Ar-H stretch (q_{11}). The one anharmonic term that is included is the cubic coupling term of the form ½ $f_3 q_1^2 q_{11}$, and the value of all the constants are obtained from a calculation at the MP2/6-311++G(d,p) level of theory/basis, as implemented in Gaussian. This gives a Hamiltonian of the form

$$H = \frac{p_1^2}{2} + \frac{p_{11}^2}{2} + \frac{\omega_1^2}{2} q_1^2 + \frac{\omega_{11}^2}{2} q_{11}^2 + \frac{f_3}{2} q_1^2 q_{11}.$$

In the present analysis, the energies and wave functions are obtained by employing an adiabatic approximation in which the OH stretch is treated as the high frequency mode and the eigenvalues and eigenvectors of the Hamiltonian

$$h_1(q_{11}) = \frac{p_1^2}{2} + \left(\frac{\omega_1^2}{2} + \frac{f_3}{2} q_{11} \right) q_1^2$$

are evaluated as functions of q_{11}. This yields expressions for the energies of

$$E_{n_1}(q_{11}) = \eta\sqrt{\omega_1^2 + f_3 q_{11}}\left(n_1 + \frac{1}{2}\right)$$
$$\approx \eta\omega_1\left(1 + \frac{f_3}{2\omega_1^2} q_{11}\right)\left(n_1 + \frac{1}{2}\right)$$

The above approximation is introduced to make the problem analytically solvable, but solving the problem numerically without invoking the approximation yields essentially the same results.

In the second step, we solve for the eigenvalues of h_{11}:

$$h_{11;n_1} = \frac{p_{11}^2}{2} + \frac{\omega_{11}^2}{2} q_{11}^2 + \frac{\eta f_3}{2\omega_1}\left(n_1 + \frac{1}{2}\right) q_{11} + \eta\omega_1\left(n_1 + \frac{1}{2}\right)$$
$$= \frac{p_{11}^2}{2} + \frac{\omega_{11}^2}{2}\left(q_{11} + \frac{\eta f_3}{2\omega_1\omega_{11}^2}\left(n_1 + \frac{1}{2}\right)\right)^2 - \frac{\eta^2 f_3^2}{8\omega_1^2\omega_{11}^2}\left(n_1 + \frac{1}{2}\right)^2 + \eta\omega_1\left(n_1 + \frac{1}{2}\right)$$

which yields

$$E_{n_1,n_{11}} = \eta\omega_1\left(n_1 + \frac{1}{2}\right) + \eta\omega_{11}\left(n_{11} + \frac{1}{2}\right) - \frac{\eta^2 f_3^2}{8\omega_1^2\omega_{11}^2}\left(n_1 + \frac{1}{2}\right)^2$$

Here the corresponding wave functions are harmonic oscillators, and they are centered around

$$q_{11}^{\min}(n_1) = -\frac{\eta f_3}{2\omega_1\omega_{11}^2}\left(n_1 + \frac{1}{2}\right)$$

rather than $q_{11}=0$.

The overlap of shifted harmonic oscillator eigenstates are well-known, and within a Franck-Condon treatment the intensities of combination bands involving one quantum of excitation in the OH stretch and n_{11} quanta in the Ar-H stretch are given by

$$I_{n_{11}} = \frac{e^{-\Delta q_{11}^2/2}\left(\Delta q_{11}\right)^{2n_{11}}}{2^{n_{11}} n_{11}!}$$

where (in dimensionless coordinates)

$$\Delta q_{11}\left(n_1\right) = -\frac{\eta f_3 n_1 \sqrt{\omega_{11}}}{2\omega_1 \omega_{11}^2} = -\frac{\tilde{F}_3 n_1}{2\tilde{\omega}_{11}}$$

Using the values from the electronic structure calculations, $\tilde{\omega}_1 = 3503$ cm^{-1}, $\tilde{\omega}_{11} = 130.6$ cm^{-1}, and $\tilde{F}_3 =$ 72.79 cm^{-1} leads to the prediction that the fundamental of the OH stretch gets 96.2% of the integrated intensity while the remaining 3.8% would go to the combination band involving one quantum in each mode.

Complete citation for reference 34:

Frisch, M. J.; Trucks, G. W.; Schlegel, H. B.; Scuseria, G. E.; Robb, M. A.; Cheeseman, J. R.; Montgomery, J. A. Jr.; Vreven, T.; Kudin, K. N.; Burant, J. C.; Millam, J. M.; Iyengar, S. S.; Tomasi, J.; Barone, V.; Mennucci, B.; Cossi, M.; Scalmani, G.; Rega, N.; Petersson, G. A.; Nakatsuji, H.; Hada, M.; Ehara, M.; Toyota, K.; Fukuda, R.; Hasegawa, J.; Ishida, M.; Nakajima, T.; Honda, Y.; Kitao, O.; Nakai, H.; Klene, M.; Li, X.; Knox, J. E.; Hratchian, H. P.; Cross, J. B.; Adamo, C.; Jaramillo, J.; Gomperts, R.; Stratmann, R. E.; Yazyev, O.; Austin, A. J.; Cammi, R.; Pomelli, C.; Ochterski, J. W.; Ayala, P. Y.; Morokuma, K.; Voth, G. A.; Salvador, P.; Dannenberg, J. J.; Zakrzewski, V. G.; Dapprich, S.; Daniels, A. D.; Strain, M. C.; Farkas, O.; Malick, D. K.; Rabuck, A. D.; Raghavachari, K.; Foresman, J. B.; Ortiz, J. V.; Cui, Q.; Baboul, A. G.; Clifford, S.; Cioslowski, J.; Stefanov, B. B.; Liu, G.; Liashenko, A.; Piskorz, P.

Komaromi, I.; Martin, R. L.; Fox, D. J.; Keith, T.; Al-Laham, M. A.; Peng, C. Y.; Nanayakkara, A.; Challacombe, M.; Gill, P. M. W.; Johnson, B.; Chen, W.; Wong, M. W.; Gonzalez, C. and Pople, J. A. Gaussian 03 (Revision B.02), Gaussian, Inc., Pittsburgh PA, 2003.

APPENDIX TO CHAPTER 6

ANALYSIS OF THE COMBINATION BAND AT 3317 CM^{-1}

We follow an approach that is similar to the one taken by Myshakin et al in their analysis of complexes of $CH_3NO_2^-$ and $CH_3CO_2^-$ with H_2O [J. Chem. Phys. **2003**, *119*, 10138]. In the present analysis, the Hamiltonian is reduced to the two normal coordinates, which are treated in the harmonic approximation. The two chosen coordinates are the OH stretch (q_1) and the Ar-H stretch (q_{13}). The one anharmonic term that is included is the cubic coupling term of the form ½ $f_3 q_1^2 q_{13}$, and the value of all the constants are obtained from a calculation at the B3LYP/aug-cc-pVTZ level of theory/basis, as implemented in Gaussian09. This gives a Hamiltonian of the form

$$H = \frac{p_1^2}{2} + \frac{p_{13}^2}{2} + \frac{\omega_1^2}{2} q_1^2 + \frac{\omega_{11}^2}{2} q_{13}^2 + \frac{f_3}{2} q_1^2 q_{13}.$$

In the present analysis, the energies and wave functions are obtained by employing an adiabatic approximation in which the O−H stretch is treated as the high frequency mode and the eigenvalues and eigenvectors of the Hamiltonian

$$h_1(q_{13}) = \frac{p_1^2}{2} + \left(\frac{\omega_1^2}{2} + \frac{f_3}{2} q_{13} \right) q_1^2$$

are evaluated as functions of q_{11}. This yields expressions for the energies of

$$E_{n_1}(q_{13}) = \hbar\sqrt{\omega_1^2 + f_3 q_{13}}\left(n_1 + \frac{1}{2}\right)$$
$$\approx \hbar\omega_1\left(1 + \frac{f_3}{2\omega_1^2} q_{13}\right)\left(n_1 + \frac{1}{2}\right)$$

The above approximation is introduced to make the problem analytically solvable, but solving the problem numerically without invoking the approximation yields essentially the same results.

In the second step, we solve for the eigenvalues of h_{11}:

$$h_{13;n_1} = \frac{p_{13}^2}{2} + \frac{\omega_{13}^2}{2} q_{13}^2 + \frac{\hbar f_3}{2\omega_1}\left(n_1 + \frac{1}{2}\right) q_{13} + \hbar\omega_1\left(n_1 + \frac{1}{2}\right)$$
$$= \frac{p_{13}^2}{2} + \frac{\omega_{13}^2}{2}\left(q_{13} + \frac{\hbar f_3}{2\omega_1\omega_{13}^2}\left(n_1 + \frac{1}{2}\right)\right)^2 - \frac{\hbar^2 f_3^2}{8\omega_1^2\omega_{13}^2}\left(n_1 + \frac{1}{2}\right)^2 + \hbar\omega_1\left(n_1 + \frac{1}{2}\right)$$

which yields

$$E_{n_1,n_{13}} = \hbar\omega_1\left(n_1 + \frac{1}{2}\right) + \hbar\omega_{13}\left(n_{13} + \frac{1}{2}\right) - \frac{\hbar^2 f_3^2}{8\omega_1^2\omega_{13}^2}\left(n_1 + \frac{1}{2}\right)^2$$

Here the corresponding wave functions are harmonic oscillators, and they are centered around

$$q_{13}^{\min}(n_1) = -\frac{\hbar f_3}{2\omega_1\omega_{13}^2}\left(n_1 + \frac{1}{2}\right)$$

rather than q_{13}=0.

The overlap of shifted harmonic oscillator eigenstates are well-known, and within a Franck-Condon treatment the intensities of combination bands involving one quantum of excitation in the O−H stretch and n_{13} quanta in the Ar−H stretch are given by

$$I_{n_{13}} = \frac{e^{-\Delta q_{13}^2/2}\left(\Delta q_{13}\right)^{2n_{13}}}{2^{n_{13}} n_{13}!}$$

where (in dimensionless coordinates)

$$\Delta q_{13}\left(n_1\right) = -\frac{\mathsf{h} f_3 n_1 \sqrt{\omega_{13}}}{2\omega_1 \omega_{13}^2} = -\frac{\tilde{F}_3 n_1}{2\tilde{\omega}_{13}}$$

Using the values from the electronic structure calculations, $\tilde{\omega}_1 = 3255$ cm^{-1}, $\tilde{\omega}_{13} = 115.8$ cm^{-1}, and $\tilde{F}_3 = -92.31$ cm^{-1} leads to the prediction that the fundamental of the O−H stretch gets 95.7% of the integrated intensity while the remaining 4.3% would go to the combination band involving one quantum in each mode.

Full Gaussian09 reference:

Gaussian 09, Revision D.01, Frisch, M. J.; Trucks, G. W.; Schlegel, H. B.; Scuseria, G. E.; Robb, M. A.; Cheeseman, J. R.; Scalmani, G.; Barone, V.; Mennucci, B.; Petersson, G. A.; Nakatsuji, H.; Caricato, M.; Li, X.; Hratchian, H. P.; Izmaylov, A. F.; Bloino, J.; Zheng, G.; Sonnenberg, J. L.; Hada, M.; Ehara, M.; Toyota, K.; Fukuda, R.; Hasegawa, J.; Ishida, M.; Nakajima, T.; Honda, Y.; Kitao, O.; Nakai, H.; Vreven, T.; Montgomery, J. A., Jr.; Peralta, J. E.; Ogliaro, F.; Bearpark, M.; Heyd, J. J.; Brothers, E.; Kudin, K. N.; Staroverov, V. N.; Kobayashi, R.; Normand, J.; Raghavachari, K.; Rendell, A.; Burant, J. C.; Iyengar, S. S.; Tomasi, J.; Cossi, M.; Rega, N.; Millam, N. J.; Klene, M.; Knox, J. E.; Cross, J. B.; Bakken, V.; Adamo, C.; Jaramillo, J.; Gomperts, R.; Stratmann, R. E.; Yazyev, O.; Austin, A. J.; Cammi, R.; Pomelli, C.; Ochterski, J. W.; Martin, R. L.; Morokuma, K.; Zakrzewski, V. G.; Voth, G. A.; Salvador, P.; Dannenberg, J. J.; Dapprich, S.; Daniels, A. D.; Farkas, Ö.; Foresman, J. B.; Ortiz, J. V.; Cioslowski, J.; Fox, D. J. Gaussian, Inc., Wallingford CT, 2009.